**DOKUZ EYLÜL UNIVERSITY**

**GRADUATE SCHOOL OF NATURAL AND APPLIED SCIENCES**

# FAILURE STRENGTH OF LAMINATED COMPOSITE PLATES WITH MULTI-PIN LOADED HOLES

**by**

**Özer TEKİNŞEN**

**November, 2006**

**İZMİR**

# FAILURE STRENGTH OF LAMINATED COMPOSITE PLATES WITH MULTI-PIN LOADED HOLES

**A Thesis Submitted to the**

**Graduate School and Applied Sciences of Dokuz Eylül University**

**In Partial Fulfillment of the Requirements for the Degree of Master of Science**

**in Mechanical Engineering, Mechanics Program**

**by**

**Özer TEKİNŞEN**

**November, 2006**

**İZMİR**

## M.Sc. THESIS EXAMINATION RESULT FORM

We have read the thesis entitled **"FAILURE STRENGTH OF LAMINATED COMPOSITE PLATES WITH MULTI-PIN LOADED HOLES"** completed by **ÖZER TEKİNŞEN** under supervision of **PROF. Dr. RAMAZAN KARAKUZU** and we certify that in our opinion it is fully adequate, in scope and in quality, as a thesis for the degree of Master of Science.

Prof. Dr. Ramazan KARAKUZU

Supervisor

Prof. Dr. Onur SAYMAN

(Committee Member)

Assist. Prof. Dr. Mustafa TOPARLI

(Committee Member)

Prof. Dr. Cahit Helvacı

Director

Graduate School of Natural and Applied Sciences

**ACKNOWLEDGEMENTS**

I would like to express my sincere gratitude to my supervisor, Prof. Dr. Ramazan KARAKUZU, for his excellent guidance and continuous encouragement throughout the preparation of this study.

I also would like to thank Prof. Dr. Onur SAYMAN for his academic support and encouragement through my M.Sc program.

I also extend my sincere thanks to research assistants Mr.Mehmet AKTAŞ, Mr.Cesim ATAŞ, Mr.B.Murat İÇTEN, Mr.Yusuf ARMAN and Mr.Faruk ŞEN for their help during both experimental and numerical phase of this study.

Thanks go out to "Izoreel Kompozit İzole Malzemeler Sanayi ve Tic.Ltd.Şti." company that helped me for the production of glass-epoxy composite laminates.

I would also like to express my sincere gratitude to TÜBİTAK-BİDEB (Bilim İnsanı Destekleme Daire Başkanlığı) for their scholarship support.

Finally, I am deeply indebted to my family for their support, patience and understanding throughout my life.

**Özer TEKİNŞEN**

**FAILURE STRENGTH OF LAMINATED COMPOSITE PLATES**

**WITH MULTI-PIN LOADED HOLES**

## ABSTRACT

The aim of this investigation is to study the failure behavior and the effect of different geometries of glass-epoxy laminated composite plate which is subjected to a traction force by 4 rigid pins. The behavior of multi-pin loaded composite plates which have the stacking sequence of $[0/90/\pm45]_S$ and approx. 60% fiber volume fraction has been observed experimentally and numerically.

The quantity of the different geometries investigated in this study were 72 which consist of 2 geometric series (Series A, Series B) and 3 different hole distance parameters (The ratio of 'edge distance' to 'hole / pin diameter' E/D:2,3,4 ; The ratio of 'Longitudinal hole distance' to 'hole / pin diameter' F/D:2.4.6 ; The ratio of 'Transverse hole distance' to 'hole / pin diameter' G/D:2,4,6,8)

The three-dimensional finite element method was used to obtain stress distribution of the material. For analyzes, LUSAS 13.6 finite element analyze software has been chosen. During the study geometric non-linear analyze method and "Hashin Failure Criteria" have been selected to determine the "Failure Mode" and the "Failure Load".

The results of numerical and experimental study have been plotted and compared with each other.

**Keywords:** glass-epoxy composite, pin loading, failure mode, failure load

# ÇOKLU PİM YÜKLEMELİ LAMİNE KOMPOZİT PLAKLARIN HASAR DAYANIMI

## ÖZ

Bu araştırmanın amacı hasar davranışı ve 4 rijid pim ile çeki yükü uygulanmış cam lifi-epoksi kompozit plakasının farklı geometrilerinin etkisini ve hasar davranışını incelemektir.

$[0/90/\pm45]_S$ dizilimine sahip ve hacimce fiber yüzdesi yaklaşık %60 olan çoklu-pim yüklemeli kompozit plakaların davranışı deneysel ve nümerik olarak incelenmiştir.

Bu çalışmada incelenen farklı geometri sayısı 72 olup, 2 geometrik seri (Seri A ve Seri B) ve 3 farklı delik mesafe parametresinden (Kenar mesafesinin delik/pim çapına oranı E/D:2,3,4 ; Boylamasına delik mesafesinin delik/pim çapına oranı F/D:2,4,6 ; Enlemesine delik mesafesinin delik/pim çapına oranı G/D:2,4,6,8) oluşur.

Malzemenin gerilme dağılımlarını elde etmek üzere üç boyutlu sonlu eleman metodu kullanıldı. Analizlerde LUSAS 13.6 sonlu eleman analiz yazılımı seçildi. Çalışma esnasında, "Hasar modu" ve "Hasar Yükü"nü belirlemek üzere geometrik doğrusal olmayan analiz metodu ve "Hashin hasar kriteri" tercih edildi.

Nümerik ve deneysel çalışma sonuçları grafiğe aktarıldı ve kendi içlerinde karşılaştırıldı.

**Anahtar Sözcükler:** cam lifi-epoksi kompozit, pimle yükleme, hasar modu, hasar yükü

**CONTENTS**

**M.Sc. THESIS EXAMINATION FORM** ..... ii
**ACKNOWLEDGEMENTS** ..... iii
**ABSTRACT** ..... iv
**ÖZ** ..... v

**CHAPTER ONE - INTRODUCTION** ..... 1

**CHAPTER TWO - INTRODUCTION TO COMPOSITE MATERIALS** ..... 10

2.1 Definition & Background: ..... 10

2.2 Classification of Composite Materials: ..... 12

2.3 The Matrix and Reinforcement: ..... 14

2.4 Functions of Fibers and Matrix: ..... 15

2.5 Special Features of Composites ..... 16

2.6 Drawbacks of Composites ..... 20

2.7 Composites Markets ..... 22

2.8 Barriers in Composite Markets ..... 32

**CHAPTER THREE - STRUCTURAL ANALYSIS OF COM. MATERIALS** ..... 33

3.1 Classical Analysis ..... 33

3.2 Finite Element Analysis ..... 39

**CHAPTER FOUR - NUMERICAL STUDY** ..... 43

4.1 Objective ..... 43

4.2 Explanation of the Numerical Study: ..... 43

**CHAPTER FIVE - EXPERIMENTAL STUDY**.....46

5.1 Objective.....46

5.2 Problem Statement and Experimental Details .....46

5.3 Determination of Mechanical Properties.....49

**CHAPTER SIX - RESULTS AND DISCUSSION** .....55

**CHAPTER SEVEN - CONCLUSION** .....101

**REFERENCES** .....103

# CHAPTER ONE

## INTRODUCTION

In structural applications such as in aircraft, spacecraft, automotive and civil engineering structures, composite components are often fastened to other structural members by mechanically-fastened (bolted, riveted or pinned) joints. Although it is the preferred joining technique in many cases, it is still associated with difficulties. The presence of a hole in a laminated plate subjected to external loading introduces a disturbance in the stress field. Stress concentrations are generated in the vicinity of the hole. Inserting a fastener into the hole and reacting load through the contact between the fastener and the hole surface will make the stress concentrations even more severe causing severely reduce the overall strength of the structure.

Considering that the joints are very often critical part of a structure, the soundness of their design procedures on the overall weight and cost of the product, reliable and general joint design methods in composite structures are required to avoid unnecessary weight and both product and in-service cost penalties.

To exploit the full potential of composite materials in structural elements, the strength and failure of mechanically fastened joints in composite plates must be understand and they must be properly designed to achieve an efficient structure. (Dano et al., 2006) , (Ekh, 2006) , (Gülem, 2004)

Owing to the significance of the problem, several investigators have developed analytical procedures for calculating the strength of bolted joints in composite materials. (Chang, 1983)

A large part of the literature published so far on mechanically-fastened joints present experimental results on the effect of the stacking sequence, geometric properties, clearance between the hole and the pin, and the degree of lateral clamping pressure exerted by the bolt. (Dano et al., 2000)

Lekhnitskii (1968) and later Savin (1968) analyzed problems related to the determination of the stress distribution in anisotropic plates weakened by an opening and deformed by forces applied to the mid plane.

Green and Zerna (1968) independently proposed a formulation for the deformation of anisotropic elastic materials containing stress raisers.

Whitney and Nuismer (1974) introduced two related failure criteria: the point stress and the average stress failure criterion to evaluate the strength of composite plates containing through the thickness discontinuities.

Konish and Whitney (1975) proposed an approximate solution to the stress distribution in the vicinity of flaws to investigate the influence of hole size on composite strength.

Collings (1977) has discussed the effects of variables such as ply orientation, laminate thickness and bolt clamping pressure.

Mathews and Quinn (1977) have experimentally studied the effect of stacking sequence on the pin bearing strength in glass fibre-reinforced laminates which have different ply angle directions. The results suggested that placing the 90º layer (normal to the applied load) at or next to the surface increases the bearing strength.

Pyner and Matthews (1979) have made experimental investigation about comparison of single and multi hole bolted joints in glass-fibre-reinforced plastics. The results suggested that the joint strength expressed as the load/bolt, decreases as the joint geometry becomes increasingly complex.

Chang, Scott and Springer (1982) have developed a user-friendly computer code (designated as BOLT) which can be used to calculate the maximum load and which can be applied to joints involving fiber-reinforced laminates with different ply orientations, different material properties, and different configurations, including different hole sizes, hole positions and thickness. They have used Yamada failure criterion.

Collings (1982) has tested CFRP for a range of laminate configurations and hole sizes, and investigated the relation between joint strength and W/D, E/D and t/d.

Chang et al. (1984)a have extended their analysis to T300/1034-C laminates containing a pin-loaded hole or two pin-loaded holes in parallel or in series.

Chang et al. (1984)b have developed a model and corresponding computer code to determine failure strength and failure mode of composite laminates containing a pin loaded hole even when the material exhibits non-linearly elastic behaviour.

Fu-Kuo et al. (1984) have investigated failure analysis using T300/1034-L graphite-epoxy materials. The specimens have one or two holes. They used Yamada-Sun failure criteria.

Kretsis and Matthews (1985) showed that as the width of the specimen decreases, there is a point where the made of failure changes from one of bearing mode to one of tension mode, using E glass fiber-reinforced plastic and carbon fiber-reinforced plastic. A similar behaviour between the end distance and the shear-out mode of failure was found. They concluded that lay-up had a great effect on both joint strength and failure mechanism. They concluded that lay-up had a great effect on both joint strength and failure mechanism. The bearing strength, failure load and failure modes are investigated in pin-loaded glass-vinylester laminated composite plate and the effects of changing the geometric parameters are observed. The three-dimensional finite element method is used to determine the failure load and failure mode using Hashin failure criteria. The mechanical properties of the laminated composite plate are obtained from standard tests.

Chang (1986) has performed an analysis to evaluate the effect of the assumed pin load distribution. The calculations have utilized a finite element method of stress analysis combined with the Yamada–Sun failure criterion applied along the Chang–Scott–Springer characteristic curve.

Fu-Kuo and Kuo-Yen (1987) have studied non-linear failure analysis of Yamada Sun failure criteria. They have used T300/1034-C graphite-epoxy composites that have different ply orientation angles.

Akay and Kong (1991) have investigated failure analysis of pinned-joint Kevlar fiber-reinforced epoxy laminates experimentally.

Herrington and Sabbaghian (1992) and later Khashaba (1996) showed that, the load–pin displacement curve of bolted joint specimens had a linear behavior up to a point, followed by an unstable non-linear behavior. They defined the bearing failure as the maximum load just prior to unstable, non-linear behavior.

Hironori and Kenji (1993) have studied failure analysis for three materials which are shin asahikasei carbon fiber, toray, and nippon steel. They took the directions of plies $[0/\pm45/90]_{3s.}$

Maikuma and Kubomura (1993) reported in their review two failure criteria for calculating the bearing strength of FRP composites. The first criterion was based on the half of the maximum bearing load, while the second criterion was based on the first peak load, using the load–pin displacement curve.

Naby and Hollaway (1993) have investigated behavior of bolted joints in pultruded composite materials experimentally. They obtained the critical end distance and showed that this distance depends on the width of the joint.

Persson et al. (1993) predicted the delamination initiation in laminates with pin-loaded holes using the strain energy density criterion.

Chen, Chiu and Chin (1994) have studied the influence of weave structure on pin-loaded strength of orthogonal 3D composites. They evaluated the influences of reinforcement type, weave structure, specimen width-to-diameter ratio and edge distance-to hole diameter ratio.

Chen and Lee (1995) used the maximum stress theory to predict in-plane fibre, matrix and shear failure and the Ye delamination criterion (1988) in a progressive damage model.

Gamble et al. (1995) used a modified version of the Hill-criterion in a progressive damage model. The criterion was able to predict fibre failure, matrix splitting and delamination.

Lessard & Shokrieh (1995) have numerically investigated 2D progressive damage modeling of composite pinned-joint failure. They have applied fiber tensile-compressive, shearing, matrix tensile-compressive and fiber-matrix shearing criteria.

Larry and Mahmood (1995) have numerically investigated 2D progressive damage modeling of graphite epoxy composite pinned-joint failure. They analyzed laminates that have different ply angle directions. In addition, they used fiber tensile-compressive, shearing, matrix tensile-compressive, and fiber-matrix shearing criteria. In their study, the specimens where the hole is located too close to the sides, W/D<3, or too close to the edge E/D<3, were characterized as weak.

Hollmann (1996) has calculated the bolt bearing strength which was based on the ultimate failure loads. Theoretically, the load at which the stresses have exceeded a prescribed limit in any of the plies along an approximately chosen curve (denoted as the characteristic curve) considered as a failure criterion by any investigators.

Khashaba (1996) has conducted an experimental study to determine the notched and pin bearing strength of GFRP composites having various values of fiber volume fractions. The results show that fiber volume fraction has a significant effect on load-pin bearing displacement behavior and the value of W/D must be greater than 5 for the development of full bearing strength of the composite laminates.

Shokrieh et al. (1996) have developed a progressive fatigue modeling technique which includes a progressive failure analysis. At that study a set of stress-based failure criteria were used to predict matrix tension, matrix compression, fibre tension, fibre compression, fibre-matrix shear out, delamination tension and delamination compression.

Hung et al. (1996) have investigated failure analysis of T800/3900-2 graphite-epoxy materials by using Hashin failure criteria.

Hamada and Maekawa (1996) have examined failure analysis of quasi-isotropic carbon epoxy T300/#2500 laminates numerically and experimentally.

A three dimensional finite element model to perform stress analysis of single and multi bolted double shear lap connections of glass fiber reinforced plastic has been used by Hassan et al. (1996) with using ANSYS program.

Hong-Sheng et al. (1996) have obtained the effect of clamping pressure on the bearing strength of bolted joints.

Mahmood and Larry (1996) have investigated non-linear three dimensional stress of pin-loaded composites which have $[O_4/90_4]_s$ and $[90_4/0_4]_s$ orientation ply angle.

Usama (1996) has obtained the pin bearing strength of randomly oriented GFRP composites having various values of fiber volume fractions.

Hiroyuki et al. (1996) have carried out failure analysis using Yamada Sun failure criteria for different ply angle directions.

Kim et al (1998) have performed a progressive failure analysis to predict the failure loads of pin loaded composites.

A large part of the literature published so far on mechanically fastened joints present experimental results on the effect of the dimensions, clearance between the hole and the pin, and the stacking sequence. Several numerical methods have also been investigated to predict failure of pinned joints. Most of them are reviewed in detail by Camanho & Matthews (1997).

Aktaş and Karakuzu (1998) have carried out failure load, failure mode, and propagation of failure in composite plate pinned-joints, both theoretically and experimentally.

Ozbay (1998) has investigated buckling of symmetrically laminated composite plates with semicircular holes by using the finite-element method and applying first-order shear deformation theory.

Aktas and Karakuzu (1999) have carried out a failure analysis of mechanically fastened carbon-fiber reinforced epoxy composite plate of arbitrary orientation. In that work, failure load and failure mode have been analyzed experimentally and numerically using Tsai-Hill and fiber tensile-compressive failure criteria. They found that full bearing strength was developed when E/D and W/D ratios were equal to or greater than 4.

Camanho & Matthews (1999) have developed a 3D finite element model to predict damage progression and strength of mechanically fastened joints in carbon fibre reinforced plastics. To predict the failure mode, Hashin failure criteria has been used and compared with the experimental results.

Dahsin (1999) has investigated thickness effect of pinned joints for composites. He has studied the interaction between the pin diameter and composite thickness. Results show that thick composites with small pins and thin composites with large pins had lower efficiencies for joint stiffness and joint strength than those having similar dimensions between pin diameter and composite thickness.

Pierron and Cerisier (2000) have carried out a numerical and experimental study to determine the stiffness and the bearing strength of bolted woven composite joints. In addition, they have studied for the influence of the clearance.

Dano, Gendron & Piccard (2000) have performed progressive failure analysis of pin loaded composite plate to predict the bearing stress pin displacement curve until joint failure occurs. In that analysis, contact between the pin and the hole, progressive damage, large deformation theory, and a non-linear shear stress–strain relationship have been taken into account.

Okutan, Aslan and Karakuzu (2001) have investigated the failure strength of pin-loaded woven fiber-glass reinforced epoxy laminates experimentally and have observed the effects of changing the with-to-hole diameter (W/D) and the ratio of edge distance to hole diameter (E/D) on the bearing strength of woven laminated composites. They have tested single-hole pin loaded specimens for their tensile response. They have observed failure propagation and failure type on the specimens.

Icten and Karakuzu (2002) have concerned with the prediction and examination of the behaviours of the pin-loaded carbon–epoxy composite plates. The failure mode and bearing strength are investigated numerically and experimentally. Two-dimensional finite element method is used to determine the failure load and failure mode using Hoffman and Hashin criteria.

Icten and Sayman (2003) have investigated failure load and failure mode in an aluminum–glass–epoxy sandwich composite plate, with a circular hole, which is subjected to a traction force by a pin. To evaluate the effects of joint geometry and fiber orientation on the failure strength and failure mode, parametric studies were performed experimentally.

Icten, Okutan and Karakuzu (2003) have investigated mechanical behaviour and damage development of pin-loaded woven glass fiber–epoxy composites,

numerically and experimentally. To verify the numerical predictions of mechanical behaviour, a series of material configurations ($[(0/90)_3]_S$ _ $[(\pm45)_3]_S$) and 20 different geometries.

Sallam (2003) investigated the behavior of notched and finger tight bolted joint in unidirectional carbon fiber reinforced epoxy composites with different diameter/width ratios. He found that, based on the net cross-section area, the composite materials were insensitive to the notch size under static and fatigue loads. The failure mode of the used bolted joint was shear out, where the strength of the bolted joint mainly depends on the size of the contact area between the hole and the bolt.

Khashaba et al. (2005) have investigated the influence of certain factors on the strength of bolted joints in $[0/\pm45/90]_s$ glass fiber reinforced epoxy (GFRE) composites. These factors were including the tightening torque and the washer outer diameter size. The mechanical properties (tensile, compressive, and in-plane shear) of GFRE laminates have been determined experimentally and theoretically. The experimental results showed that under the same tightening torque, the slope of load–displacement diagrams of bolted joints (stiffness) increased with decreasing washer size.

Aktaş (2005) has carried out static and dynamic experimental studies to investigate both the static and dynamic bearing strengths of a pinned-joint carbon epoxy composite plate with $[0°/45°/-45°/90°]_s$ and $[90°/45°/-45°/0°]_s$ stacking configurations. The experiments showed that the static bearing strengths reach their upper limit when E/D and W/D ratios are equal to or greater than 4 for both [0°/ 45°/-45°/90°]s and [90°/45°/-45°/0°]s stacking sequences. The fatigue strength, on the other hand, reduced by up to 65% as E/D and W/D ratios increased for both stacking configurations.

Karakuzu et al. (2006)a have studied the bearing strength, failure mode and failure load in a woven laminated glass-vinylester composite plate with circular hole subjected to a traction force by a rigid pin. These are investigated for two variables; the distance from the free edge of the plate-to-the diameter of the hole (E/D) ratio (1, 2, 3, 4, 5), and the width of rectangular plate-to-the diameter of the hole (W/ D) ratio

(2, 3, 4, 5), numerically and experimentally. Hashin failure criteria is used in the failure analysis.

Karakuzu et al. (2006)b have performed experimental and numerical study on the bearing strength, failure load and failure mode of pin loaded woven kevlar-epoxy plate was presented. In numerical study, Hashin, Hoffman and Maximum Stress failure criteria were used to predict the failure load and failure mode. Experimental results concerning damage progression and ultimate strength of the joint were obtained and compared with these predictions. To develop the full bearing strength the critical values of in-plane geometric parameters were investigated. In parametric studies, one of the variables was changed while the others are constant. It was seen that the results obtained numerically and experimentally are close to each other.

Wang et al. (2006) has carried out an experimental investigation to understand the bearing strength of stitched and unstitched uniweave T300/QY9512 laminates with single-lap single-bolt joint configuration. The objectives of the studies are to determine the effects of stitching node position, stacking sequence, and hygrothermal environment on the bearing strength and the load–displacement curves of stitched laminates. A three-dimensional finite element model is developed to investigate the bearing properties of mechanically fastened joints in unstitched and stitched laminates. Hashin's three-dimensional failure criterion is used to predict the progressive ply failure. The results showed that the bearing strength decreased when the stitching node position was close to the hole boundary.

The objective of this research is to study the failure behavior and investigate the effect of different geometries and different ply orientations of glass-epoxy laminated composite plate which is subjected to traction force by 4 rigid pins. The numerical and experimental studies implemented with particular attention given to the sensitivity of the model to different geometric dimensions. The three-dimensional finite element method was used to obtain stress distribution of the material. During the study “Hashin Failure Criteria” has been selected to determine the “Failure Mode” and the “Failure Load”. The mechanical properties of the composite material were obtained from the standard test methods.

# CHAPTER TWO

# INTRODUCTION TO COMPOSITE MATERIALS

## 2.1 Definition & Background

A composite material is made by combining two or more materials to give a unique combination of properties. The above definition is more general and can include metals alloys, plastic co-polymers, minerals, and wood. Fiber-reinforced composite materials differ from the above materials in that the constituent materials are different at the molecular level and are mechanically separable. In bulk form, the constituent materials work together but remain in their original forms. The final properties of composite materials are better than constituent material properties.

The concept of composites was not invented by human beings; it is found in nature. An example is wood, which is a composite of cellulose fibers in a matrix of natural glue called lignin. The shell of invertebrates, such as snails and oysters, is an example of a composite. Such shells are stronger and tougher than man-made advanced composites. Scientists have found that the fibers taken from a spider's web are stronger than synthetic fibers. In India, Greece, and other countries, husks or straws mixed with clay have been used to build houses for several hundred years. Mixing husk or sawdust in a clay is an example of a particulate composite and mixing straws in a clay is an example of a shortfiber composite. These reinforcements are done to improve performance.

The main concept of a composite is that it contains matrix materials. Typically, composite material is formed by reinforcing fibers in a matrix resin as shown in Figure 2.1. The reinforcements can be fibers, particulates, or whiskers, and the matrix materials can be metals, plastics, or ceramics.

The reinforcements can be made from polymers, ceramics, and metals. The fibers can be continuous, long, or short. Composites made with a polymer matrix have become more common and are widely used in various industries. They can be thermoset or thermoplastic resins.

The reinforcing fiber or fabric provides strength and stiffness to the composite, whereas the matrix gives rigidity and environmental resistance. Reinforcing fibers are found in different forms, from long continuous fibers to woven fabric to short chopped fibers and mat. Each configuration results in different properties. The properties strongly depend on the way the fibers are laid in the composites. All of the above combinations or only one form can be used in a composite. The important thing to remember about composites is that the fiber carries the load and its strength is greatest along the axis of the fiber. Long continuous fibers in the direction of the load result in a composite with properties far exceeding the matrix resin itself. The same material chopped into short lengths yields lower properties than continuous fibers, as illustrated in Figure 2.2. Depending on the type of application (structural or nonstructural) and manufacturing method, the fiber form is selected. For structural applications, continuous fibers or long fibers are recommended; whereas for nonstructural applications, short fibers are recommended. Injection and compression molding utilize short fibers, whereas filament winding, pultrusion, and roll wrapping use continuous fibers.

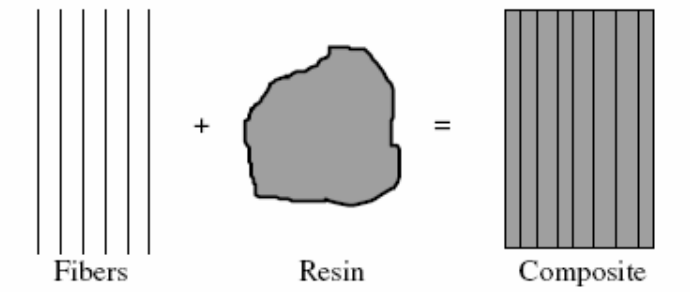



Figure 2.1 Formation of a composite material using fibers and resin.

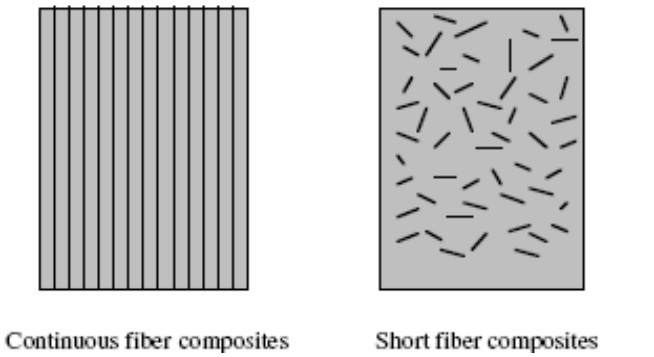



Figure 2.2 Continuous fiber and short fiber composites.

## 2.2 Classification of Composite Materials

It's known that composites have two (or more) chemically distinct phases on a microscopic scale, separated by a distinct interface, and it is important to be able to specify these constituents. The constituent that is continuous and is often, but not always, present in the greater quantity in the composite is termed the matrix. The normal view is that it is the properties of the matrix. That is improved upon when incorporating another constituent to produce a composite. A composite may have a ceramic, metallic or polymeric matrix. The mechanical properties of these classes of material differ considerably. As a generalization, polymers have low strengths and Young's moduli, ceramics are strong, stiff and brittle, and metals have intermediate strengths and moduli, together with good ductilities, i.e. they are not brittle.

The second constituent is known to as the reinforcing phase, or reinforcement, as it enhances or reinforces the mechanical properties of the matrix. In most cases the reinforcement is harder, stronger and stiffer than the matrix, although there are some exceptions; for example, ductile metal reinforcement in a ceramic matrix and rubberlike reinforcement in a brittle polymer matrix. At least one of the dimensions of the reinforcement is small, say less than 500 μm and sometimes only of the order of a micrometer. The geometry of the reinforcing phase is one of the major parameters in determining he effectiveness of the reinforcement; in other words, the mechanical properties of composites are a function of the shape and dimensions of the reinforcement. We usually describe the reinforcement as being either fibrous or particulate. Figure 2.3 represents a commonly employed classification scheme for composite materials which utilizes this designation for the reinforcement (Fig. 2.3 - Block A)

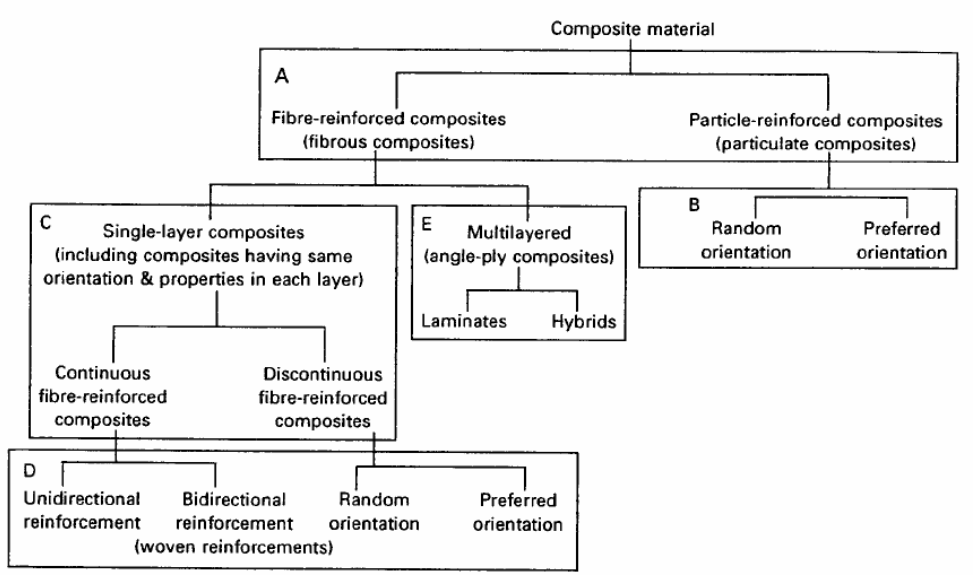



Figure 2.3 Classification of Composite Materials

Particulate reinforcements have dimensions that are approximately equal in all directions the shape of the reinforcing particles may be spherical, cubic, platelet or any regular or irregular geometry. The arrangement of the particulate reinforcement may be random or with a preferred orientation, and this characteristic is also used as a part of the classification scheme (Fig 2.3 Block B). In the majority of particulate-reinforced composites the orientation of the particles is considered, for practical purposes, to be random.

A fibrous reinforcement is characterized y its length being much greater than its cross-section dimensions. However, the ratio of length to a cross-section dimension, known as the aspect ratio, can vary considerably. In single-layer composites long fibres with high aspect ratios give what are called continuous fibre-reinforced composites, whereas discontinuous fibre composites are fabricated using short fibres of low aspect ratio (Fig 2.3 Block C). The orientation of the discontinuous fibres may be random or preferred. The frequently encountered preferred orientation in the case of a continuous fibre composite is termed unidirectional and the corresponding random situation can be approximated to by bidirectional woven reinforcement (Fig 2.3 Block D).

Multilayered composites are another category, and commonly used form, of fibre-reinforced composites. These are classified as either laminates or hybrids (Fig 2.3 Block E). Laminates are sheet constructions which are made by stacking layers (also called plies or laminae and usually unidirectional) in a specified sequence. The layers are often in the form of 'prepreg' (fibres pre-impregnated with partly cured resin) which are consolidated in an autoclave. A laminate may have between 4 and 400 layers and the fibre orientation changes from layer to layer in a regular manner through the thickness of the laminate, e.g. a 0/90/0 stacking sequence results in a cross-ply composite.

Hybrids are composites with mixes fibres and are becoming commonplace. The fibres may be mixed within a ply or layer by layer, and these composites are designed to benefit from the different properties of the fibres employed. For example, a mixture of glass and carbon fibres incorporated into a polymer matrix gives a relatively inexpensive composite, owing to the low cost of glass fibres, but with mechanical properties enhanced by the excellent stiffness of carbon.

### 2.3 The Matrix and Reinforcement

Most composites are designed to exploit an improvement in mechanical properties. Even for composites produced essentially for their physical properties, the mechanical properties can play an important role during component manufacture and service. The strengths of fibres are generally much higher than those of their monolithic counterparts owing to the presence of defects in the latter.

There are of course many properties other than strength that should be taken into account when selecting a reinforcement. In the case of fibres the flexibility is important as it determines whether the fibers may be easily woven or not, and influences the choice of method for composite manufacture. The flexibility of a fibre depends on Young's modulus and the diameter of the fibre, decreasing as diameter increases.

Clearly, single fibres, because of their small cross-section dimensions, are not directly usable in structural applications. This problem may be overcome by embedding the fibres in a material to hold the fibres apart, to protect the surface of the fibres, and to facilitate the production of components. The embedding material is

the matrix. The amount of reinforcement that can be incorporated in a given matrix is limited by a number of factors. For example with particulate-reinforced metals the reinforcement content is usually kept to less than 40 vol% (0.4 volume fraction) owing to processing difficulties and increasing brittleness at higher contents. On the other hand, the processing methods for fibre-reinforced polymers are capable of producing composites with a high proportion of fibres, and the upper limit of about 70 vol% (0.7 volume fraction) is set by the need to avoid fibre-fibre contact, which results in fibre damage.

Finally the fact that the reinforcement is bonded to the matrix means that any loads applies to a composite are carried by both constituents. As in most cases the reinforcement is the stiffer and stronger constituent, it is the principal load-bearer. The matrix is said to have transferred the load to the reinforcement.

### 2.4 Functions of Fibers and Matrix

A composite material is formed by reinforcing plastics with fibers. To develop a good understanding of composite behavior, one should have a good knowledge of the roles of fibers and matrix materials in a composite. The important functions of fibers and matrix materials are discussed below.

The main functions of the fibers in a composite are:

- To carry the load. In a structural composite, 70 to 90% of the load is carried by fibers.
- To provide stiffness, strength, thermal stability, and other structural properties in the composites.
- To provide electrical conductivity or insulation, depending on the type of fiber used.

A matrix material fulfills several functions in a composite structure, most of which are vital to the satisfactory performance of the structure. Fibers in and of themselves are of little use without the presence of a matrix material or binder. The important functions of a matrix material include the following:

- The matrix material binds the fibers together and transfers the load to the fibers. It provides rigidity and shape to the structure.

- The matrix isolates the fibers so that individual fibers can act separately. This stops or slows the propagation of a crack.

- The matrix provides a good surface finish quality and aids in the production of net-shape or near-net-shape parts.

- The matrix provides protection to reinforcing fibers against chemical attack and mechanical damage (wear).

- Depending on the matrix material selected, performance characteristics such as ductility, impact strength, etc. are also influenced. A ductile matrix will increase the toughness of the structure. For higher toughness requirements, thermoplastic-based composites are selected.

- The failure mode is strongly affected by the type of matrix material used in the composite as well as its compatibility with the fiber.

**2.5 Special Features of Composites**

Composites have been routinely designed and manufactured for applications in which high performance and light weight are needed. They offer several advantages over traditional engineering materials as discussed below.

- Composite materials provide capabilities for part integration. Several metallic components can be replaced by a single composite component.

- Composite structures provide in-service monitoring or online process monitoring with the help of embedded sensors. This feature is used to monitor fatigue damage in aircraft structures or can be utilized to monitor the resin flow in an RTM (resin transfer molding) process. Materials with embedded sensors are known as “smart” materials.

- Composite materials have a high specific stiffness (stiffness-to-density ratio). Composites offer the stiffness of steel at one fifth the weight and equal the stiffness of aluminum at one half the weight.

♦ The specific strength (strength-to-density ratio) of a composite material is very high. Due to this, airplanes and automobiles move faster and with better fuel efficiency. The specific strength is typically in the range of 3 to 5 times that of steel and aluminum alloys. Due to this higher specific stiffness and strength, composite parts are lighter than their counterparts.

♦ The fatigue strength (endurance limit) is much higher for composite materials. Steel and aluminum alloys exhibit good fatigue strength up to about 50% of their static strength. Unidirectional carbon/epoxy composites have good fatigue strength up to almost 90% of their static strength.

♦ Composite materials offer high corrosion resistance. Iron and aluminum corrode in the presence of water and air and require special coatings and alloying. Because the outer surface of composites is formed by plastics, corrosion and chemical resistance are very good.

♦ Composite materials offer increased amounts of design flexibility. For example, the coefficient of thermal expansion (CTE) of composite structures can be made zero by selecting suitable materials and lay-up sequence. Because the CTE for composites is much lower than for metals, composite structures provide good dimensional stability.

♦ Net-shape or near-net-shape parts can be produced with composite materials. This feature eliminates several machining operations and thus reduces process cycle time and cost.

♦ Complex parts, appearance, and special contours, which are sometimes not possible with metals, can be fabricated using composite materials without welding or riveting the separate pieces. This increases reliability and reduces production times. It offers greater manufacturing feasibility.

♦ Composite materials offer greater feasibility for employing design for manufacturing (DFM) and design for assembly (DFA) techniques. These techniques help minimize the number of parts in a product and thus reduce assembly and joining time. By eliminating joints, high-strength structural parts

can be manufactured at lower cost. Cost benefit comes by reducing the assembly time and cost.

♦ Composites offer good impact properties, as shown in Figures 2.4 and 2.5. Figure 2.4 shows impact properties of aluminum, steel, glass/epoxy, kevlar/epoxy, and carbon/epoxy continuous fiber composites. Glass and Kevlar composites provide higher impact strength than steel and aluminum. Figure 2.5 compares impact properties of short and long glass fiber thermoplastic composites with aluminum and magnesium. Among thermoplastic composites, impact properties of long glass fiber nylon 66 composite (NylonLG60) with 60% fiber content, short glass fiber nylon 66 composite (NylonSG40) with 40% fiber content, long glass fiber polypropylene composite (PPLG40) with 40% fiber content, short glass fiber polypropylene composite (PPSG40) with 40% fiber content, long glass fiber PPS composite (PPSLG50) with 50% fiber content, and long glass fiber polyurethane composite (PULG60) with 60% fiber content are described. Long glass fiber provides three to four times improved impact properties than short glass fiber composites.

♦ Noise, vibration, and harshness (NVH) characteristics are better for composite materials than metals. Composite materials dampen vibrations an order of magnitude better than metals. These characteristics are used in a variety of applications, from the leading edge of an airplane to golf clubs.

♦ By utilizing proper design and manufacturing techniques, cost-effective composite parts can be manufactured. Composites offer design freedom by tailoring material properties to meet performance specifications, thus avoiding the over-design of products. This is achieved by changing the fiber orientation, fiber type, and/or resin systems.

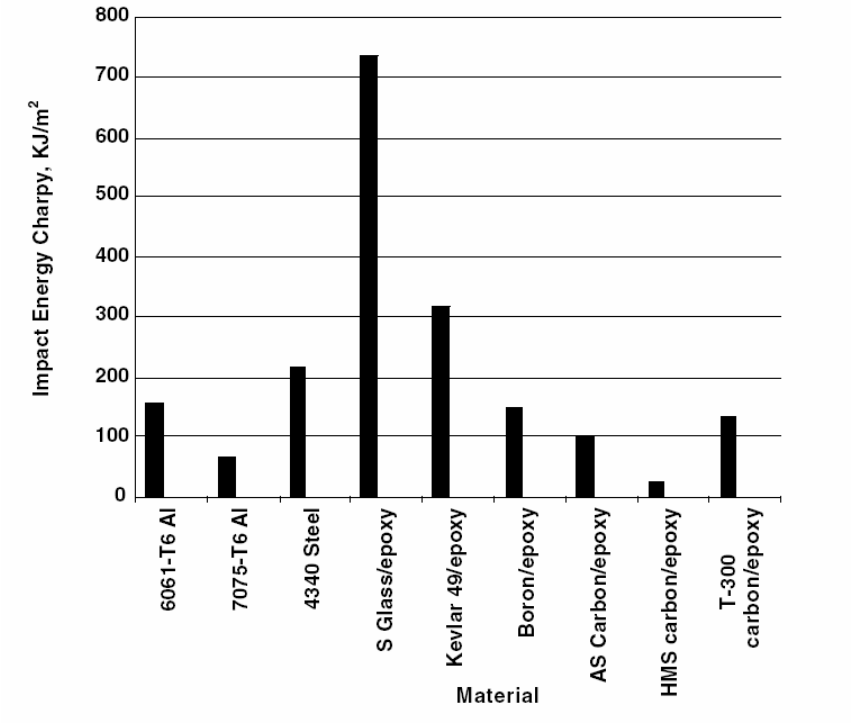



Figure 2.4 Impact properties of various engineering materials. Unidirectional composite materials with about 60% fiber volume fraction are used.

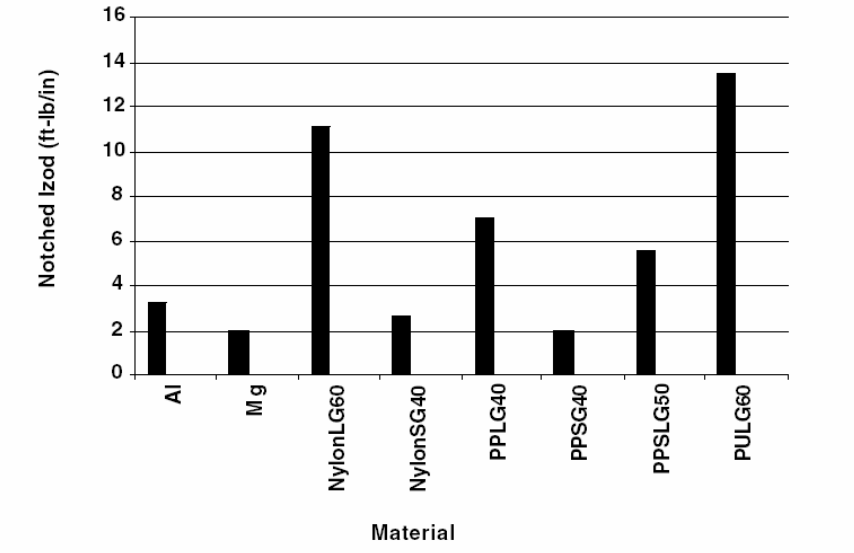



Figure 2.5 Impact properties of long glass (LG) and short glass (SG) fibers reinforced thermoplastic composites. Fiber weight percent is written at the end in two digits.

- Glass-reinforced and aramid-reinforced phenolic composites meet FAA and JAR requirements for low smoke and toxicity. This feature is required for aircraft interior panels, stow bins, and galley walls.

- The cost of tooling required for composites processing is much lower than that for metals processing because of lower pressure and temperature requirements. This offers greater flexibility for design changes in this competitive market where product lifetime is continuously reducing.

### 2.6 Drawbacks of Composites

Although composite materials offer many benefits, they suffer from the following disadvantages:

- The materials cost for composite materials is very high compared to that of steel and aluminum. It is almost 5 to 20 times more than aluminum and steel on a weight basis. For example, glass fiber costs $1.00 to $8.00/lb; carbon fiber costs $8 to $40/lb; epoxy costs $1.50/lb; glass/epoxy prepreg costs $12/lb; and carbon/epoxy prepreg costs $12 to $60/lb. The cost of steel is $0.20 to $1.00/lb and that of aluminum is $0.60 to $1.00/lb.

- In the past, composite materials have been used for the fabrication of large structures at low volume (one to three parts per day). The lack of high-volume production methods limits the widespread use of composite materials. Recently, pultrusion, resin transfer molding (RTM), structural reaction injection molding (SRIM), compression molding of sheet molding compound (SMC), and filament winding have been automated for higher production rates. Automotive parts require the production of 100 to 20,000 parts per day. For example, Corvette volume is 100 vehicles per day, and Ford-Taurus volume is 2000 vehicles per day. Steering system companies such as Delphi Saginaw Steering Systems and TRW produce more than 20,000 steering systems per day for various models. Sporting good items such as golf shafts are produced on the order of 10,000 pieces per day.

- Classical ways of designing products with metals depend on the use of machinery and metals handbooks, and design and data handbooks. Large design

databases are available for metals. Designing parts with composites lacks such books because of the lack of a database.

♦ The temperature resistance of composite parts depends on the temperature resistance of the matrix materials. Because a large proportion of composites uses polymer-based matrices, temperature resistance is limited by the plastics' properties. Average composites work in the temperature range –40 to +100°C. The upper temperature limit can range between +150 and +200°C for high-temperature plastics such as epoxies, bismaleimides, and PEEK. Table 2.1 shows the maximum continuous-use temperature for various polymers.

♦ Solvent resistance, chemical resistance, and environmental stress cracking of composites depend on the properties of polymers. Some polymers have low resistance to solvents and environmental stress cracking.

♦ Composites absorb moisture, which affects the properties and dimensional stability of the composites.

Table 2.1 Maximum Continuous-Use Temperatures for Various Thermosets and Thermoplastics

| **Materials** | **Maximum Continuous-Use Temperature (°C)** |
|---|---|
| Thermosets | |
| Vinylester | 60–150 |
| Polyester | 60–150 |
| Phenolics | 70–150 |
| Epoxy | 80–215 |
| Cyanate esters | 150–250 |
| Bismaleimide | 230–320 |
| Thermoplastics | |
| Polyethylene | 50–80 |
| Polypropylene | 50–75 |
| Acetal | 70–95 |
| Nylon | 75–100 |
| Polyester | 70–120 |
| PPS | 120–220 |
| PEEK | 120–250 |
| Teflon | 200–260 |

## 2.7 Composites Markets

There are many reasons for the growth in composite applications, but the primary impetus is that the products fabricated by composites are stronger and lighter. Today, it is difficult to find any industry that does not utilize the benefits of composite materials. The largest user of composite materials today is the transportation industry, having consumed 1.3 billion pounds of composites in 2000. Composite materials have become the materials of choice for several industries.

In the past three to four decades, there have been substantial changes in technology and its requirement. This changing environment created many new needs and opportunities, which are only possible with the advances in new materials and their associated manufacturing technology.

In the past decade, several advanced manufacturing technology and material systems have been developed to meet the requirements of the various market segments. Several industries have capitalized on the benefits of composite materials. The vast expansion of composite usage can be attributed to the decrease in the cost of fibers, as well as the development of automation techniques and high-volume production methods. For example, the price of carbon fiber decreased from $150.00/lb in 1970 to about $8.00/lb in 2000. This decrease in cost was due to the development of low-cost production methods and increased industrial use.

Broadly speaking, the composites market can be divided into the following industry categories: aerospace, automotive, construction, marine, corrosion resistant equipment, consumer products, appliance/business equipment, and others. U.S. composite shipments in the above markets are shown in Figure 2.6 for the years 1999 and 2000 (projected).

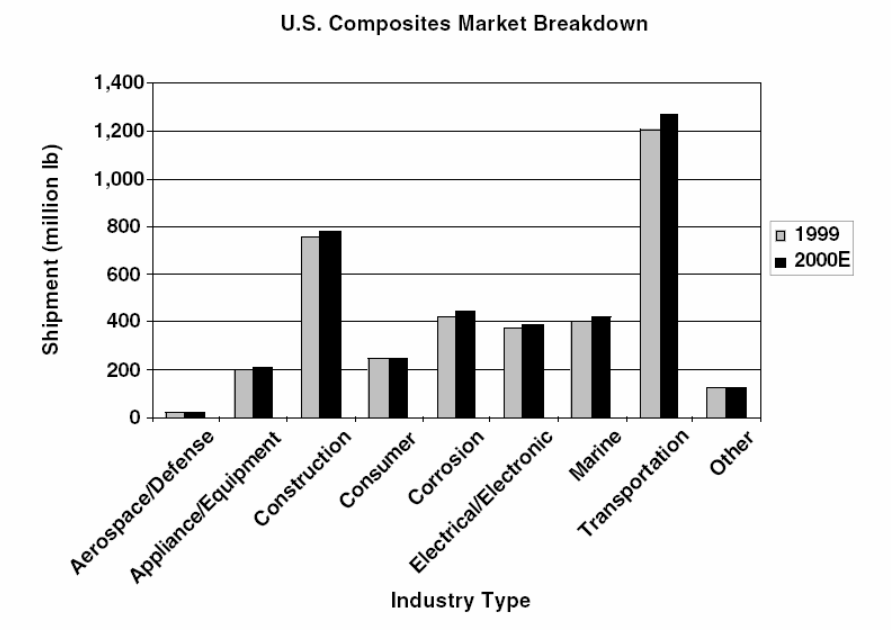



Figure 2.6 Composite shipments in various industries in 1999 and those projected for 2000.

### *2.7.1 The Aerospace Industry*

The aerospace industry was among the first to realize the benefits of composite materials. Airplanes, rockets, and missiles all fly higher, faster, and farther with the help of composites. Glass, carbon, and Kevlar fiber composites have been routinely designed and manufactured for aerospace parts. The aerospace industry primarily uses carbon fiber composites because of their high-performance characteristics. The hand lay-up technique is a common manufacturing method for the fabrication of aerospace parts; RTM and filament winding are also being used.

In 1999, the aerospace industry consumed 23 million pounds of composites, as shown in Figure 2.7. Military aircrafts, such as the F-11, F-14, F-15, and F-16, use composite materials to lower the weight of the structure. The composite components used in the above-mentioned fighter planes are horizontal and vertical stabilizers, wing skins, fin boxes, flaps, and various other structural components as shown in Table 2.2. Typical mass reductions achieved for the above components are in the range of 20 to 35%. The mass saving in fighter planes increases the payload capacity as well as the missile range.

Figure 2.7.a, Figure 2.7.b and Figure 2.7.c show the typical composite structures used in commercial aircraft and Figure 2.8.a and Figure 2.8.b shows the typical composite structures used in military aircraft. Composite components used in engine and satellite applications are shown in Figures 2.9 and 2.10, respectively.

Table 2.2 Composite Components in Aircraft Applications

| **Composite Components** | |
|---|---|
| F-14 | Doors, horizontal tails, fairings, stabilizer skins |
| F-15 | Fins, rudders, vertical tails, horizontal tails, speed brakes, stabilizer skins |
| F-16 | Vertical and horizontal tails, fin leading edge, skins on vertical fin box |
| B-1 | Doors, vertical and horizontal tails, flaps, slats, inlets |
| AV-8B | Doors, rudders, vertical and horizontal tails, ailerons, flaps, fin box, fairings |
| Boeing 737 | Spoilers, horizontal stabilizers, wings |
| Boeing 757 | Doors, rudders, elevators, ailerons, spoilers, flaps, fairings |
| Boeing 767 | Doors, rudders, elevators, ailerons, spoilers, fairings |

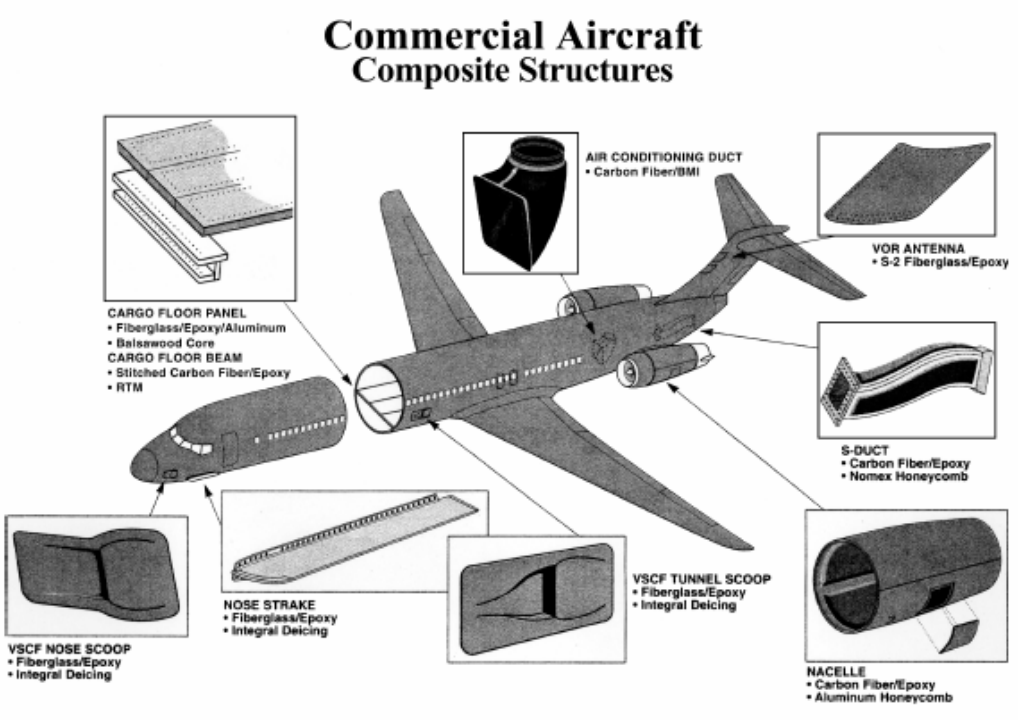



Figure 2.7.a Typical composite structures used in commercial aircraft.

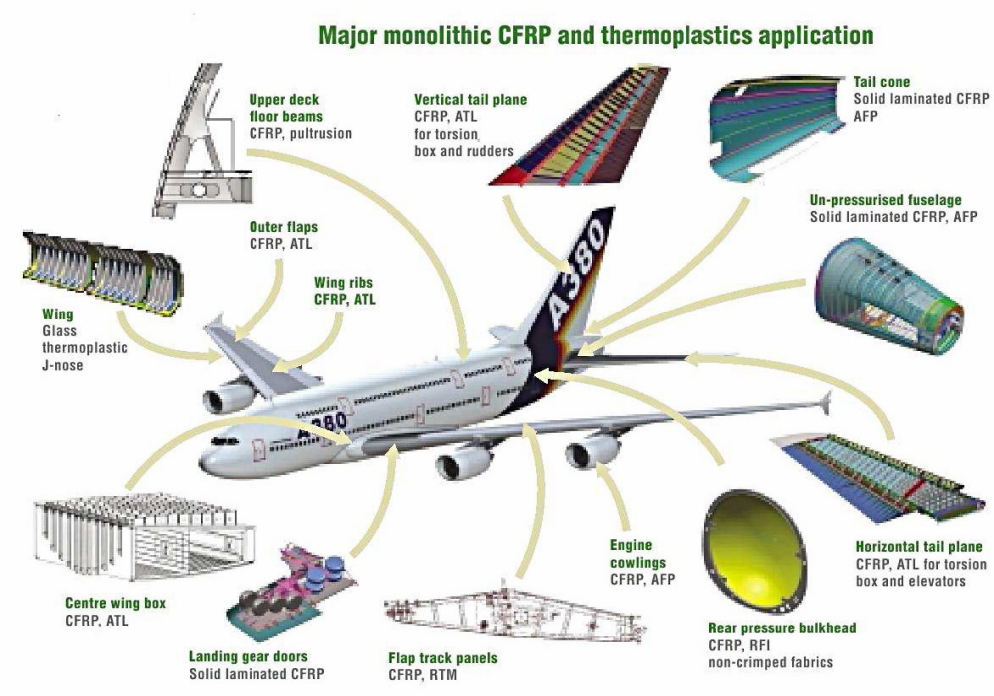



Figure 2.7.b Major composite parts on the Airbus A380.

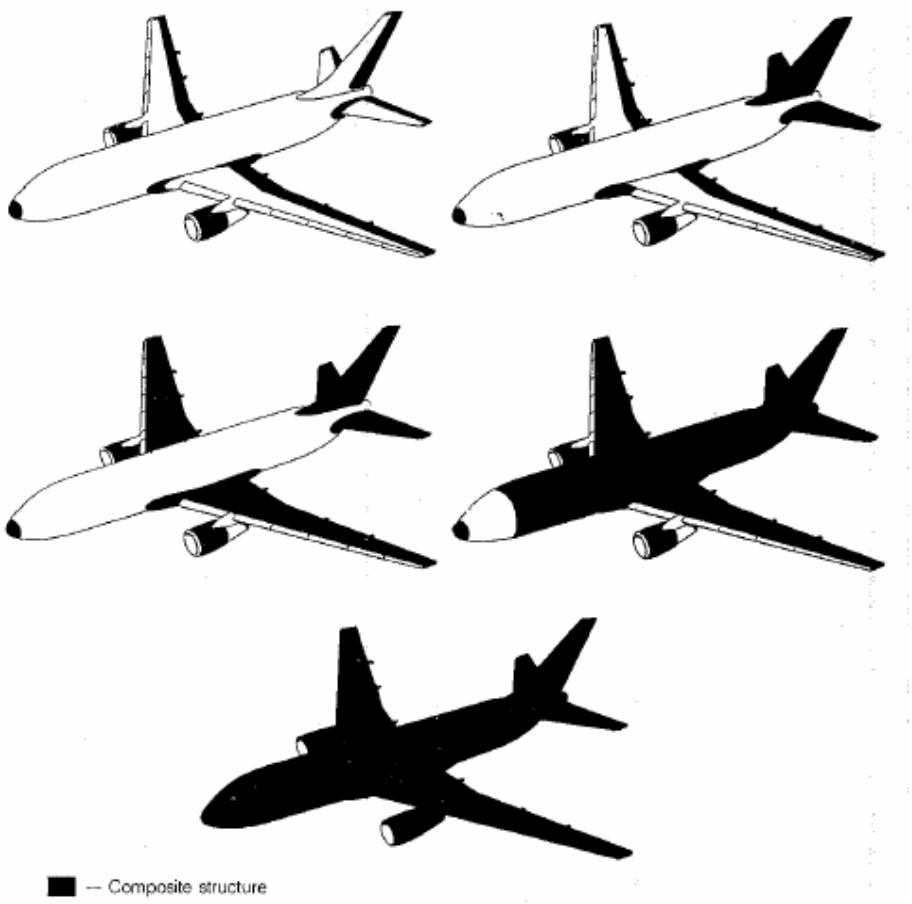



Figure 2.7.c The progressive use of composites on commercial transport airframes

The major reasons for the use of composite materials in spacecraft applications include weight savings as well as dimensional stability. In low Earth orbit (LEO), where temperature variation is from –100 to +100°C, it is important to maintain dimensional stability in support structures as well as in reflecting members. Carbon epoxy composite laminates can be designed to give a zero coefficient of thermal expansion. Typical space structures are tubular truss structures, face sheets for the payload bay door, antenna reflectors, etc. In space shuttle composite materials provide weight savings of 2688 lb per vehicle.

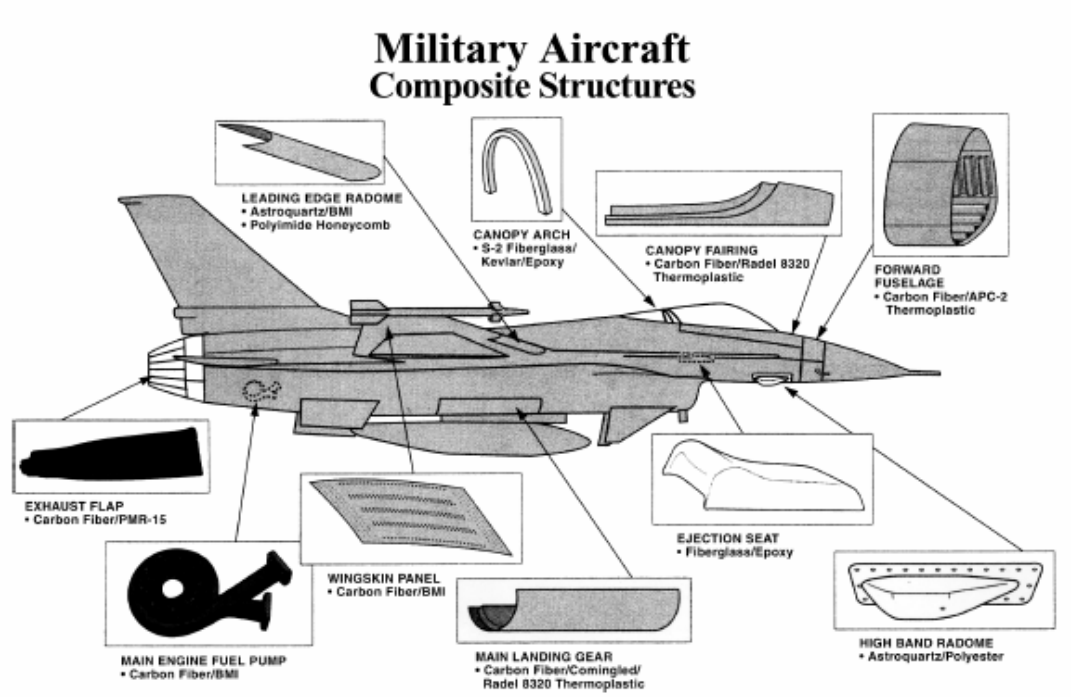



Figure 2.8.a Typical composite structures used in military aircraft

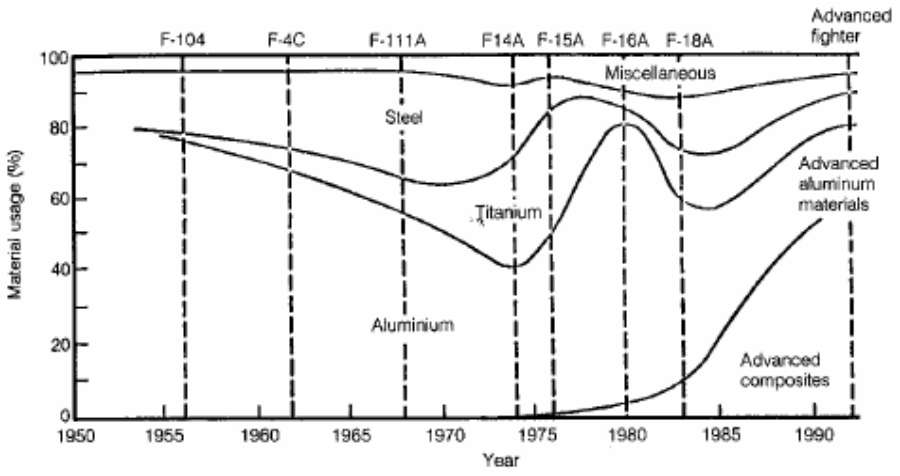



Figure 2.8.b Progress in using composite materials on military fighter aircraft

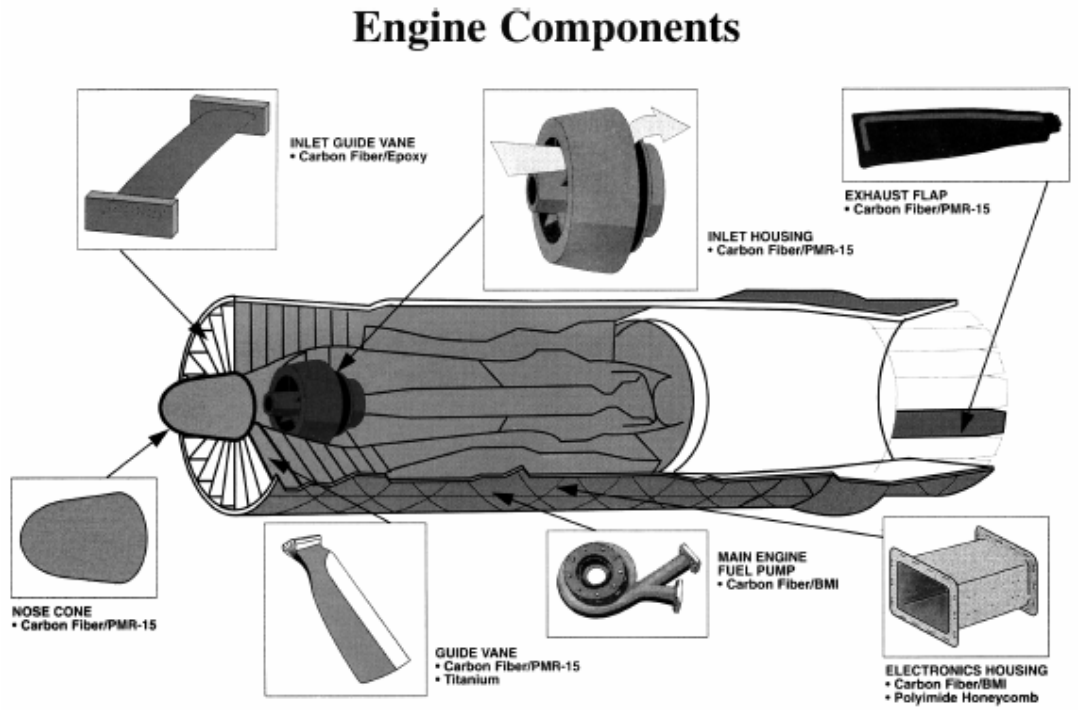



Figure 2.9 Composite components used in engine applications

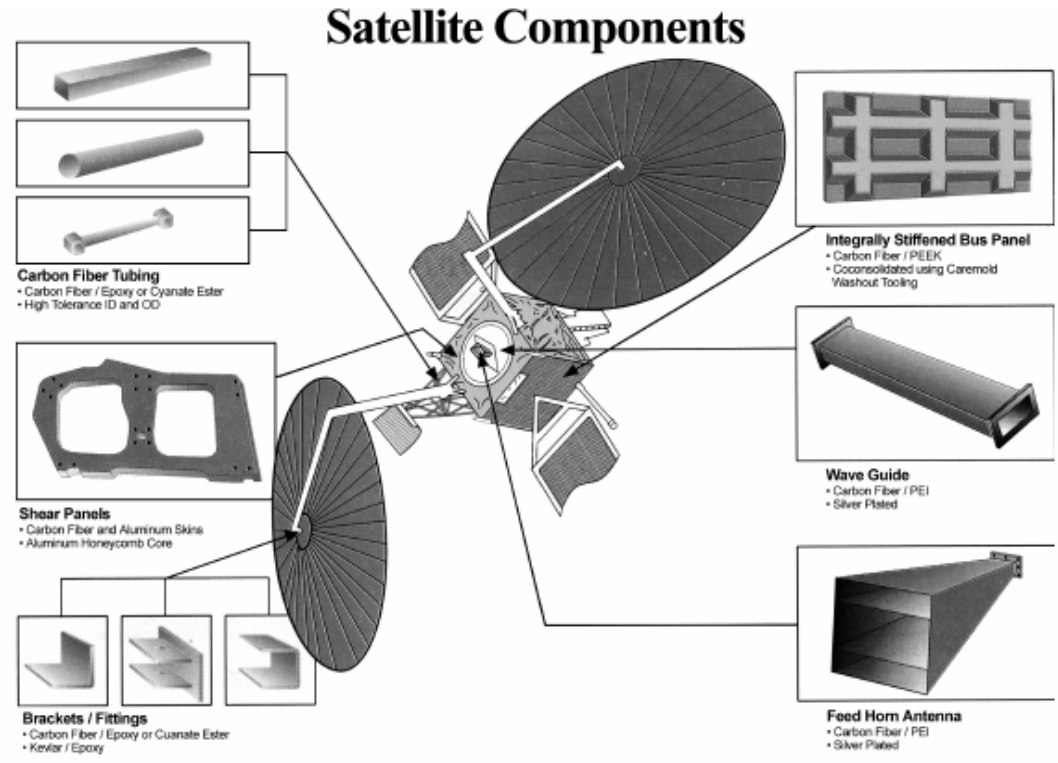



Figure 2.10 Composite components used in satellite applications

Passenger aircrafts such as the Boeing 747 and 767 use composite parts to lower the weight, increase the payload, and increase the fuel efficiency. The components made out of composites for such aircrafts are shown in Table 2.2

### *2.7.2 The Automotive Industry*

Composite materials have been considered the “material of choice” in some applications of the automotive industry by delivering high-quality surface finish, styling details, and processing options. Manufacturers are able to meet automotive requirements of cost, appearance, and performance utilizing composites. Today, composite body panels have a successful track record in all categories — from exotic sports cars to passenger cars to small, medium, and heavy truck applications. In 2000, the automotive industry used 318 million pounds of composites.

Because the automotive market is very cost-sensitive, carbon fiber composites are not yet accepted due to their higher material costs. Automotive composites utilize glass fibers as main reinforcements. Table 2.3 provides a breakdown of automotive composite usage by applications, matrix materials, and manufacturing methods.



Figure 2.11 Composite applications in automotive industry

Table 2.3 Average use of composites in automobiles per year, 1988-1993

| **Applications** | **Usage (kg x 106)** | **Matrix Material** | **Usage (kg x 106)** | **Manufacturing Process** | **Usage (kg x 106)** |
|---|---|---|---|---|---|
| Bumper beam | 42 | Polyester (TS) | 42 | SMC (comp. mold) | 40 |
| Seat/load floor | 14 | Polypropylene | 22 | GMT (comp. mold) | 20 |
| Hood | 13 | Polycarbonate/PBT | 10 | Injection molding | 13 |
| Radiator support | 4 | Polyethylene | 4 | Ext. blow mold | 5 |
| Roof panel | 4 | Epoxy | 4 | Filament wound | 3 |
| Other | 11 | Other | 7 | Other | 8 |
| Total | 89 | Total | 89 | Total | 89 |

### *2.7.3 The Sporting Goods Industry*

Sports and recreation equipment suppliers are becoming major users of composite materials. The growth in structural composite usage has been greatest in high-performance sporting goods and racing boats. Anyone who has visited a sporting goods store can see products such as golf shafts, tennis rackets, snow skis, fishing rods, etc. made of composite materials. These products are light in weight and provide higher performance, which helps the user in easy handling and increased comfort.

### *2.7.4 Marine Applications*

Composite materials are used in a variety of marine applications such as passenger ferries, power boats, buoys, etc. because of their corrosion resistance and light weight, which gets translated into fuel efficiency, higher cruising speed, and portability. The majority of components is made of glass-reinforced plastics (GRP) with foam and honeycomb as core materials. About 70% of all recreational boats are made of composite materials according to a 361-page market report on the marine industry. According to this report total annual domestic boat shipments in the United States was $8.85 billion and total composite shipments in the boating industry worldwide is estimated as 620 million lbs in 2000.

Composites are also used in offshore pipelines for oil and gas extractions. The motivation for the use of GRP materials for such applications includes reduced

handling and installation costs as well as better corrosion resistance and mechanical performance. Another benefit comes from the use of adhesive bonding, which minimizes the need for a hot work permit if welding is employed.

### *2.7.5 Consumer Goods*

Composite materials are used for a wide variety of consumer good applications, such as sewing machines, doors, bathtubs, tables, chairs, computers, printers, etc. The majority of these components are short fiber composites made by molding technology such as compression molding, injection molding, RTM, and SRIM.

### *2.7.6 Construction and Civil Structures*

The construction and civil structure industries are the second major users of composite materials. Construction engineering experts and engineers agree that the U.S. infrastructure is in bad shape, particularly the highway bridges. Some 42% of this nation's bridges need repair and are considered obsolete, according to Federal Highway Administration officials. The federal government has budgeted approximately $78 billion over the next 20 years for major infrastructure rehabilitation. The driving force for the use of glass-and carbon-reinforced plastics for bridge applications is reduced installation, handling, repair, and life-cycle costs as well as improved corrosion and durability. It also saves a significant amount of time for repair and installation and thus minimizes the blockage of traffic. Composite usage in earthquake and seismic retrofit activities is also booming. The columns wrapped by glass/epoxy, carbon/epoxy, and aramid/epoxy show good potential for these applications.

### *2.7.7 Industrial Applications*

The use of composite materials in various industrial applications is growing. Composites are being used in making industrial rollers and shafts for the printing industry and industrial drive shafts for cooling-tower applications. Filament winding shows good potential for the above applications. Injection molded, short fiber composites are used in bushings, pump and roller bearings, and pistons. Composites are also used for making robot arms and provide improved stiffness, damping, and response time.

## 2.8 Barriers in Composite Markets

The primary barrier to the use of composite materials is their high initial costs in some cases, as compared to traditional materials. Regardless of how effective the material will be over its life cycle, industry considers high upfront costs, particularly when the life-cycle cost is relatively uncertain. This cost barrier inhibits research into new materials. In general, the cost of processing composites is high, especially in the hand lay-up process. Here, raw material costs represent a small fraction of the total cost of a finished product. There is already evidence of work moving to Asia, Mexico, and Korea for the cases where labor costs are a significant portion of the total product costs. The recycling of composite materials presents a problem when penetrating a high-volume market such as the automotive industry, where volume production is in the millions of parts per year. With the new government regulations and environmental awareness, the use of composites has become a concern and poses a big challenge for recycling. (Matthews et al., 2000), (Mazumdar, 2002), (Chun, 2002)

# CHAPTER THREE

# STRUCTURAL ANALYSIS OF COMPOSITE MATERIALS

## 3.1 Classical Analysis

The use of classical (continuum) methods of stress analysis has developed over many decades to give techniques that can be applied satisfactorily to a vast range of situations. Such analyses are based on the application of the equations of equilibrium and compatibility, together with the stress-strain relations for the material, to produce governing equations which must be solved to obtain displacements and stresses. Usually, assumptions must be made before a solution can be affected. So, for example, problems are considered as one-or two-dimensional, as when considering beams and plates, respectively. Often we take the material to be isotropic, but many analyses also exist for anisotropic materials.

When calculated the mechanical properties of composites it is convenient to start by considering a composite in which all the fibres are aligned in one direction (i.e. a unidirectional composite). This basic 'building block' can then be used to predict the behaviour of continuous fibre multidirectional laminates, as well as short fibre, non-aligned systems.

The essential point about a unidirectional fibre composite is that its stiffness (and strength) are different in different directions. This behaviour contrasts with a metal with a random orientation of grains, or other isotropic material, which has the same elastic properties in all directions.

In a unidirectional composite the fibre distribution implies that the behaviour is essentially isotropic in a cross-section perpendicular to the fibres (Fig. 3.1). In other words, if we were to conduct a mechanical test by applying a stress in the '2' direction or in the '3' direction (both normal to the fibre's longitudinal axis), we would obtain the same elastic properties from each test. We say the material is 'transversely isotropic'. Clearly the properties in the longitudinal ('1') direction are very different from those in the other two directions. We call such a material 'orthotropic'. The elastic properties are symmetric with respect to the chosen (1-2-3) axes, which are usually called the 'principal material axes'.

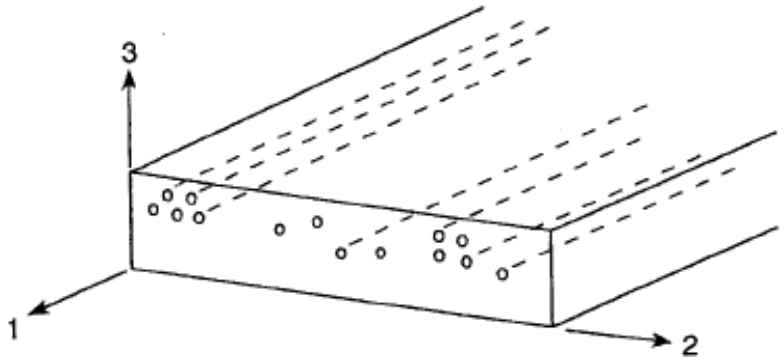



Figure 3.1 Orientation of principal material axes.

### *3.1.1 Basic Stress-Strain Relations*

The stress-strain relations for the unidirectional material can readily be found, provided we take account of the fact that the properties are direction-dependent. Considering the composite illustrated in Fig. 3.1, we see that if the directions of the applied stresses coincide with the principal material axes ('specially orthotropic'), the strains in terms of the stresses are given by

$$\begin{Bmatrix} \varepsilon_1 \\ \varepsilon_2 \\ \varepsilon_3 \\ \gamma_{23} \\ \gamma_{31} \\ \gamma_{12} \end{Bmatrix} = \begin{bmatrix} S_{11} & S_{12} & S_{13} & 0 & 0 & 0 \\ S_{12} & S_{22} & S_{23} & 0 & 0 & 0 \\ S_{13} & S_{23} & S_{33} & 0 & 0 & 0 \\ 0 & 0 & 0 & S_{44} & 0 & 0 \\ 0 & 0 & 0 & 0 & S_{55} & 0 \\ 0 & 0 & 0 & 0 & 0 & S_{66} \end{bmatrix} \begin{Bmatrix} \sigma_1 \\ \sigma_2 \\ \sigma_3 \\ \tau_{23} \\ \tau_{31} \\ \tau_{12} \end{Bmatrix} \tag{3.1}$$

where,

$$S_{11} = \frac{1}{\mathrm{E}_1},\ S_{12} = -\frac{\nu_{12}}{\mathrm{E}_1} = -\frac{\nu_{21}}{\mathrm{E}_2},\ S_{13} = -\frac{\nu_{13}}{\mathrm{E}_1} = -\frac{\nu_{31}}{\mathrm{E}_3},\ S_{23} = -\frac{\nu_{23}}{\mathrm{E}_2} = -\frac{\nu_{32}}{\mathrm{E}_3}$$

$$S_{22} = \frac{1}{\mathrm{E}_2},\ S_{33} = \frac{1}{\mathrm{E}_3},\ S_{44} = \frac{1}{G_{23}},\ S_{55} = \frac{1}{G_{31}},\ S_{66} = \frac{1}{G_{12}} \tag{3.2}$$

The strain-stress relations in Eq. 3.1 can be inverted to obtain the stress-strain relations:

$$\begin{Bmatrix}\sigma_1\\ \sigma_2\\ \sigma_3\\ \tau_{23}\\ \tau_{31}\\ \tau_{12}\end{Bmatrix}=\begin{bmatrix}C_{11} & C_{12} & C_{13} & 0 & 0 & 0\\ C_{12} & C_{22} & C_{23} & 0 & 0 & 0\\ C_{13} & C_{23} & C_{33} & 0 & 0 & 0\\ 0 & 0 & 0 & C_{44} & 0 & 0\\ 0 & 0 & 0 & 0 & C_{55} & 0\\ 0 & 0 & 0 & 0 & 0 & C_{66}\end{bmatrix}\begin{Bmatrix}\varepsilon_1\\ \varepsilon_2\\ \varepsilon_3\\ \gamma_{23}\\ \gamma_{31}\\ \gamma_{12}\end{Bmatrix} \tag{3.3}$$

The stiffness matrix, $C_{ij}$, for an orthotropic material in terms of the engineering constants, is obtained by inversion of the compliance matrix, $S_{ij}$. The stiffness' in Eq. (3.3) are

$$C_{11}=\frac{1-\upsilon_{23}\upsilon_{32}}{\mathrm{E}_2\mathrm{E}_3\Delta},\ C_{22}=\frac{1-\upsilon_{13}\upsilon_{31}}{\mathrm{E}_1\mathrm{E}_3\Delta},\ C_{12}=\frac{\upsilon_{21}+\upsilon_{31}\upsilon_{23}}{\mathrm{E}_2\mathrm{E}_3\Delta}=\frac{\upsilon_{12}+\upsilon_{32}\upsilon_{13}}{\mathrm{E}_1\mathrm{E}_3\Delta}$$

$$C_{23}=\frac{\upsilon_{32}+\upsilon_{12}\upsilon_{31}}{\mathrm{E}_1\mathrm{E}_3\Delta}=\frac{\upsilon_{23}+\upsilon_{21}\upsilon_{13}}{\mathrm{E}_1\mathrm{E}_2\Delta},\ C_{13}=\frac{\upsilon_{31}+\upsilon_{21}\upsilon_{32}}{\mathrm{E}_2\mathrm{E}_3\Delta}=\frac{\upsilon_{13}+\upsilon_{12}\upsilon_{23}}{\mathrm{E}_1\mathrm{E}_2\Delta} \tag{3.4}$$

$$C_{33}=\frac{1-\upsilon_{12}\upsilon_{21}}{\mathrm{E}_1\mathrm{E}_2\Delta},\ C_{44}=G_{23},\ C_{55}=G_{31},\ C_{66}=G_{12}$$

where,

$$\Delta=\frac{1-\upsilon_{12}\upsilon_{21}-\upsilon_{23}\upsilon_{32}-\upsilon_{31}\upsilon_{13}-2\upsilon_{21}\upsilon_{32}\upsilon_{13}}{\mathrm{E}_1\mathrm{E}_2\mathrm{E}_3} \tag{3.5}$$

The principal directions of orthotropy often do not coincide with coordinate directions that are geometrically natural to the solution of the problem. For this reason a method of transforming stress-strain relations from one coordinate system to another is needed.

The principal material axes and θ, is the angle from the *x* axis to 1 axis, are shown in Figure 3.2.

The stress transformations between x-y-z and 1-2-3 are,

$$\begin{Bmatrix}\sigma_{xx}\\ \sigma_{yy}\\ \sigma_{zz}\\ \sigma_{yz}\\ \sigma_{xz}\\ \sigma_{xy}\end{Bmatrix}=\begin{bmatrix}\cos^2\theta & \sin^2\theta & 0 & 0 & 0 & -\sin 2\theta\\ \sin^2\theta & \cos^2\theta & 0 & 0 & 0 & \sin 2\theta\\ 0 & 0 & 1 & 0 & 0 & 0\\ 0 & 0 & 0 & \cos\theta & \sin\theta & 0\\ 0 & 0 & 0 & -\sin\theta & \cos\theta & 0\\ \sin\theta\cos\theta & -\sin\theta\cos\theta & 0 & 0 & 0 & \cos^2\theta-\sin^2\theta\end{bmatrix}\begin{Bmatrix}\sigma_1\\ \sigma_2\\ \sigma_3\\ \sigma_4\\ \sigma_5\\ \sigma_6\end{Bmatrix} \quad (3.6)$$

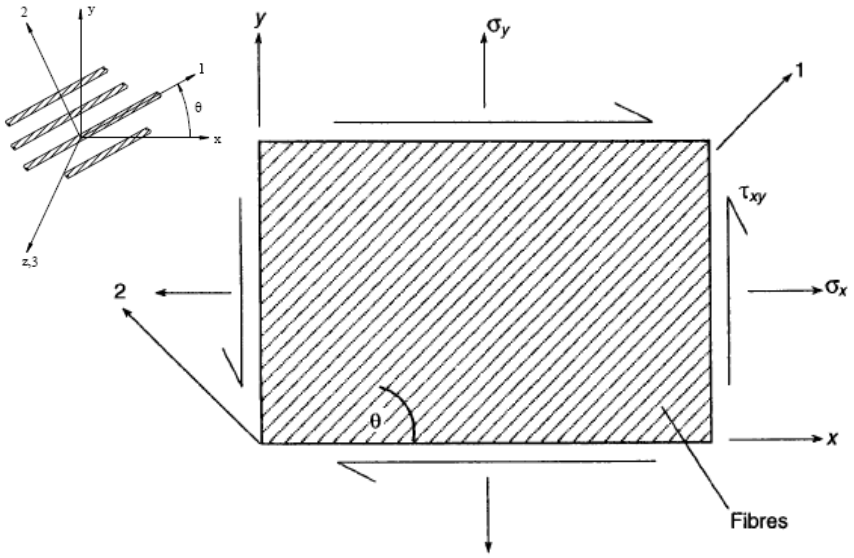



Fig 3.2 Unidirectional lamina with principal axes rotating by θ relative to the ***x-y*** axes.

The strain-stress relations in x-y-z coordinates are;

$$\begin{Bmatrix}\varepsilon_{xx}\\ \varepsilon_{yy}\\ \varepsilon_{zz}\\ \gamma_{yz}\\ \gamma_{xz}\\ \gamma_{xy}\end{Bmatrix}=\begin{bmatrix}\overline{S}_{11} & \overline{S}_{12} & \overline{S}_{13} & 0 & 0 & \overline{S}_{16}\\ \overline{S}_{12} & \overline{S}_{22} & \overline{S}_{23} & 0 & 0 & \overline{S}_{26}\\ \overline{S}_{13} & \overline{S}_{23} & \overline{S}_{33} & 0 & 0 & \overline{S}_{36}\\ 0 & 0 & 0 & \overline{S}_{44} & \overline{S}_{45} & 0\\ 0 & 0 & 0 & \overline{S}_{45} & \overline{S}_{55} & 0\\ \overline{S}_{16} & \overline{S}_{26} & \overline{S}_{36} & 0 & 0 & \overline{S}_{66}\end{bmatrix}\begin{Bmatrix}\sigma_{xx}\\ \sigma_{yy}\\ \sigma_{zz}\\ \sigma_{yz}\\ \sigma_{xz}\\ \sigma_{xy}\end{Bmatrix} \quad (3.7)$$

The transformed compliance coefficients $S_{ij}$ , referred to the (x, y, z) system,

$$\overline{S}_{11}=S_{11}\cos^4\theta-2S_{16}\cos^3\theta\sin\theta+(2S_{12}+S_{66})\cos^2\theta\sin^2\theta-2S_{26}\cos\theta\sin^3\theta+S_{22}\sin^4\theta$$

$$\begin{aligned}
\overline{S}_{12} &= S_{12}\cos^4\theta - (S_{16}-S_{26})\cos^3\theta\sin\theta + (S_{11}+S_{22}-S_{66})\cos^2\theta\sin^2\theta \\
&\quad + (S_{26}-S_{16})\cos\theta\sin^3\theta + S_{12}\sin^4\theta \\
\overline{S}_{13} &= S_{13}\cos^2\theta - S_{36}\cos\theta\sin\theta + S_{23}\sin^2\theta \\
\overline{S}_{16} &= S_{16}\cos^4\theta + (2S_{11}-2S_{12}-S_{66})\cos^3\theta\sin\theta + 3(S_{26}-S_{16})\cos^2\theta\sin^2\theta \\
&\quad + (S_{66}+2S_{12}-2S_{22})\cos\theta\sin^3\theta + S_{26}\sin^4\theta \\
\overline{S}_{22} &= S_{22}\cos^4\theta + 2S_{26}\cos^3\theta\sin\theta + (2S_{12}+S_{66})\cos^2\theta\sin^2\theta \\
&\quad + 2S_{16}\cos\theta\sin^3\theta + S_{11}\sin^4\theta \\
\overline{S}_{23} &= S_{23}\cos^2\theta + S_{36}\cos\theta\sin\theta + S_{13}\sin^2\theta \\
\overline{S}_{26} &= S_{26}\cos^4\theta + (2S_{12}-2S_{22}+S_{66})\cos^3\theta\sin\theta + 3(S_{16}-S_{26})\cos^2\theta\sin^2\theta \\
&\quad + (2S_{11}-2S_{12}-S_{66})\cos\theta\sin^3\theta - S_{16}\sin^4\theta \\
\overline{S}_{33} &= S_{33} \\
\overline{S}_{36} &= 2(S_{13}-S_{23})\cos\theta\sin\theta + S_{36}(\cos^2\theta-\sin^2\theta) \\
\overline{S}_{44} &= S_{44}\cos^2\theta + 2S_{45}\cos\theta\sin\theta + S_{55}\sin^2\theta \\
\overline{S}_{45} &= S_{45}(\cos^2\theta-\sin^2\theta) + (S_{55}-S_{44})\cos\theta\sin\theta \\
\overline{S}_{55} &= S_{55}\cos^2\theta - 2S_{45}\cos\theta\sin\theta + S_{44}\sin^2\theta \\
\overline{S}_{66} &= S_{66}(\cos^2\theta-\sin^2\theta) + 4(S_{16}-S_{26})(\cos^2\theta-\sin^2\theta)\cos\theta\sin\theta \\
&\quad + 4(S_{11}+S_{22}-2S_{12})\cos^2\theta\sin^2\theta
\end{aligned} \tag{3.8}$$

The stress-strain relations in x-y-z coordinates are,

$$\begin{Bmatrix} \sigma_{xx} \\ \sigma_{yy} \\ \sigma_{zz} \\ \sigma_{yz} \\ \sigma_{xz} \\ \sigma_{xy} \end{Bmatrix} = \begin{bmatrix} \overline{C}_{11} & \overline{C}_{12} & \overline{C}_{13} & 0 & 0 & \overline{C}_{16} \\ \overline{C}_{21} & \overline{C}_{22} & \overline{C}_{23} & 0 & 0 & \overline{C}_{26} \\ \overline{C}_{31} & \overline{C}_{32} & \overline{C}_{33} & 0 & 0 & \overline{C}_{36} \\ 0 & 0 & 0 & \overline{C}_{44} & \overline{C}_{45} & 0 \\ 0 & 0 & 0 & \overline{C}_{45} & \overline{C}_{55} & 0 \\ \overline{C}_{16} & \overline{C}_{26} & \overline{C}_{36} & 0 & 0 & \overline{C}_{66} \end{bmatrix} \begin{Bmatrix} \varepsilon_{xx} \\ \varepsilon_{yy} \\ \varepsilon_{zz} \\ \gamma_{yz} \\ \gamma_{xz} \\ \gamma_{xy} \end{Bmatrix} \tag{3.9}$$

The transformed compliance coefficients $C_{ij}$ , referred to the (x, y, z) system,

$$\overline{C}_{11} = C_{11}\cos^4\theta - 4C_{16}\cos^3\theta\sin\theta + (2C_{12} + C_{66})\cos^2\theta\sin^2\theta - 4C_{26}\cos\theta\sin^3\theta + C_{22}\sin^4\theta$$

$$\overline{C}_{12} = C_{12}\cos^4\theta + 2(C_{16} - C_{26})\cos^3\theta\sin\theta + (C_{11} + C_{22} - 4C_{66})\cos^2\theta\sin^2\theta + 2(C_{26} - C_{16})\cos\theta\sin^3\theta + C_{12}\sin^4\theta$$

$$\overline{C}_{13} = C_{13}\cos^2\theta - 2C_{36}\cos\theta\sin\theta + C_{23}\sin^2\theta$$

$$\overline{C}_{16} = C_{16}\cos^4\theta + (C_{11} - C_{12} - 2C_{66})\cos^3\theta\sin\theta + 3(C_{26} - C_{16})\cos^2\theta\sin^2\theta + (2C_{66} + C_{12} - C_{22})\cos\theta\sin^3\theta - C_{26}\sin^4\theta$$

$$\overline{C}_{22} = C_{22}\cos^4\theta + 4C_{26}\cos^3\theta\sin\theta + 2(C_{12} + 2C_{66})\cos^2\theta\sin^2\theta + 4C_{16}\cos\theta\sin^3\theta + C_{11}\sin^4\theta$$

$$\overline{C}_{23} = C_{23}\cos^2\theta + 2C_{36}\cos\theta\sin\theta + C_{13}\sin^2\theta$$

$$\overline{C}_{26} = C_{26}\cos^4\theta + (C_{12} - C_{22} + 2C_{66})\cos^3\theta\sin\theta + 3(C_{16} - C_{26})\cos^2\theta\sin^2\theta + (C_{11} - C_{12} - 2C_{66})\cos\theta\sin^3\theta - C_{16}\sin^4\theta$$

$$\overline{C}_{33} = C_{33}$$

$$\overline{C}_{36} = (C_{13} - C_{23})\cos\theta\sin\theta + C_{36}(\cos^2\theta - \sin^2\theta)$$

$$\overline{C}_{44} = C_{44}\cos^2\theta + 2C_{45}\cos\theta\sin\theta + C_{55}\sin^2\theta$$

$$\overline{C}_{45} = C_{45}(\cos^2\theta - \sin^2\theta) + (C_{55} - C_{44})\cos\theta\sin\theta$$

$$\overline{C}_{55} = C_{55}\cos^2\theta - 2C_{45}\cos\theta\sin\theta + C_{44}\sin^2\theta$$

$$\overline{C}_{66} = 2(C_{16} - C_{26})\cos^3\theta\sin\theta + (C_{11} + C_{22} - 2C_{12} - 2C_{66})\cos^2\theta\sin^2\theta + 2(C_{26} - C_{16})\cos\theta\sin^3\theta + C_{66}(\cos^4\theta + \sin^4\theta) \tag{3.10}$$

Note that $C_{14}$, $C_{15}$, $C_{16}$, $C_{24}$, $C_{25}$, $C_{26}$, $C_{34}$, $C_{35}$, $C_{36}$, $C_{45}$, $C_{46}$, and $C_{56}$ are zero for an orthotropic material.

## 3.2 Finite Element Analysis

Finite Element (FE) analysis is merely an alternative approach to solving the governing equations of a structural problem. Hence, FE and classical methods wil produce identical results for the same problem, provided the former method is correctly applied.

The method consists of imagining the structure to be composed of discrete parts (i.e. finite elements), which are then assembled in such way as to represent the distortion of the structure under the specified loads. Each element has an assumed displacement field, and part of the skill of applying the method is in selecting appropriate elements of the correct size and distributions (the FE 'mesh').

The FE method was initially developed for isotropic materials and the majority of elements available (the 'library') in any software package would be for such materials. To apply the technique to composites requires different element formulations that adequately represent their anisotropic, or orthotropic, stiffness and strength, as well as the laminated form of construction often used.

### *3.2.1 Three-Dimensional Finite Element Method*

In the three-dimensional finite element formulation, the displacements, traction components, and distributed body force values are the functions of the position indicated by (*x, y, z).* The displacement vector **u** is given as

$$\mathbf{u} = (u,v,w)^T \tag{3.19}$$

where *u,* v and w are the *x, y* and *z* components of **u**, respectively. The stress and strains are given by

$$\begin{aligned} \sigma &= \left[\sigma_{xx}, \sigma_{yy}, \sigma_{zz}, \sigma_{yz}, \sigma_{xz}, \sigma_{xy}\right]^T \\ \varepsilon &= \left[\varepsilon_{xx}, \varepsilon_{yy}, \varepsilon_{zz}, \gamma_{yz}, \gamma_{xz}, \gamma_{xy}\right]^T \end{aligned} \tag{3.20}$$

From Figure 3.6, representing the three- dimensional problem in a general setting, the body force and traction vector are given by

$$\mathbf{f} = [\, f_x, f_y, f_z \,]^T \;, \quad \mathbf{T} = [\, T_x, T_y, T_z \,]^T \tag{3.21}$$

The body force **f** has dimensions of force per unit volume, while the traction force **T** has dimensions of force per unit area.

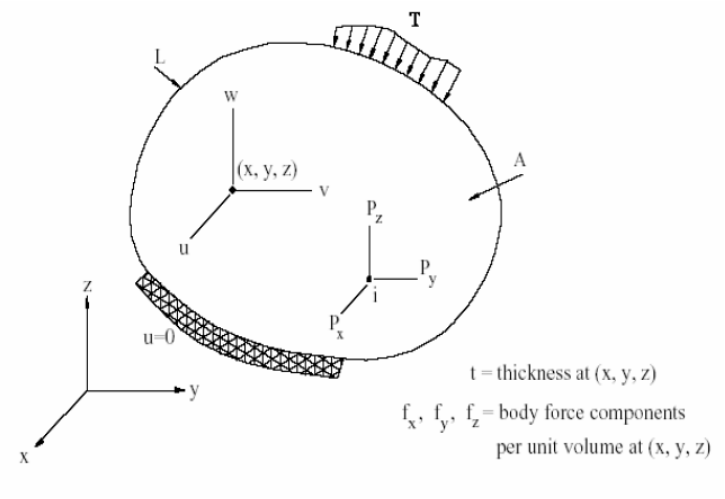



Figure 3.6 Three dimensional problem

### *3.2.2 The sixteen-Node Brick Element*

The sixteen-node brick element is a simple three-dimensional element used in the analysis of solid mechanics problem. A 3D isoparametric solid continuum element capable of modeling curved boundaries. The element is numbered according to right-hand screw rule in the local z-direction. Freedoms of the element are u, v, w at each node and node coordinates are x, y, z at each node. A typical sixteen-node brick element is shown in Figure 3.7

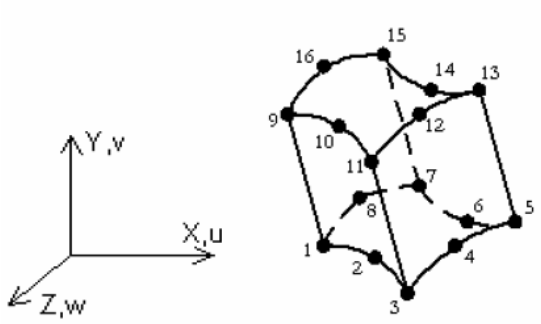



Figure 3.7 Sixteen-node brick element

Hashin failure criteria (1980) are polynomial failure criteria similar to the quadratic failure envelope except that in the Hashin formulation there are distinct

polynomials corresponding to the different modes. Hashin-type failure criteria are ideal for use in finite element models, especially when adapted to progressive damage models. Hashin proposed a set of failure criteria for predicting failure of unidirectional composites based on each failure mode.

***Tensile Fiber Mode:***

$$\left(\frac{\sigma_{11}}{X_T}\right)^2 + \frac{1}{S^2}(\sigma_{12}{}^2 + \sigma_{13}{}^2) = 1$$

or (3.22)

$$\sigma_{11} = X_T$$

***Compressive Fiber Mode:***

$$|\sigma_{11}| = X_c \tag{3.23}$$

***Tensile Matrix Mode:*** $(\sigma_{22} + \sigma_{33}) > 0$

$$\frac{1}{Y_T{}^2}(\sigma_{22} + \sigma_{33})^2 + \frac{1}{S_T{}^2}(\sigma_{33}{}^2 - \sigma_{22}\sigma_{33}) + \frac{1}{S^2}(\sigma_{12}{}^2 + \sigma_{13}) = 1 \tag{3.24}$$

***Compressive Matrix Mode:***

$$\frac{1}{Y_c{}^2}\left[\left(\frac{Y_c}{2S_T}\right) - 1\right](\sigma_{22} + \sigma_{33}) + \frac{1}{4S_T{}^2}(\sigma_{22} + \sigma_{33})^2 + \frac{1}{S_T{}^2}(\sigma_{23}{}^2 - \sigma_{22}\sigma_{33}) + \frac{1}{S^2}(\sigma_{12}{}^2 + \sigma_{13}{}^2) = 1 \tag{3.25}$$

where;

$\sigma_{11}$ is the normal stress in the direction of the fibers of the lamina.

$\sigma_{22}$, $\sigma_{33}$ are the normal stresses in the transverse directions to the fibers of the lamina.

$\sigma_{23}$, $\sigma_{13}$, $\sigma_{12}$ are the shear stresses in the lamina.

$X_T$ is the tensile strength of the fibers.

$X_C$ is the compressive strength of the fibers.

$Y_T$ is the tensile strength in the transverse direction of the fibers.

$Y_C$ is the compression strength in the transverse direction of the fibers.

S is the shear strength, in the 1-2 plane of the lamina.

$S_T$ is the transverse shear strength in the 1-3 and 2-3 planes of the lamina.

# CHAPTER FOUR

# NUMERICAL STUDY

## 4.1 Objective

The objective of the numerical study is to determine the failure loads and failure modes of the composite plates considered in experimental analysis and comparing the results with the each other.

## 4.2 Explanation of the Numerical Study

The numerical studies have been carried out by LUSAS 13.6 finite element analysis software. All of the specimens with different pin-configurations have been modeled and analyzed so that the failure loads have been determined.

Specimens modeled as a half model and symmetry boundary conditions were used to reduce the size of the model and calculation time.

While modeling meshes were graded manually by specifying the number of elements on each of the boundary lines. (See Figure 4.1)

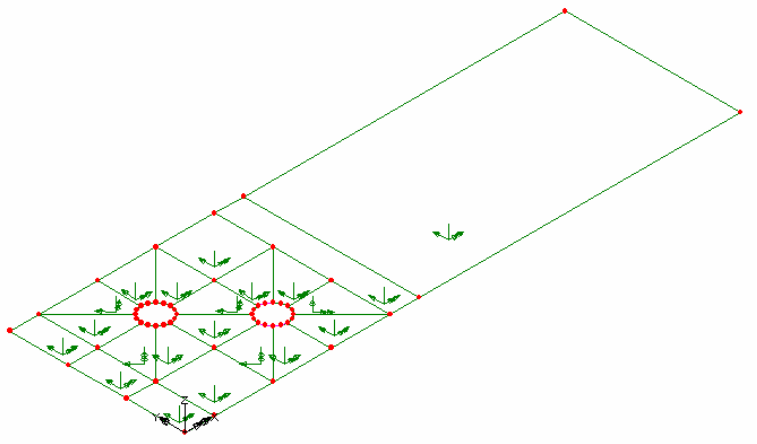


Figure 4.1 Modeling of the surfaces

After creating the surfaces, they were swept through the depth of the plate to create a volume. Then the mesh dataset Composite Brick (HX16L) were assigned to the volume. (See Figure 4.2)

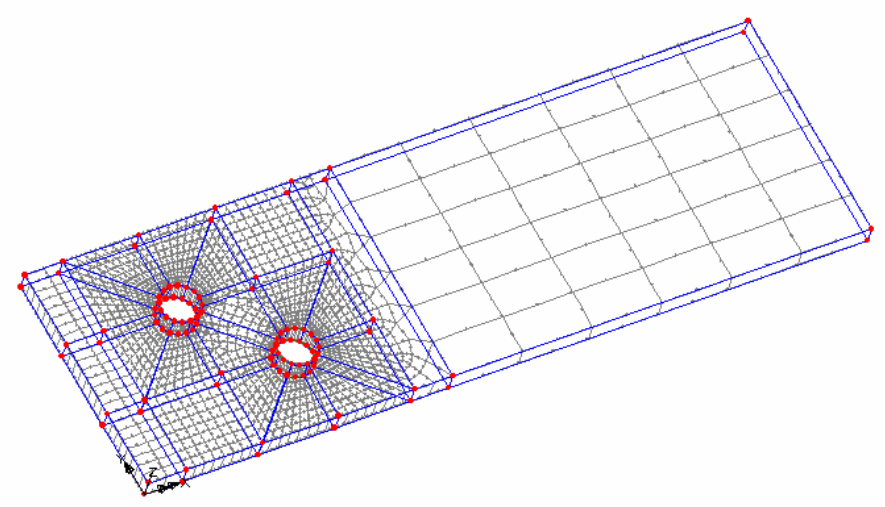


Figure 4.2 Composite Brick (HX16L) meshes.

After defining the material properties of glass-epoxy composite material indicated in Table 5.1, the ply orientations and stacking sequence of the composite plate, the boundary conditions and distributed load have been defined.

The first boundary condition was the bottom surface of the symmetrically half model. It was defined as supported on xz plane.

The second boundary condition was the supporting face of the holes. These faces have been defined to support the load by cylindrical coordinates just like the bearing load, and they've been defined as fixed x direction support for the both holes.

Finally a distributed load has been defined to the loading direction (x) of the model and after defining the failure criteria values, the analyses were carried out as geometric non-linear. (See Figure 4.3 & Figure 4.4)

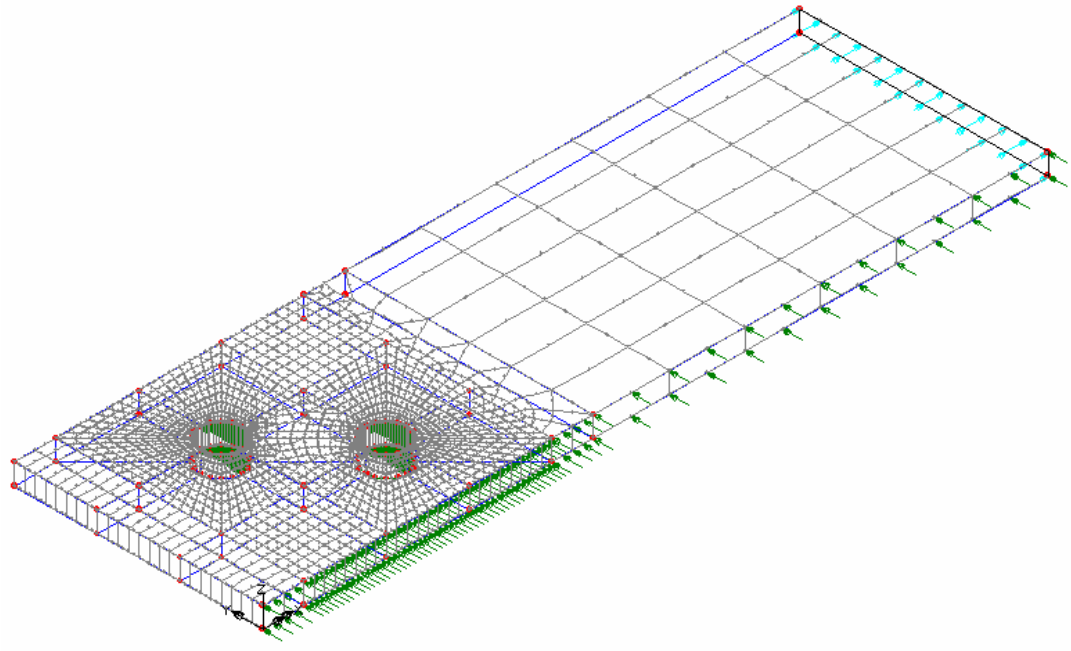


Figure 4.3 Boundary conditions of the model.

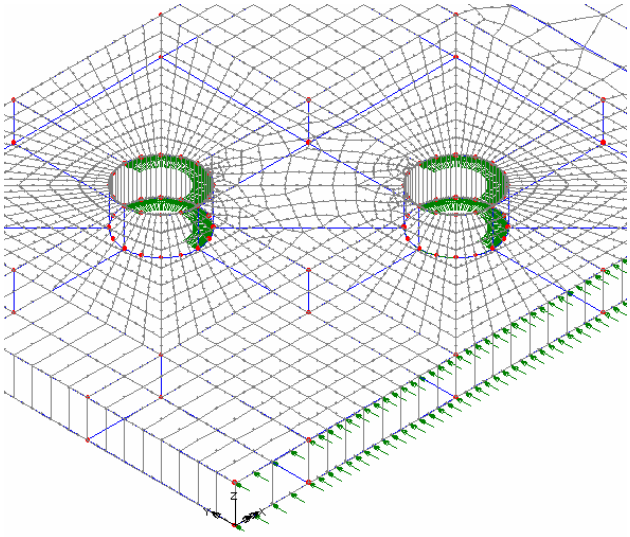


Figure 4.4 Boundary conditions of the model.

For the analyses, “geometric non-linear analyze method” and “Hashin Failure Criteria” were selected.

For each analyzed pin-configuration, failure loads have been determined and the stress contours have been plotted.

# CHAPTER FIVE

# EXPERIMENTAL STUDY

## 5.1 Objective

The objective of this research is to investigate the effect of failure behaviour of multi-pinned-joint in glass-epoxy laminated composite plate. The experimental studies have been implemented as two set of tests. The purpose of the first set of test was to determine the material properties. The second set of was implemented to determine the "Failure Modes" and the "Failure Loads" of the laminates with different hole/pin combinations.

## 5.2 Problem Statement and Experimental Details

The configuration and loading studied in this research are shown in Figure 5.1 and Figure 5.2. A uniform tensile load P was applied to the test plate which was supported by 4 rigid pins with different arrangements. Load was parallel to the plate and symmetric with respect to the centerline so that it can not create bending moments about x, y, z axes.

The laminates with stacking arrangements of $[0/90/\pm45]_S$ were selected to investigate. (The 0° direction in the stacking notation denotes the x-axis or longitudinal direction.) The fiber-volume fraction of the composite is approximately 60%. The thickness of the material is 2.5 mm.

There were mainly two series of geometric arrangement which are symmetrical about the y axes. (See Fig. 5.1)

This lay-up was chosen and 72 different geometries were used so that a variety of failure modes and failure strength could be observed.

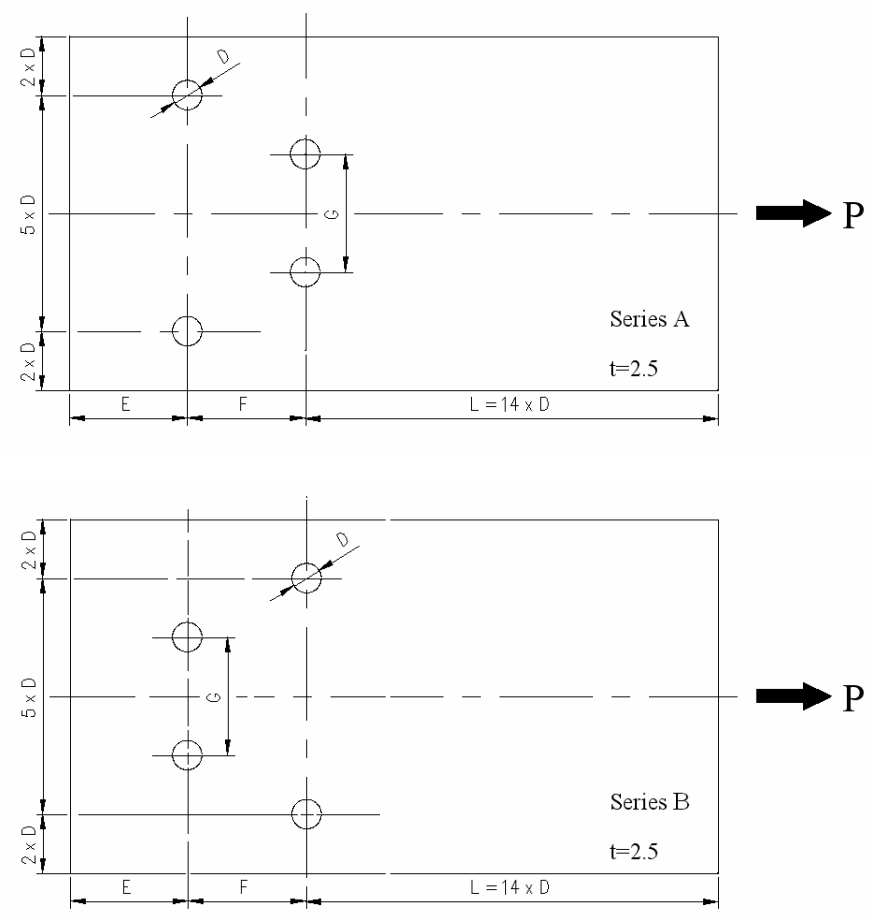



Fig. 5.1 Geometry of two series of test plates with 4 circular hole

The main parameters of the test plate can be described as follows:

- **L** – The length of the plate
- **D** – Hole / pin diameter
- **E** – Edge distance, the distance from the center of the 1st series-holes to the free edge.
- **F** – Longitudinal hole distance, the distance between the 1st-series-holes and the 2nd-series-holes along the longitudinal axis.
- **G** – Transverse hole distance, the distance between the 2nd-series-holes along the transverse axis

- **E/D –** The ratio of ‘edge distance’ to ‘hole / pin diameter’, it has been varied as 2, 3, 4 in the study.
- **F/D –** The ratio of ‘Longitudinal hole distance’ to ‘hole / pin diameter’, it has been varied as 2, 4, 6 in the study.
- **G/D –** The ratio of ‘Transverse hole distance’ to ‘hole / pin diameter’, it, has been varied as 2, 4, 6, 8 in the study.

There are, in general, three basic joint failure modes related to composite failure: net-tension, shear out and bearing, although, in practice, combinations of these failure modes are possible. Typical damages due to each mechanism are shown in Figure 5.2. Especially, the appearance of the net-tension failure is catastrophic, immediate and without warning. Therefore, the designer should choose optimal pin arrangements to avoid such catastrophic and immediate failure at structural elements in practical applications. (Okutan et al. 2001)

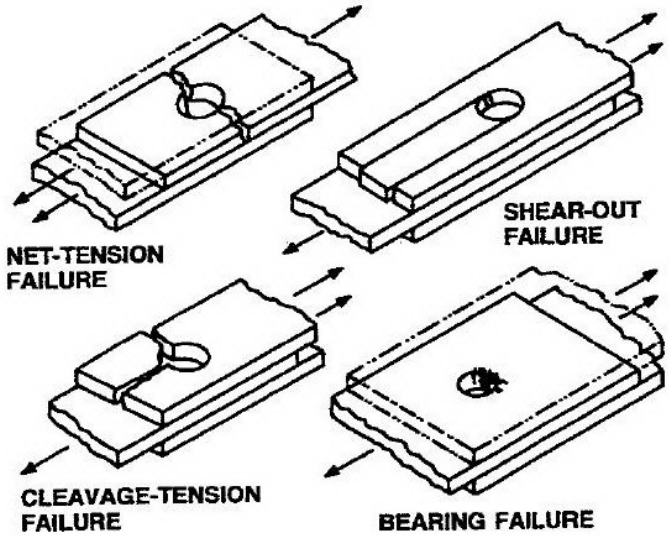



Figure 5.2 Typical failure mechanisms of the pinned-joint configuration (Jones, 1999)

### 5.3 Determination of Mechanical Properties

The elasticity modulus in direction of the fibers, $E_1$, and the Poisson's ratio $\nu_{12}$ can be determined by means of tension tests on unidirectional coupons that instrumented with electric resistance strain gages, as shown in Figure 5.3. One of them was placed to the fiber direction and the other one in the matrix direction.

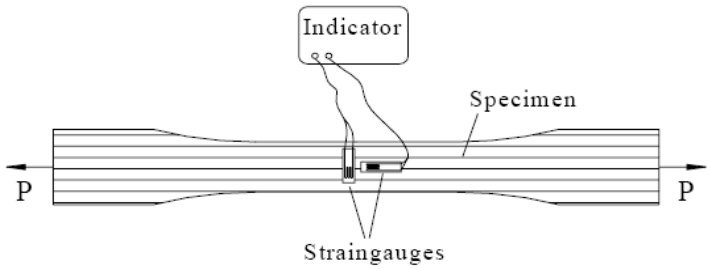



Figure 5.3 Test specimen for determination of $E_1$ and $\nu_{12}$.

The specimen which has the dimensions 150 mm x 12 mm x 1.8 mm was loaded step by step to rapture by tensile test machine. For all steps, P, $\varepsilon_1$ and $\varepsilon_2$ values were measured.

Then, $\nu_{12}$ and $E_1$ were calculated by using the equations (5.1)

$$\sigma_1 = \frac{P}{A},\ \upsilon_{12} = -\frac{\varepsilon_2}{\varepsilon_2}, E_1 = \frac{\sigma_1}{\varepsilon_1} \tag{5.1}$$

The similar test was performed to determine $E_2$. The specimen which has the dimensions 150 mm x 25.6 mm x 1.8 mm was loaded step by step to rapture by tensile test machine. For all steps, *P*, $\varepsilon_1$ and $\varepsilon_2$ values were measured. (Figure 5.4)

Then, $E_2$ was calculated by using the equations (5.2)

$$\sigma_2 = \frac{P}{A},\ E_2 = \frac{\sigma_2}{\varepsilon_2} \tag{5.2}$$

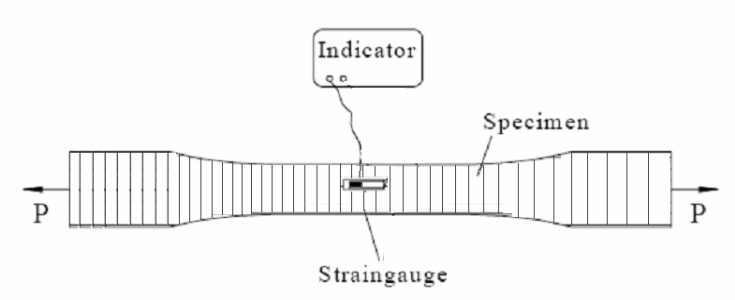



Figure 5.4 Test specimen for determination of $E_2$.

To find $X_t$, a specimen which has the dimensions 300 mm x 12 mm x 1.8 mm was loaded step by step to rapture by tensile test machine. (Figure 5.5) It was calculated from the equation (5.3)

$$X_t = \frac{P_{ult}}{A} \tag{5.3}$$

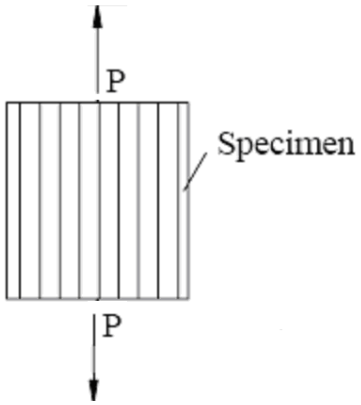



Figure 5.5 Longitudinal tension test

The similar test method was used to determine $Y_t$ (Figure 5.6). The specimen dimensions were 300 mm x 25.6 mm x 1.8 mm. The $Y_t$ value was calculated by the equation (5.4).

$$Y_t = \frac{P_{ult}}{A} \tag{5.4}$$

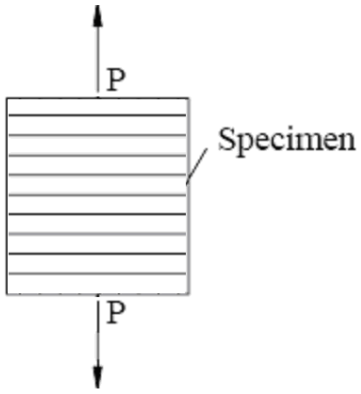



Figure 5.6 Transversal tension test

To find $X_c$, a specimen, which has the dimensions 7.5 mm x 1.8 mm and whose fiber direction coincides with the loading direction was taken and it was subjected to compressive loading (Fig.5.7). $X_c$ was also calculated by dividing the ultimate force by the cross-sectional area of the specimen. (Equation (5.5))

$$X_c = \frac{P_{ult}}{A} \tag{5.5}$$

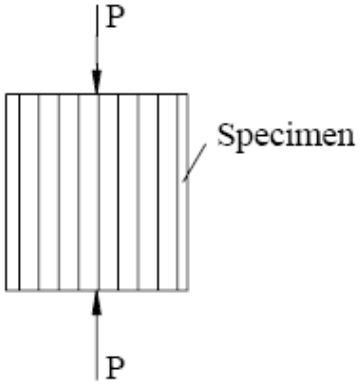



Figure 5.7 Longitudinal compression test

The similar test method was used to determine $Y_c$. (Figure 5.8) The specimen dimensions were 7.5 mm x 1.8 mm. The value was calculated by the equation (5.6).

$$Y_c = \frac{P_{ult}}{A} \tag{5.6}$$

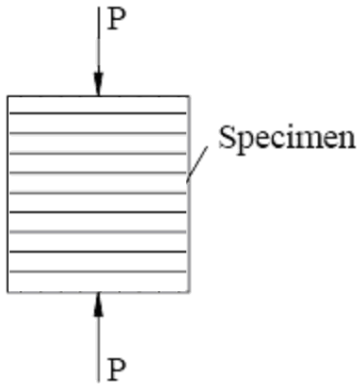



Figure 5.8 Transversal compression test

To define the shear modulus $G_{12}$, a specimen whose principal axis was on 45° was taken and a strain gauge was stuck on loading direction of the lamina (Fig.5.9). The specimen was loaded step by step up to rapture by the test machine and $G_{12}$ was calculated by measurement of the strain in the tensile direction $\varepsilon_x$.

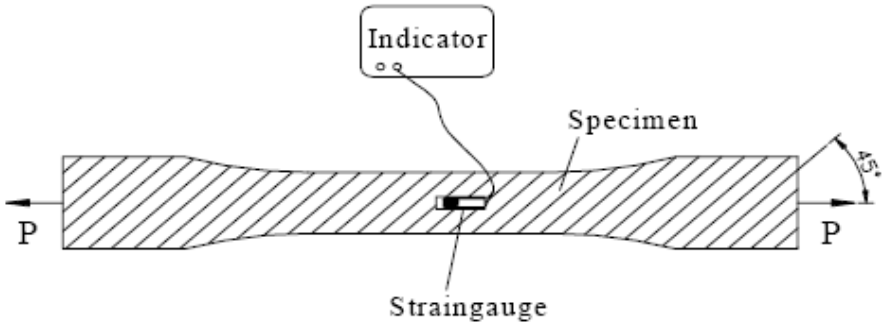



Figure 5.9 Shear Test

$$E_x = \frac{P/A}{\varepsilon_x}$$

$$G_{12} = \frac{1}{\frac{4}{E_x} - \frac{1}{E_1} - \frac{1}{E_2} + \frac{2\upsilon_{12}}{E_1}} \tag{5.7}$$

Iosipescu testing method was used to define the shear strength *S* (Fig.5.10). The dimensions of the specimen were chosen as; L=80 mm, h=20 mm, w=12 mm and $t_i$=1.8 mm. A compression test was applied to the specimen. In failure, S was calculated from

$$S = \frac{P_{\max}}{t_i c} \tag{5.5}$$

where $P_{max}$ is the failure force.

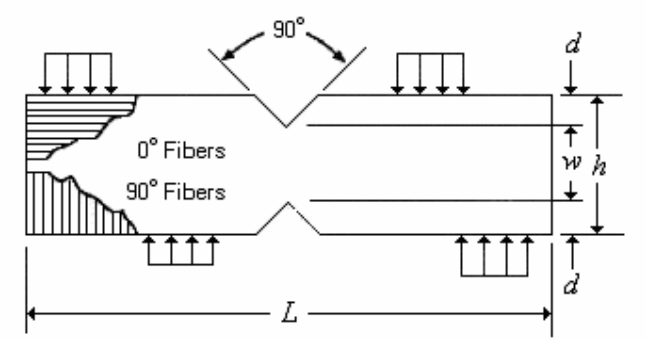



Figure 5.10.a Iosipescu test specimen and testing fixture

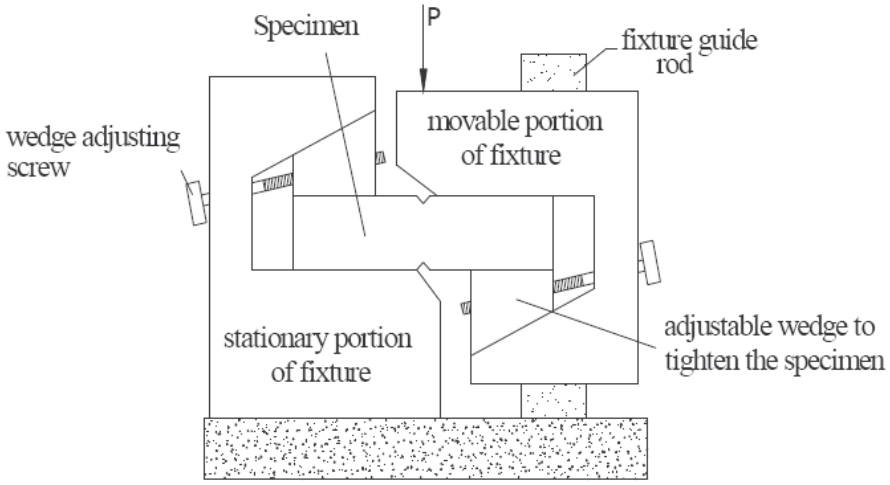



Figure 5.10.b Iosipescu test specimen and testing fixture

The mechanical properties of glass/epoxy composite plate which were obtained from the experimental study have been given in Table 5.1.

Table 5.1 Mechanical properties of glass/epoxy

| $E_1$ (GPa) | $E_2$ (GPa) | $G_{12}$ (GPa) | $\nu_{12}$ | $X_c$ (MPa) | $Y_c$ (MPa) | $X_t$ (MPa) | $Y_t$ (MPa) | $S$ (MPa) |
|---|---|---|---|---|---|---|---|---|
| 37.461 | 7.998 | 3.965 | 0.2725 | 223.37 | 109.01 | 686.77 | 73.88 | 78.59 |

Experiments were carried out in tension mode with the tensile machine. The lower edge of the specimen clamped and loaded from the steel pins by stretching the specimens at a ratio 0.5 mm/mm (Figure 5.11). The load – pin displacement diagrams for all composite configurations were plotted.

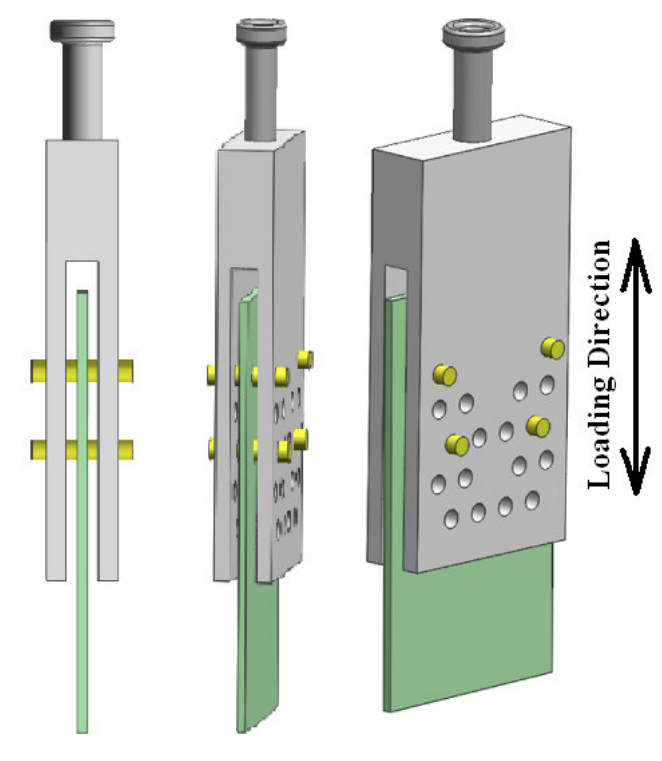



Figure 5.11 Tensile test setup – test fixture (grey), test specimen (green), and rigid pins (yellow)

# CHAPTER SIX

## RESULTS AND DISCUSSION

In this study, maximum failure load and failure mode parameters were investigated experimentally and numerically. The specimens for each pin configuration were tested for experimental study. For the numerical study all pin configurations were modeled and analyzed by LUSAS 13.6 finite element analysis software. Geometric non-linear solution with Hashin failure criterion were selected for the numerical analysis.

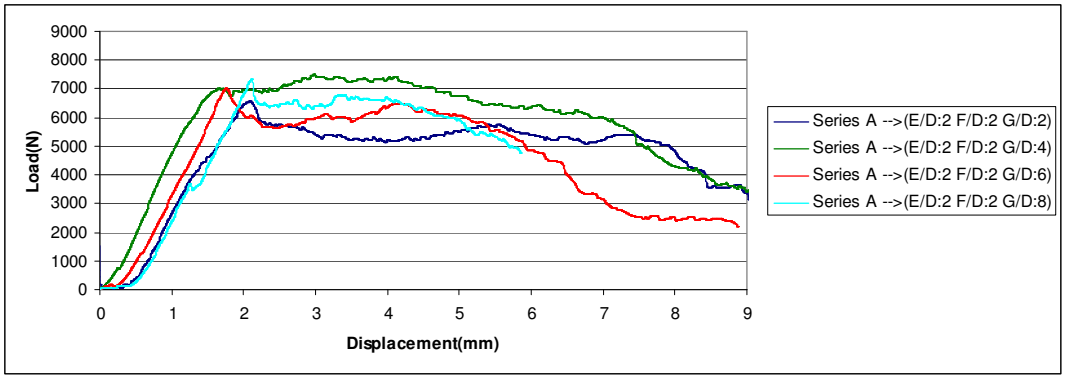
Failure load values and failure modes were investigated for three variables, E/D ratio (2,3,4), F/D ratio (2,4,6), G/D ratio (2,4,6,8).

In the experimental study, load-displacement curves have been plotted and fixed E/D ratio-configurations were compared with each other respectively (Figure 6.1 to 6.6). It was seen that curves are linear before the initial failure (elastic region). It can be say that almost all of the specimens were reached the failure loads between the displacements of 1 and 2 mm. Furthermore, specimens were carried the load up to min. 5 mm at nearly-constant load values.

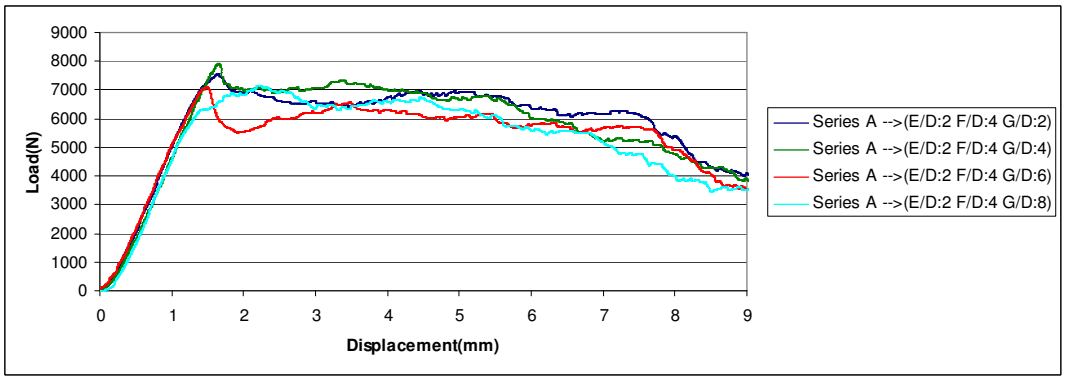
However, it was seen that the greater E/D ratio-configuration-specimens continued to carry the load up to 9 mm at nearly-constant load values.

Load vs. Pin-displacement diagrams can be seen below in Figure 6.1 to Figure 6.2 while;

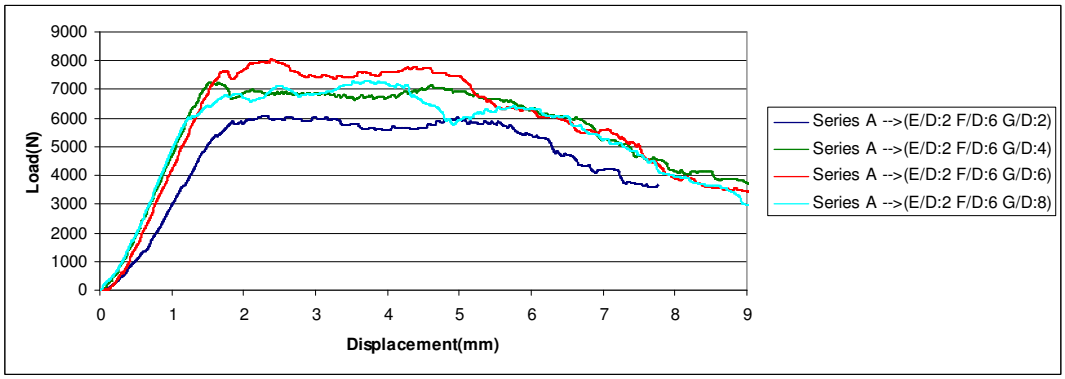
- Figure 6.1, 6.2 & 6.3 indicate the change of G/D ratio in test series A.
- Figure 6.4, 6.5 & 6.6 indicates the change of G/D ratio in test series B.




(a)

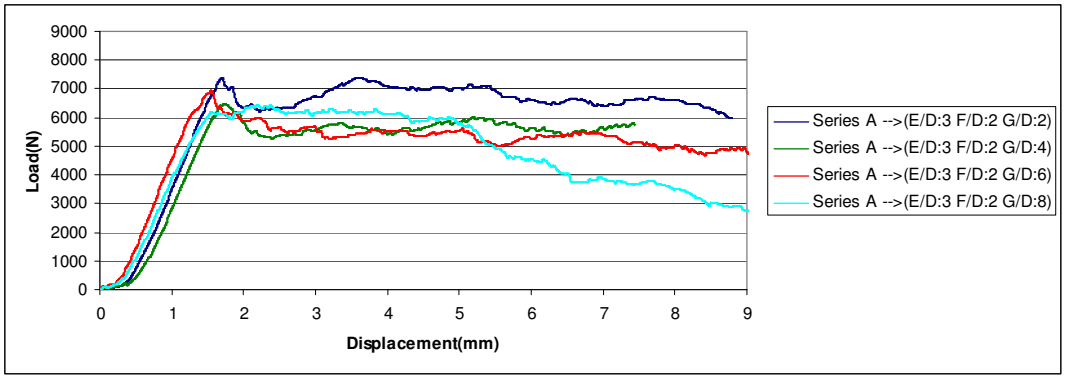



(b)

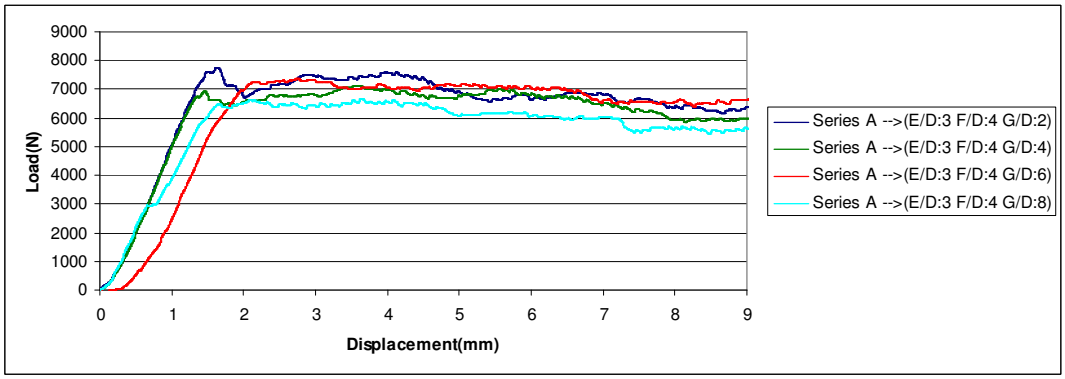



(c)

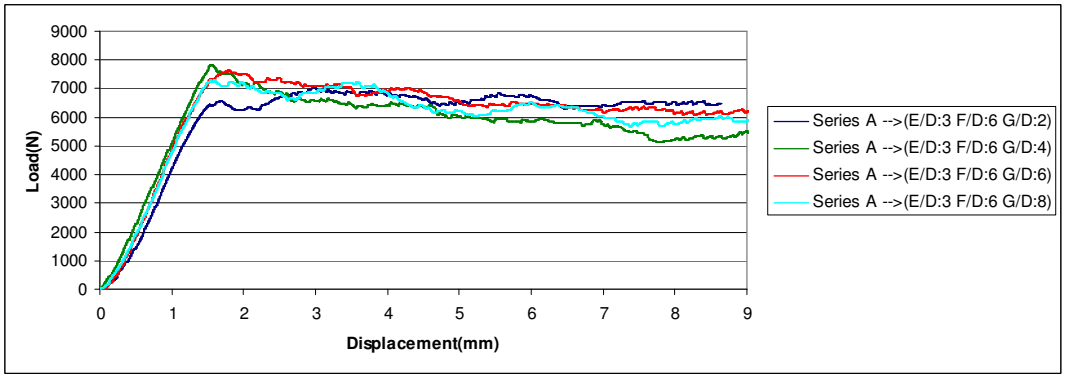
Figure 6.1 Load-Displacement curves of composite plates for test series A and E/D=2




(a)

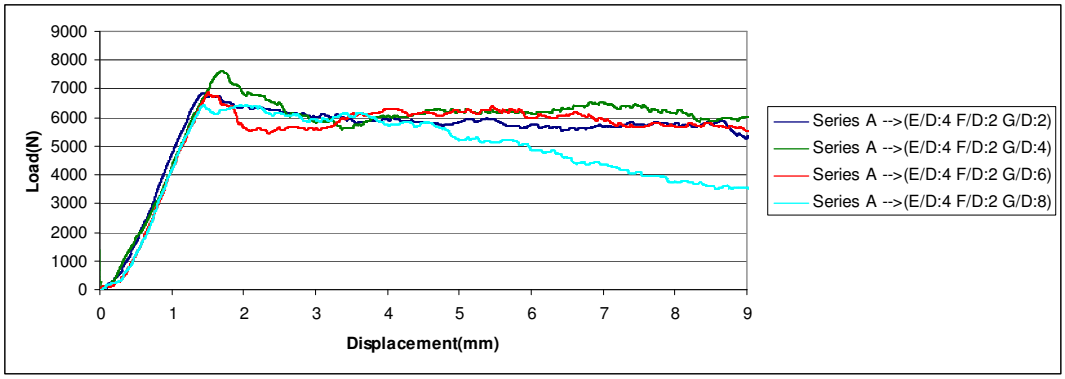



(b)

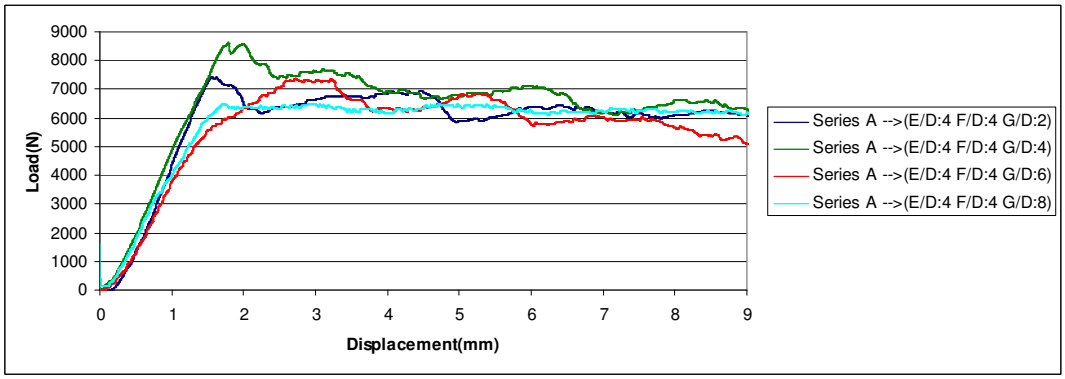



(c)

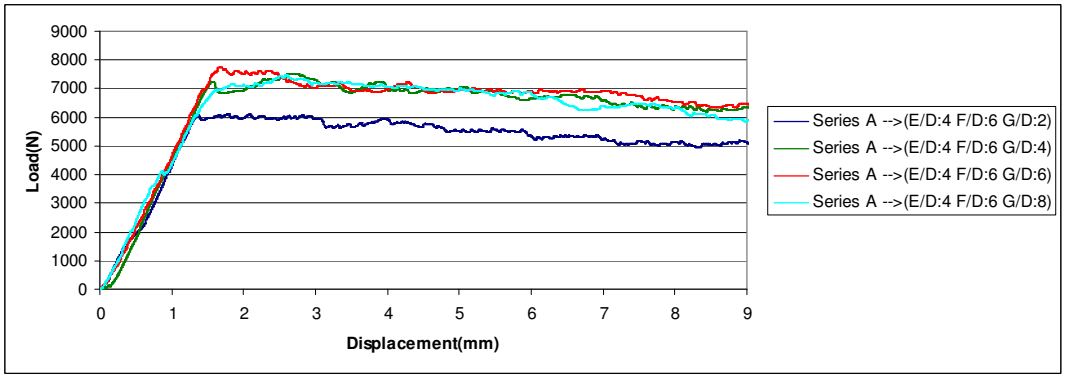
Figure 6.2 Load-Displacement curves of composite plates for test series A and E/D=3




(a)

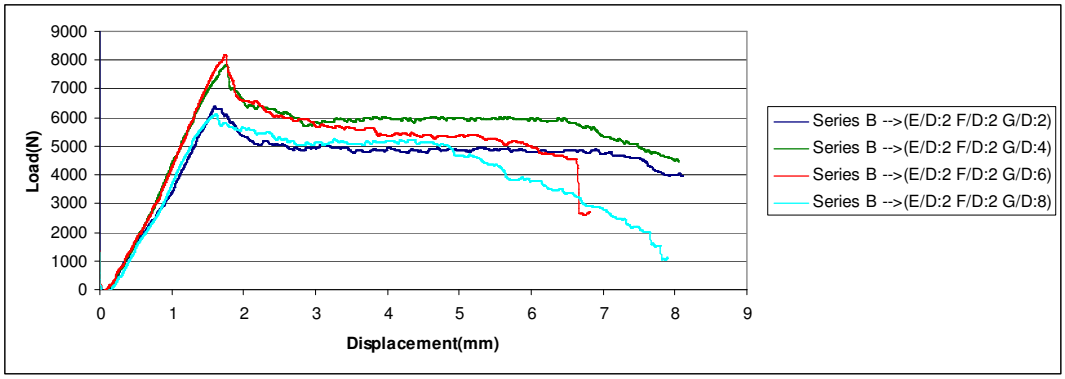



(b)

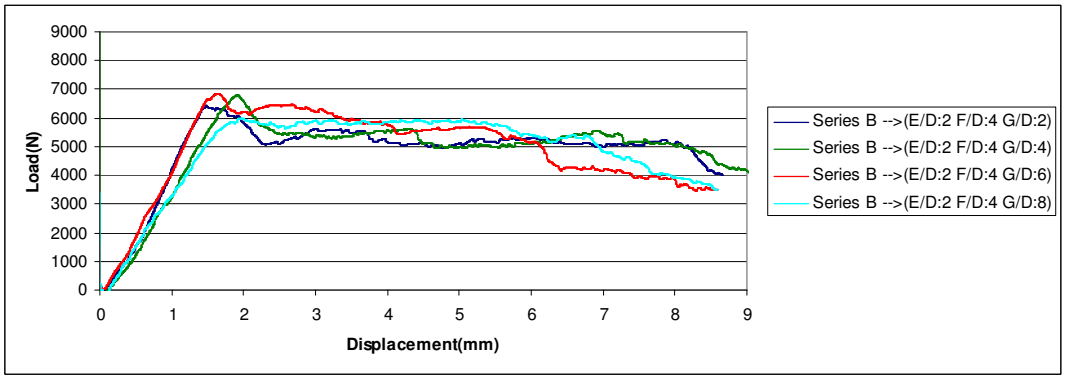



(c)

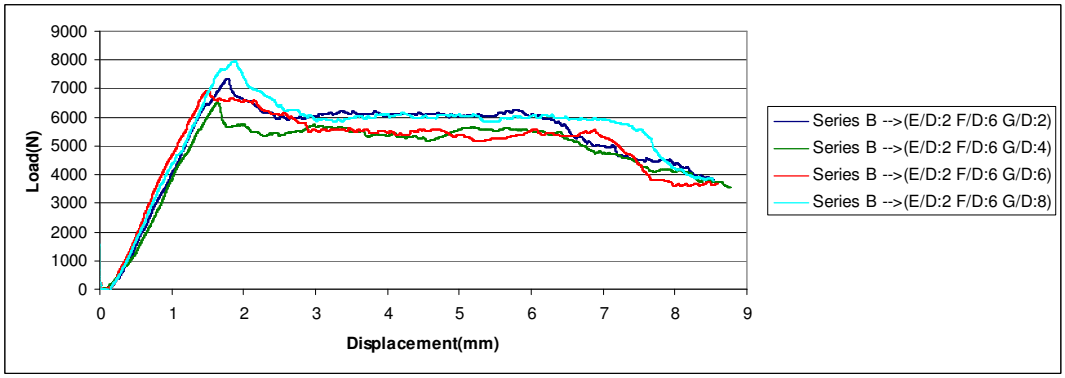
Figure 6.3 Load-Displacement curves of composite plates for test series A and E/D=4




(a)

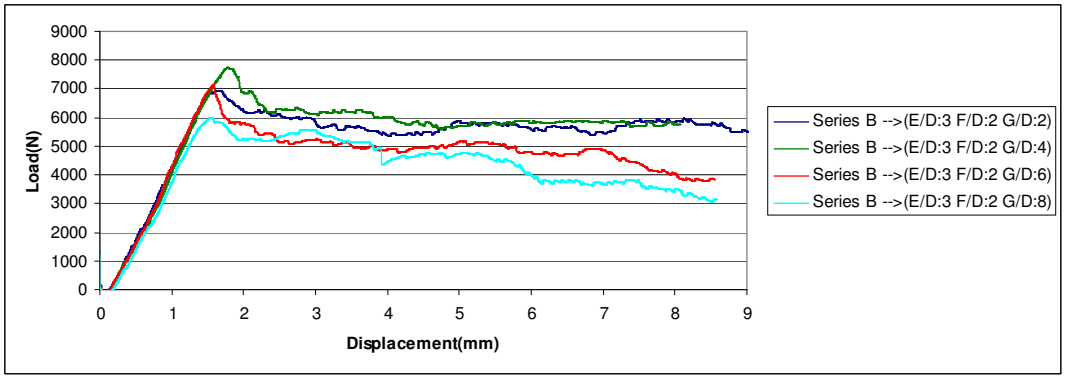



(b)

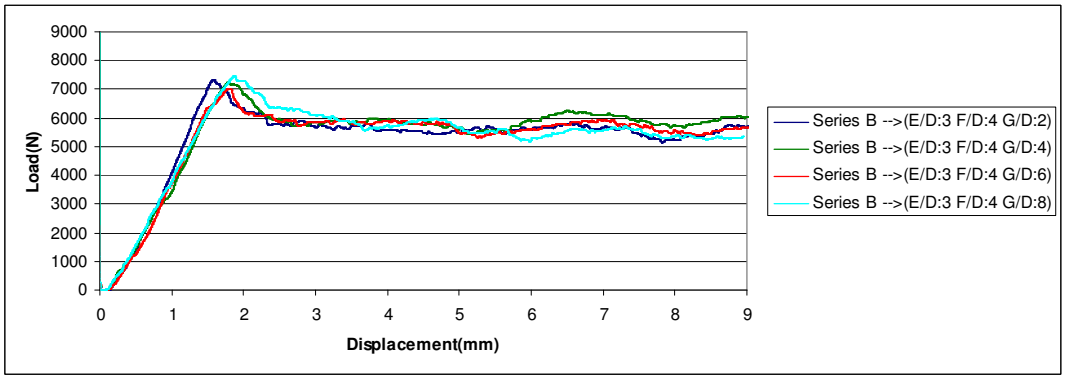



(c)

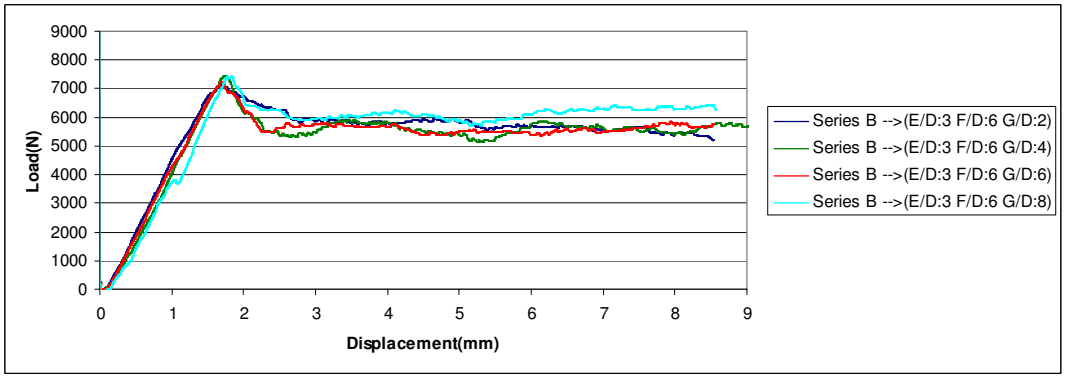
Figure 6.4 Load-Displacement curves of composite plates for test series B and E/D=2




(a)

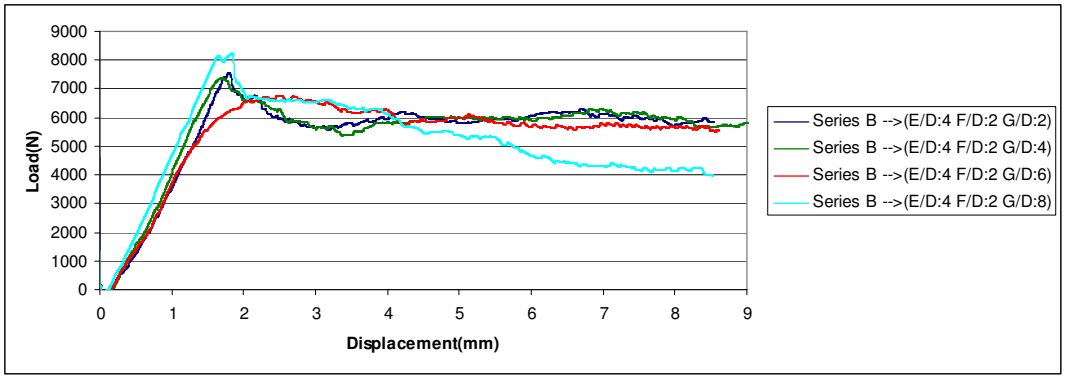



(b)

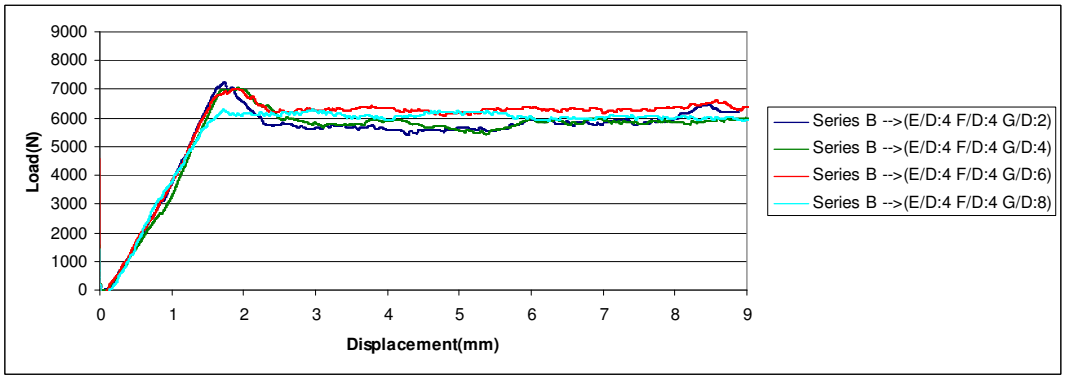



(c)

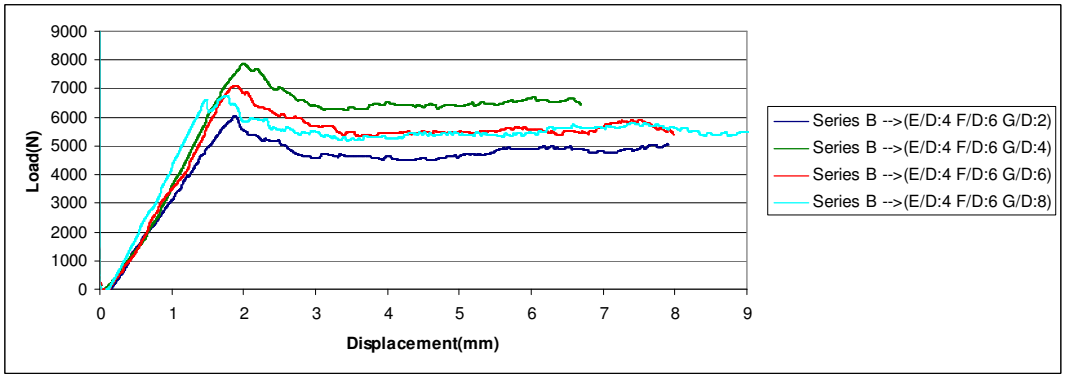
Figure 6.5 Load-Displacement curves of composite plates for test series B and E/D=3




(a)




(b)




(c)

Figure 6.6 Load-Displacement curves of composite plates for test series B and E/D=4

When we look at the failure modes of either Series A or Series B, the lowest value of the E/D (E/D=2), have the combination of “Bearing” and “Shear-out” modes. As known that it is not a secured mode, in practice the ratio of E/D=2 should not to be chosen. (Tables 6.1 & 6.4)

At the same time, for all E/D versions of the arrangement F/D=2 + G/D=8 the same failure modes, combination of “Bearing” and “Shear-out”, occurred. Although the configuration E/D=4, F/D=2, G/D=8 of the test series A has the greatest failure load value, in practice also it should not to be chosen since it is not a secured mode.

The remaining configurations have the “Bearing” mode, which is the most secured failure mode.

If we focused on the failure load values, these observations below can be determined:

For Series A, G/D=2 and F/D=6 with lower values of E/D (2,4) the laminates are the weakest.

However, the configuration E/D=4, F/D=4 and G/D=4 is the strongest and the most secured laminate of Series A.

For Series B, G/D=8 with lower values of E/D (2,3) and F/D (2,4) the laminates are the weakest.

However, the configuration of E/D=2, F/D=2 and G/D=6 is the strongest and the most secured laminate of Series B.

When G/D=8 is kept constant and considering the combinations of F/D=2, F/D=4, F/D=6, the failure load values of E/D=2, E/D=3 and E/D=4 are nearly the same.(Figure 6.7.d) So it can be say that the failure behavior of the laminates which have the rectangular-shaped hole configuration is not depend on the E/D ratio.

Table 6.1 Results & comparisons of experimental with numerical failure loads and failure modes of the composite material
(Series A, E/D=2)
(B = bearing mode, S = shear-out mode, N = net-tension mode)

| Series A E / D = 2 | | Failure Load (N) | | Failure Mode | |
|---|---|---|---|---|---|
| | | Experimental | Numerical | Exp. | Num. |
| F / D = 2 | G / D = 2 | 6585 | 10100 | B-S | B |
| | G / D = 4 | 7500 | 8721 | B-S | B |
| | G / D = 6 | 7014 | 8066 | B-S | B |
| | G / D = 8 | 7335 | 8435 | B-S | B-S |
| F / D = 4 | G / D = 2 | 7553 | 8450 | B-S | B |
| | G / D = 4 | 7907 | 7900 | B-S | B |
| | G / D = 6 | 7106 | 8172 | B-S | B |
| | G / D = 8 | 7168 | 8244 | B-S | B |
| F / D = 6 | G / D = 2 | 6085 | 7763 | B-S | B |
| | G / D = 4 | 7250 | 8338 | B-S | B |
| | G / D = 6 | 8042 | 9248 | B-S | B |
| | G / D = 8 | 7293 | 8387 | B-S | B-S |

Table 6.2 Results & comparisons of experimental with numerical failure loads and failure modes of the composite material
(Series A, E/D=3)
(B = bearing mode, S = shear-out mode, N = net-tension mode)

| Series A E / D = 3 | | Failure Load (N) | | Failure Mode | |
|---|---|---|---|---|---|
| | | Experimental | Numerical | Exp. | Num. |
| F / D = 2 | G / D = 2 | 7391 | 10150 | B | B |
| | G / D = 4 | 6493 | 8930 | B | B |
| | G / D = 6 | 6949 | 7992 | B | B |
| | G / D = 8 | 6453 | 7500 | B-S | B-S |
| F / D = 4 | G / D = 2 | 7747 | 8600 | B | B |
| | G / D = 4 | 7107 | 8173 | B | B |
| | G / D = 6 | 7379 | 7750 | B | B |
| | G / D = 8 | 6665 | 7529 | B | B |
| F / D = 6 | G / D = 2 | 7007 | 7890 | B | B |
| | G / D = 4 | 7834 | 7450 | B-S | B |
| | G / D = 6 | 7637 | 7589 | B | S |
| | G / D = 8 | 7286 | 7050 | B | B |

Table 6.2 Results & comparisons of experimental with numerical failure loads and failure modes of the composite material
(Series A, E/D=4)
(B = bearing mode, S = shear-out mode, N = net-tension mode)

| Series A E / D = 4 | | Failure Load (N) | | Failure Mode | |
|---|---|---|---|---|---|
| | | Experimental | Numerical | Exp. | Num. |
| F / D = 2 | G / D = 2 | 6856 | 7884 | B | B |
| | G / D = 4 | 7612 | 8754 | B | B |
| | G / D = 6 | 6869 | 7900 | B | B |
| | G / D = 8 | 6450 | 7418 | B-S | B-S |
| F / D = 4 | G / D = 2 | 7426 | 8625 | B | B |
| | G / D = 4 | 8621 | 9914 | B | B |
| | G / D = 6 | 7380 | 8487 | B | B |
| | G / D = 8 | 6495 | 7469 | B | B |
| F / D = 6 | G / D = 2 | 6126 | 7045 | B | B |
| | G / D = 4 | 7525 | 7200 | B | B |
| | G / D = 6 | 7752 | 8915 | B | B |
| | G / D = 8 | 7478 | 8600 | B | B |

Table 6.4 Results & comparisons of experimental with numerical failure loads and failure modes of the composite material
(Series B, E/D=2)
(B = bearing mode, S = shear-out mode, N = net-tension mode)

| Series B E / D = 2 | | Failure Load (N) | | Failure Mode | |
|---|---|---|---|---|---|
| | | Experimental | Numerical | Exp. | Num. |
| F / D = 2 | G / D = 2 | 6374 | 7459 | B-S | B |
| | G / D = 4 | 7815 | 8518 | B-S | B |
| | G / D = 6 | 8201 | 8898 | B-S | B |
| | G / D = 8 | 6105 | 8435 | B-S | B-S |
| F / D = 4 | G / D = 2 | 6419 | 7000 | B-S | B |
| | G / D = 4 | 6789 | 7591 | B-S | B |
| | G / D = 6 | 6853 | 7800 | B-S | B |
| | G / D = 8 | 5996 | 8244 | B-S | B |
| F / D = 6 | G / D = 2 | 7351 | 6675 | B-S | B |
| | G / D = 4 | 6507 | 6156 | B-S | B |
| | G / D = 6 | 6937 | 7388 | B-S | B |
| | G / D = 8 | 7968 | 8387 | B-S | B-S |

Table 6.5 Results & comparisons of experimental with numerical failure loads and failure modes of the composite material
(Series B, E/D=3)
(B = bearing mode, S = shear-out mode, N = net-tension mode)

| **Series B E / D = 3** | | **Failure Load (N)** | | **Failure Mode** | |
|---|---|---|---|---|---|
| | | **Experimental** | **Numerical** | **Exp.** | **Num.** |
| **F / D = 2** | **G / D = 2** | 6950 | 7750 | B | B |
| | **G / D = 4** | 7734 | 8169 | B | B |
| | **G / D = 6** | 7150 | 7651 | B-S | B |
| | **G / D = 8** | 5995 | 7500 | B-S | B-S |
| **F / D = 4** | **G / D = 2** | 7355 | 7238 | B | B |
| | **G / D = 4** | 7255 | 7800 | B | B-S |
| | **G / D = 6** | 7033 | 8025 | B | B |
| | **G / D = 8** | 7474 | 7529 | B | B |
| **F / D = 6** | **G / D = 2** | 7170 | 6843 | B | B |
| | **G / D = 4** | 7437 | 7250 | B | S |
| | **G / D = 6** | 7246 | 7679 | B | S |
| | **G / D = 8** | 7419 | 7050 | B | B |

Table 6.6 Results & comparisons of experimental with numerical failure loads and failure modes of the composite material
(Series B, E/D=4)
(B = bearing mode, S = shear-out mode, N = net-tension mode)

| **Series B E / D = 4** | | **Failure Load (N)** | | **Failure Mode** | |
|---|---|---|---|---|---|
| | | **Experimental** | **Numerical** | **Exp.** | **Num.** |
| **F / D = 2** | **G / D = 2** | 7546 | 7971 | B | B |
| | **G / D = 4** | 7381 | 7750 | B | B |
| | **G / D = 6** | 6754 | 7105 | B | B |
| | **G / D = 8** | 8229 | 7418 | B-S | B-S |
| **F / D = 4** | **G / D = 2** | 7240 | 7375 | B | B |
| | **G / D = 4** | 7057 | 7268 | B | B |
| | **G / D = 6** | 7025 | 7517 | B | B |
| | **G / D = 8** | 6279 | 7469 | B | B |
| **F / D = 6** | **G / D = 2** | 6033 | 6900 | B | B |
| | **G / D = 4** | 7873 | 8146 | B | S |
| | **G / D = 6** | 7113 | 7765 | B | S |
| | **G / D = 8** | 6763 | 8600 | B | B |

"Failure Load" vs. "Hole Ratio" diagrams can be seen below in Figure 6.7 to 6.30 while;

- Figure 6.7 (a to d) indicates the experimental results of the effect of F/D ratio on the failure load in test series A while G/D changes
- Figure 6.8 (a to d) indicates the experimental results of the effect of F/D ratio on the failure load in test series B while G/D changes
- Figure 6.9 (a to c) indicates the experimental results of the effect of G/D ratio on the failure load in test series A while E/D changes
- Figure 6.10 (a to c) indicates the experimental results of the effect of G/D ratio on the failure load in test series B while E/D changes
- Figure 6.11 (a to c) indicates the experimental results of the effect of G/D ratio on the failure load in test series A while F/D changes
- Figure 6.12 (a to c) indicates the experimental results of the effect of G/D ratio on the failure load in test series B while F/D changes
- Figure 6.13 (a to d) indicates the numerical results of the effect of F/D ratio on the failure load in test series A while G/D changes
- Figure 6.14 (a to d) indicates the numerical results of the effect of F/D ratio on the failure load in test series B while G/D changes
- Figure 6.15 (a to c) indicates the numerical results of the effect of G/D ratio on the failure load in test series A while E/D changes
- Figure 6.16 (a to c) indicates the numerical results of the effect of G/D ratio on the failure load in test series B while E/D changes
- Figure 6.17 (a to c) indicates the numerical results of the effect of G/D ratio on the failure load in test series A while F/D changes
- Figure 6.18 (a to c) indicates the numerical results of the effect of G/D ratio on the failure load in test series B while F/D changes
- Figure 6.19, 6.20 & 6.21 indicates the experimental & numerical failure load values of the whole versions of test series A while E/D changes

- Figure 6.22, 6.23 & 6.24 indicate the experimental & numerical failure load values of the whole versions of test series B while E/D changes
- Figure 6.25, 6.26 & 6.27 indicate differences of the experimental results of Series A & Series B while E/D changes
- Figure 6.28, 6.29 & 6.30 indicate differences of the numerical results of Series A & Series B while E/D changes

When we focused on the results figure by figure these comments below can be written;

At G/D=2 in experimental results of Series A, for E/D=2 & E/D=4 the failure load values are nearly the same for each F/D. In addition, the maximum value occurred at F/D=4 (Fig. 6.7.a)

At G/D=4 in experimental results of Series A, for E/D=2 there is no remarkable change of the failure load values. For E/D=3, the failure load increased linearly while F/D increased. (Fig. 6.7.b)

At G/D=6 in experimental results of Series A, for E/D=2 there is no remarkable change of the failure load values while F/D changes. For E/D=3 & E/D=4, failure load values are the same for each F/D, and increased linearly while F/D increased. (Fig. 6.7.c)

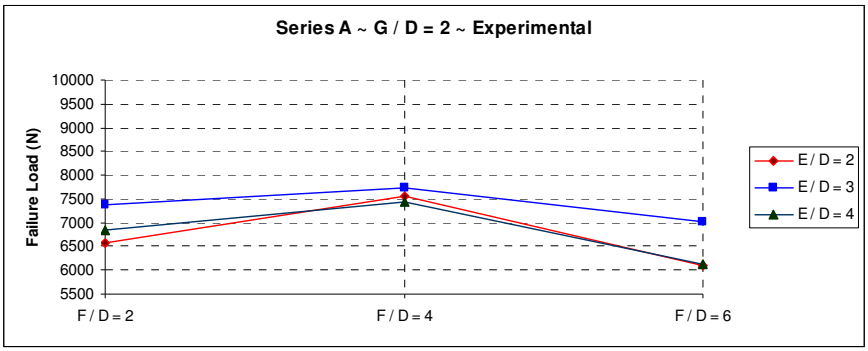
At G/D=8 in experimental results of Series A, for each E/Ds failure load values are the same for each F/D, and increased linearly while F/D increased. (Fig. 6.7.d)

At G/D=2 in experimental results of Series B, for E/D=3 failure load values are the same for all F/D (Fig. 6.8.a)

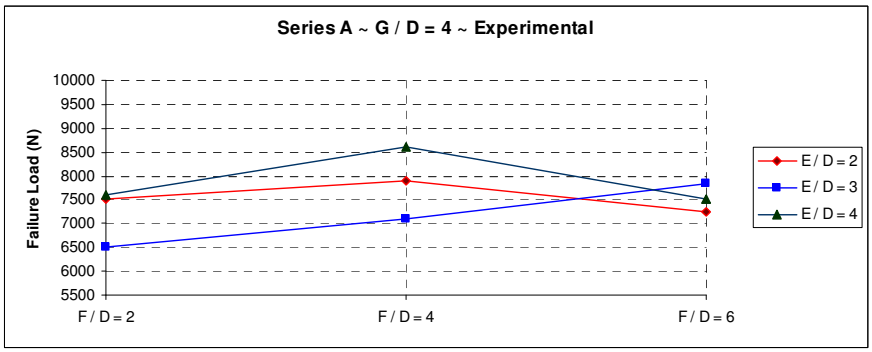
At G/D=4 in experimental results of Series B, for E/D=3 failure load values did not change for all F/D (Fig. 6.8.b)

At G/D=6 in experimental results of Series B, for each E/Ds except E/D=2 failure load values are the same for each F/D. For E/D=2 & F/D=2 the failure load is greater than the others. (Fig. 6.8.c)

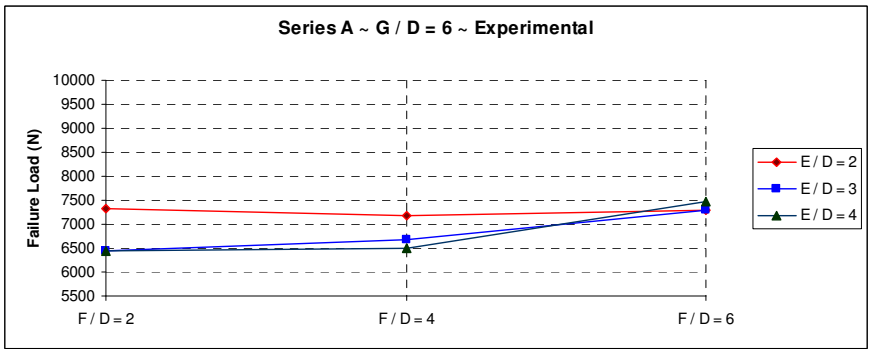
At G/D=8 in experimental results of Series B, for E/D=2 & E/D=3 failure load values are the same for F/D=2. (Fig. 6.8.d)



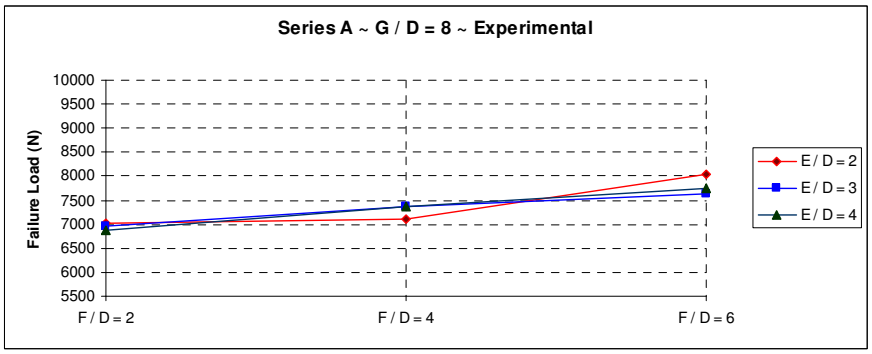

(a)




(b)

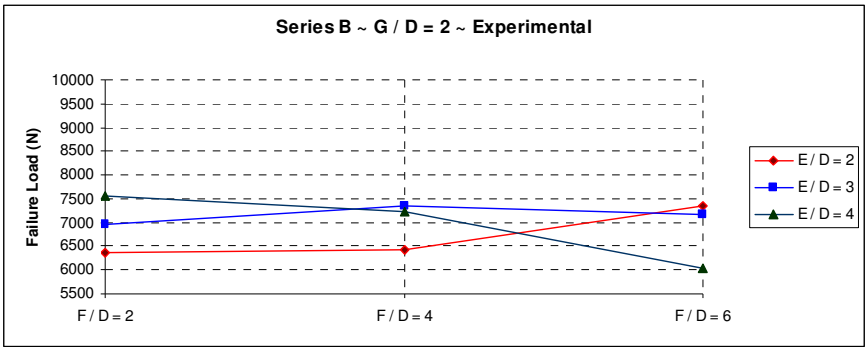



(c)

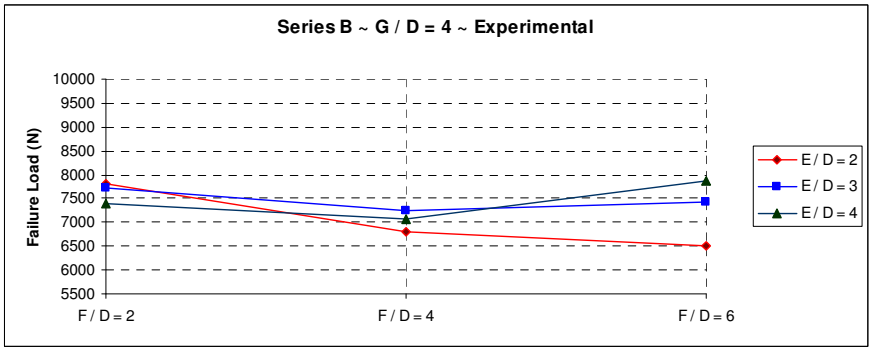



(d)

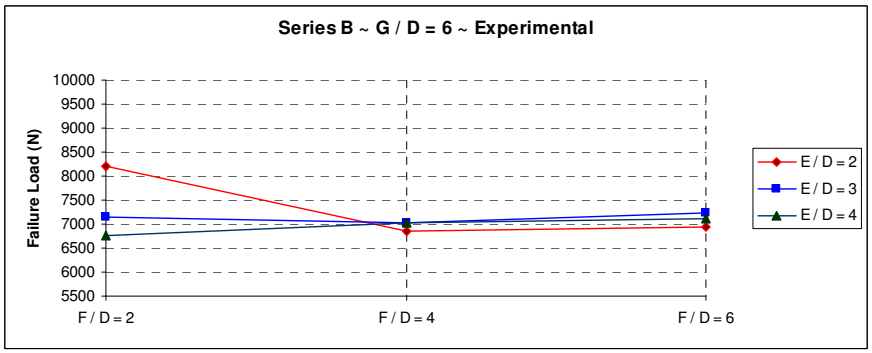
Figure 6.7 The experimental results of the effect of F/D ratio on the failure load (Change of G/D ratio in test series A)



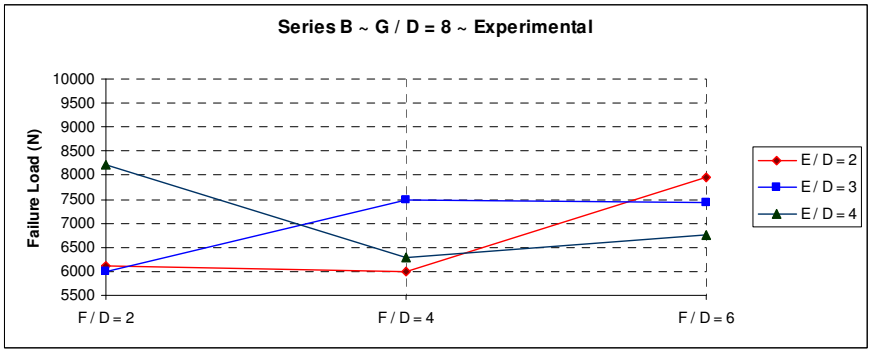

(a)




(b)




(c)




(d)

Figure 6.8 The experimental results of the effect of F/D ratio on the failure load (Change of G/D ratio in test series B)

At E/D=2 in experimental results of Series A, for F/D=2 & F/D=3 failure load values are the same for each G/D. For F/D=6 failure load increased with G/D. For F/D=4 failure load decreased with G/D (Fig. 6.9.a)

At E/D=3 in experimental results of Series A, F/D=2 & F/D=4 failure load values decreased with G/D. (Fig. 6.9.b)

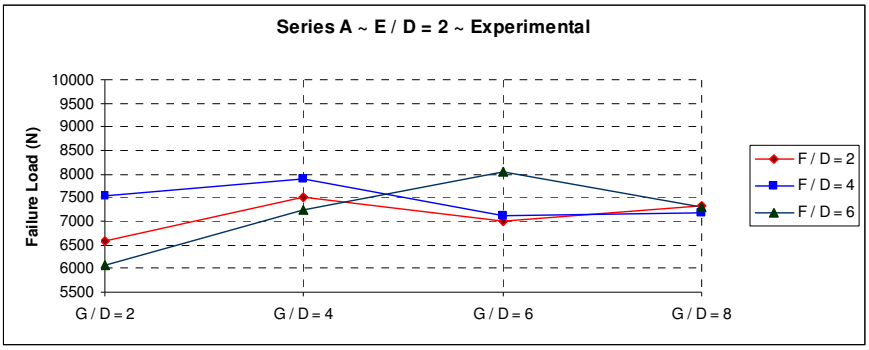
At E/D=4 in experimental results of Series A, F/D=2 & F/D=4 failure load values showed the similar behaviour while G/D increased. The maximum value occurred at F/D=4 & G/D=4 arrangement (Fig. 6.9.c)

At E/D=2 in experimental results of Series B, F/D=2 & F/D=4 failure load values are the same while G/D=8. The similar situation occurred for G/D=2 (Fig. 6.10.a)

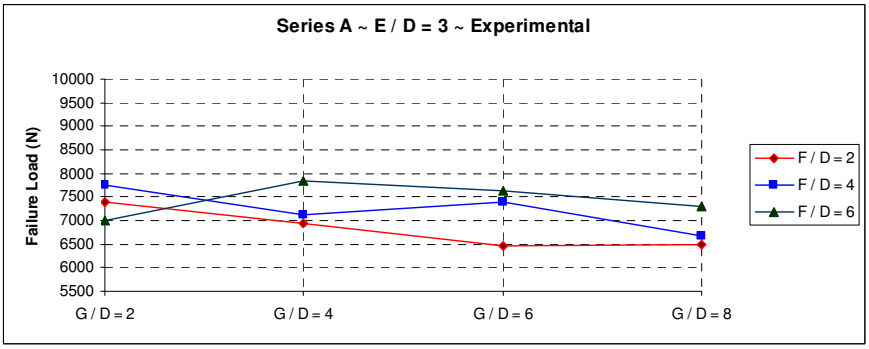
At E/D=3 in experimental results of Series B, for each G/Ds except G/D=8 failure load values are the same for each F/D. For G/D=8 & F/D=2 the failure load is the minimum. (Fig. 6.10.b)

At F/D=4 in experimental results of Series A, for all E/Ds the failure load values are the same for each G/D. The similar situation occurred for G/D=6. While G/D changes from 4 to 8 all E/Ds tends to decrease. (Fig. 6.11.b)

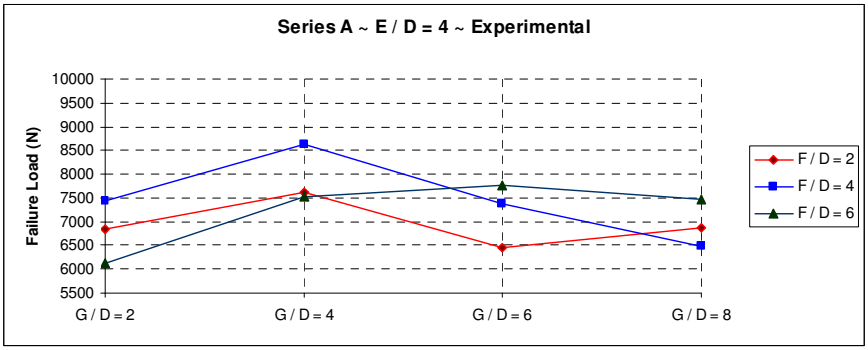
At F/D=4 in experimental results of Series B, for all E/Ds the failure load values are the same for each G/D=4 & G/D=8. While G/D=8 & E/D=3 the failure load value is maximum. (Fig. 6.12.b)




(a)

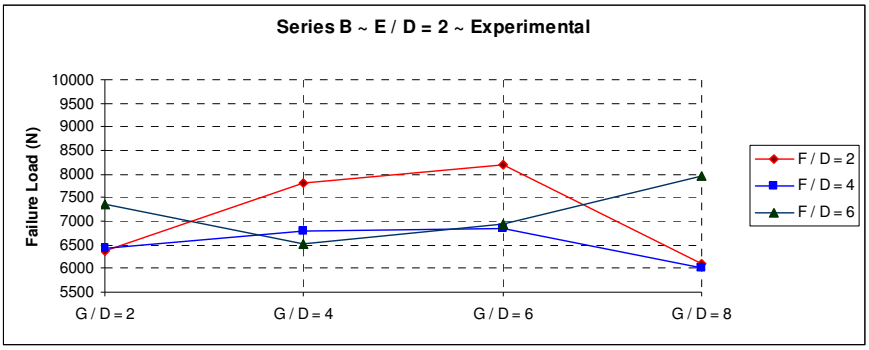



(b)

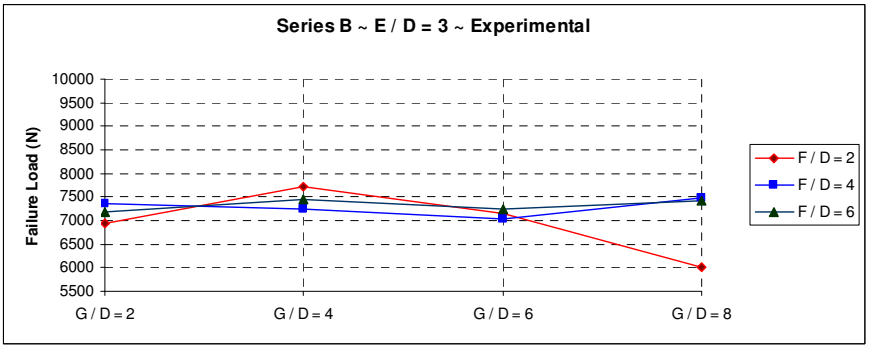



(c)

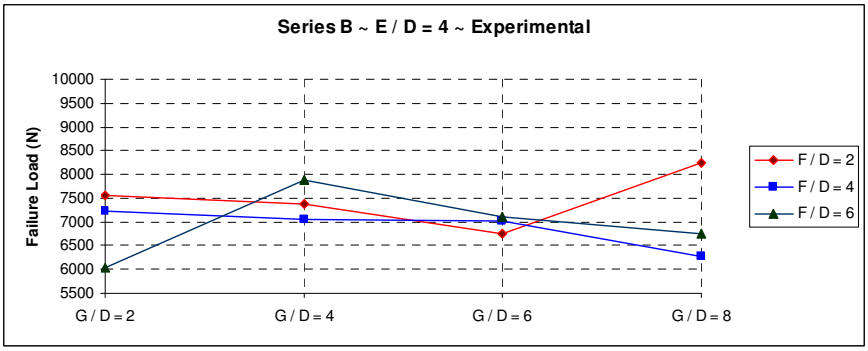
Figure 6.9 The experimental results of the effect of G/D ratio on the failure load (Change of E/D ratio in test series A)




(a)

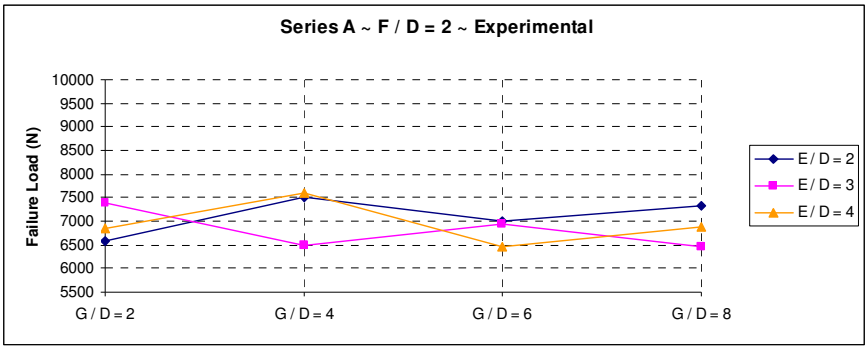



(b)

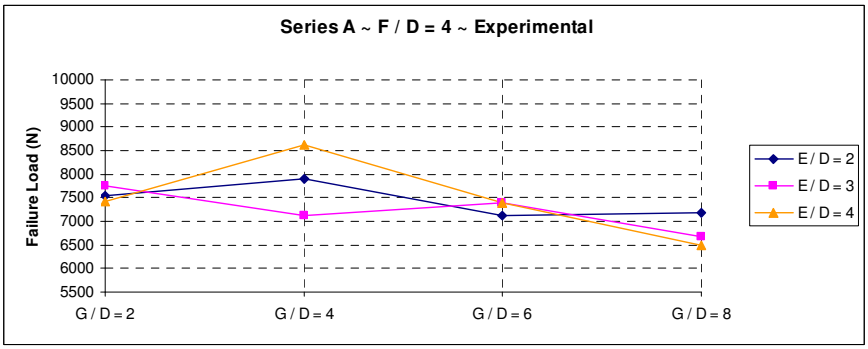



(c)

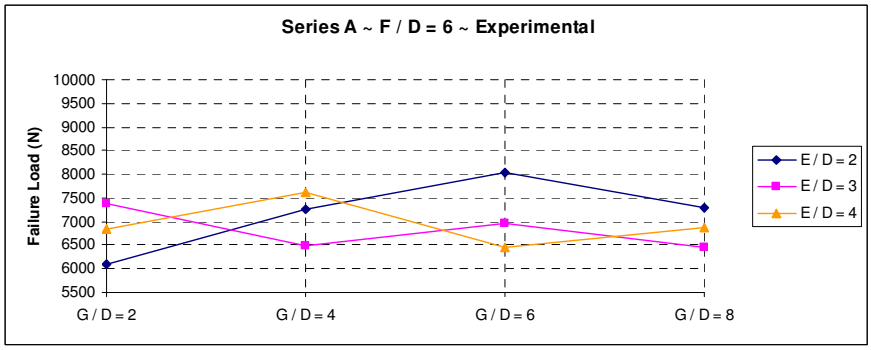
Figure 6.10 The experimental results of the effect of G/D ratio on the failure load (Change of E/D ratio in test series B)




(a)

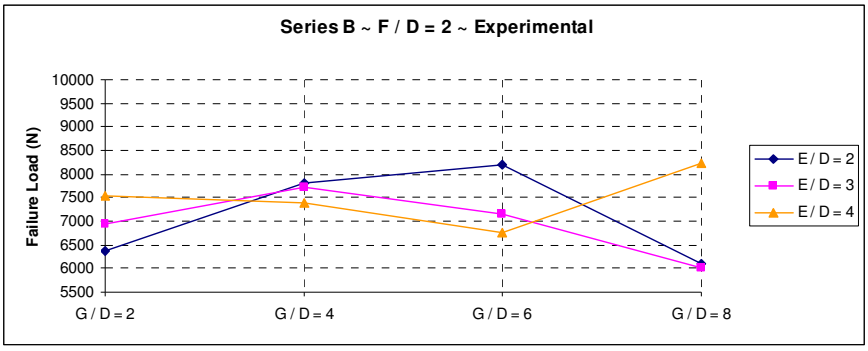



(b)

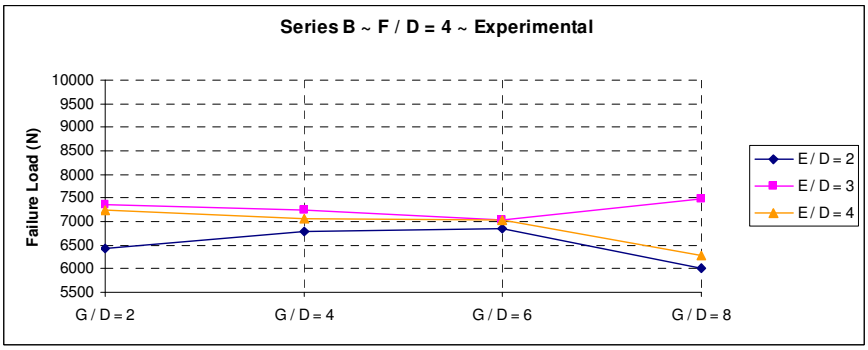



(c)

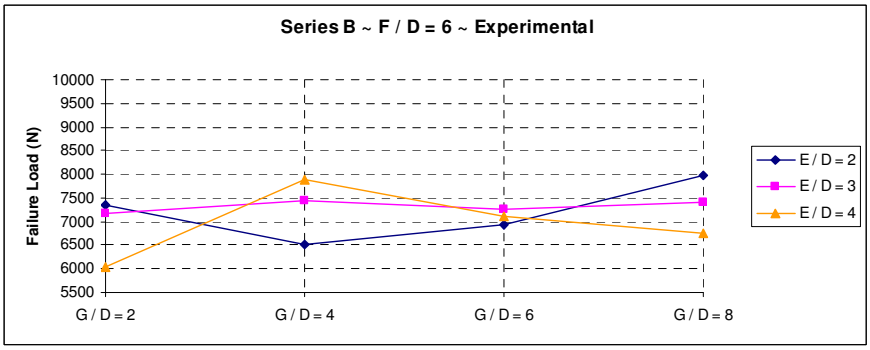
Figure 6.11 The experimental results of the effect of G/D ratio on the failure load (Change of F/D ratio in test series A)




(a)




(b)




(c)

Figure 6.12 The experimental results of the effect of G/D ratio on the failure load (Change of F/D ratio in test series B)

At experimental result of E/D=2 in series A, the minimum failure load value occured at two regions, one of them is at the minimum values of G/D & F/Ds, the other one is the minimum value of G/D & the maximum value of F/D. The failure load tended to decrease while G/D & F/D decreased. (Fig.6.19.a)

At numerical result of E/D=2 in series A, in opposition to experimental result the maximum failure load value occurred at the minimum values of G/D & F/D (Fig.6.19.b)

At experimental result of E/D=3 in series A, the minimum failure load value occurred at the maximum value of G/D and the minimum value of F/Ds. The maximum failure load value occurred at G/D=4 & F/D=6. The failure load tended to decrease while G/D increased & F/D decreased. (Fig.6.20.a)

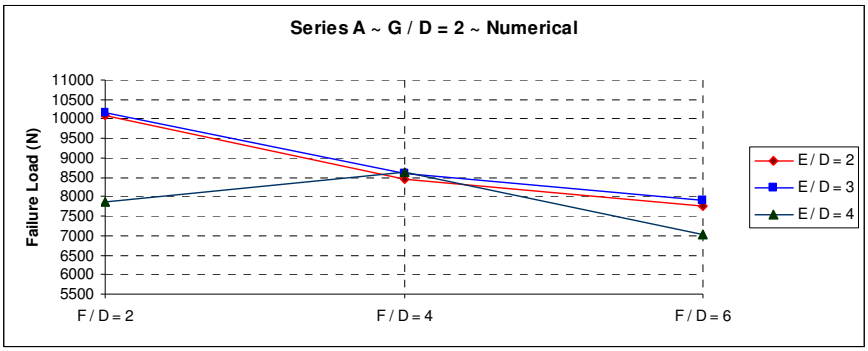
At numerical result of E/D=3 in series A, the minimum failure load value occurred at the maximum values of G/D & F/Ds. The maximum failure load value occurred at G/D=2 & F/D=2. (Fig.6.20.b)

At experimental result of E/D=4 in series A, the maximum failure load value occurred at G/D & F/D=4. The failure load tended to decrease while G/D increased & F/D decreased. (Fig.6.21.a)

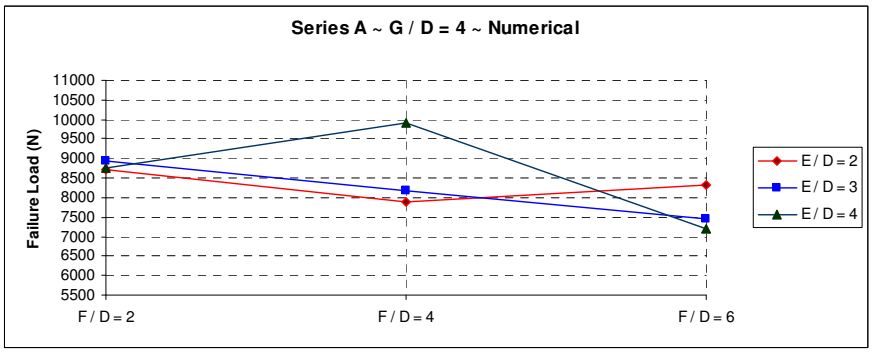
At numerical result of E/D=4 in series A, the maximum failure load value occurred at G/D & F/D=4. The failure load tended to decrease while G/D increased & F/D decreased similar to the experimental result. (Fig.6.21.b)

At experimental result of E/D=2 in series B, the minimum failure load value occured at the maximum value of G/D & the minimum value of F/D. The failure load tended to decrease while G/D increased & F/D decreased. (Fig.6.22.a)

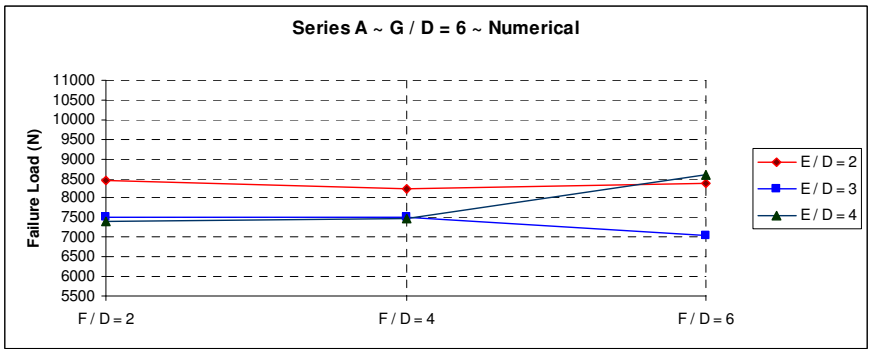
At numerical result of E/D=2 in series B, the maximum failure load value occurred at G/D=6 & the minimum value of F/D(2). The failure load tended to decrease while G/D increased & F/D decreased similar to the experimental result. (Fig.6.22.b)



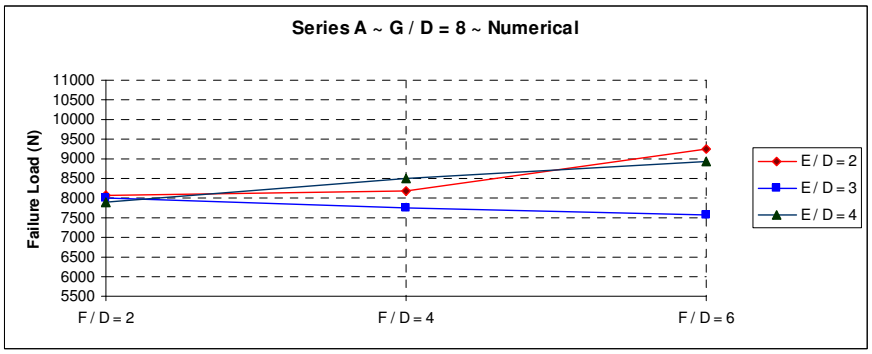

(a)




(b)

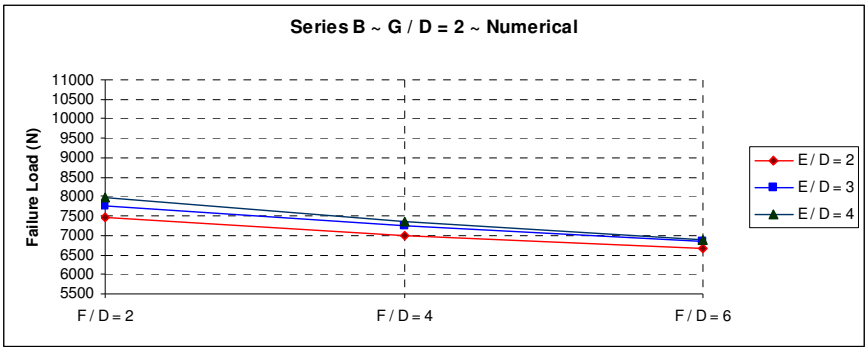



(c)

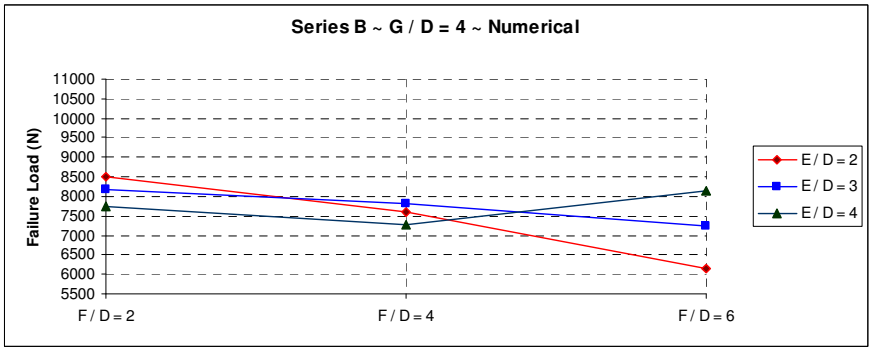



(d)

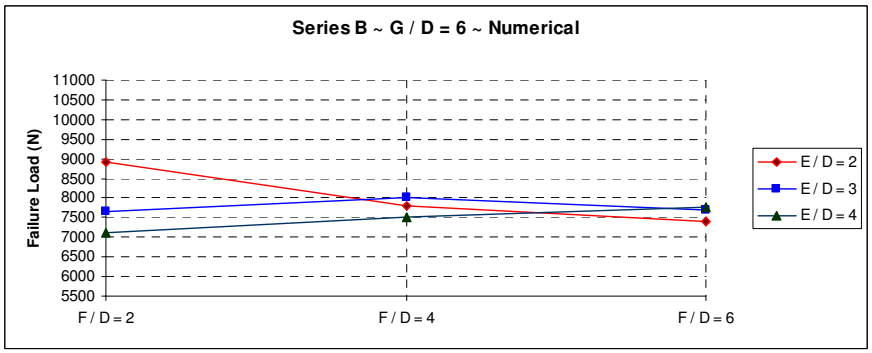
Figure 6.13 The numerical results of the effect of F/D ratio on the failure load (Change of G/D ratio in test series A)



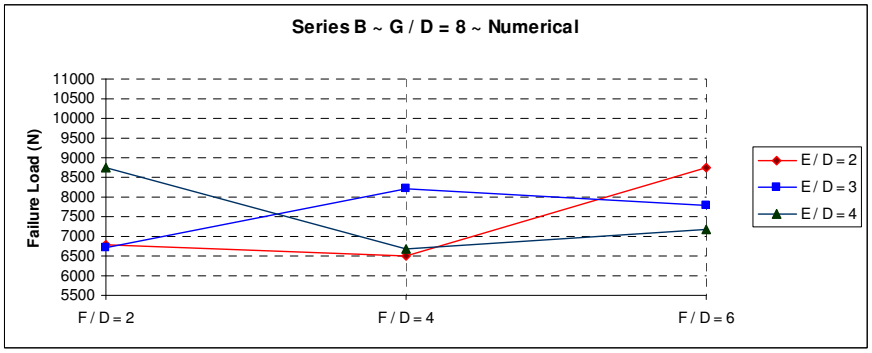

(a)




(b)

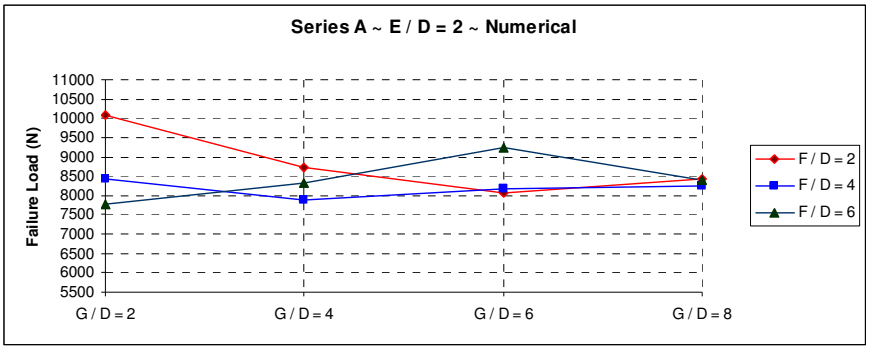



(c)

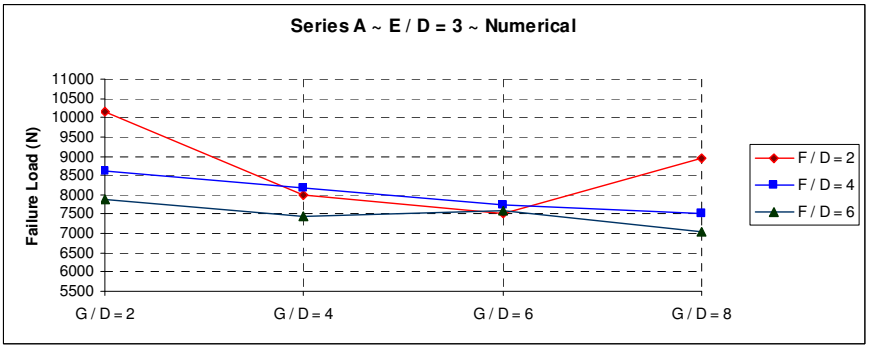



(d)

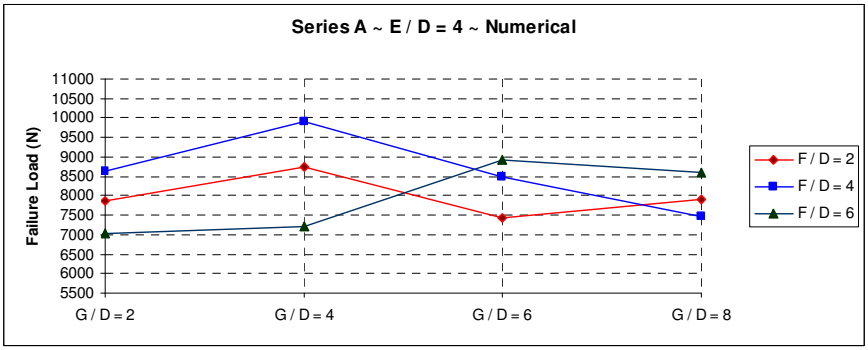
Figure 6.14 The numerical results of the effect of F/D ratio on the failure load (Change of G/D ratio in test series B)




(a)

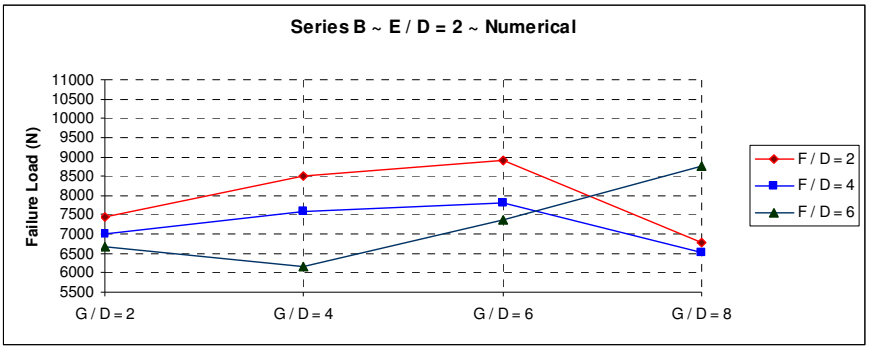



(b)

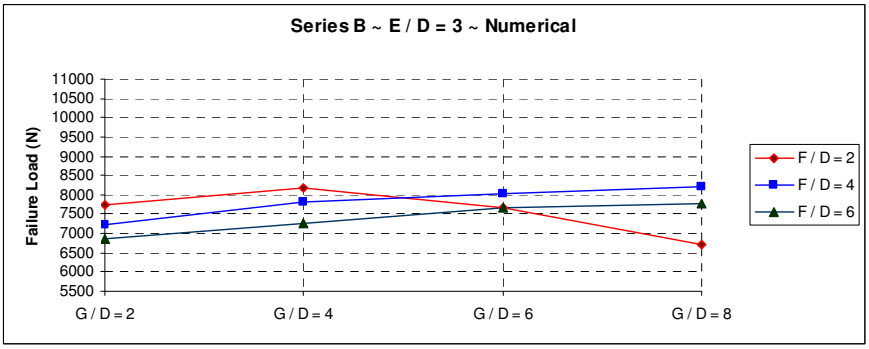



(c)

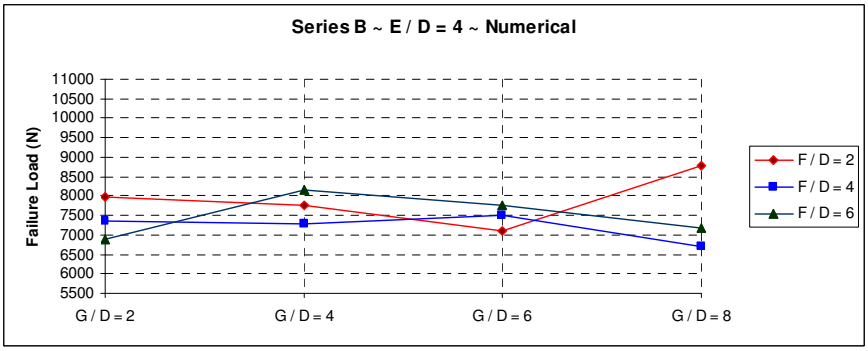
Figure 6.15 The numerical results of the effect of G/D ratio on the failure load (Change of E/D ratio in test series A)




(a)

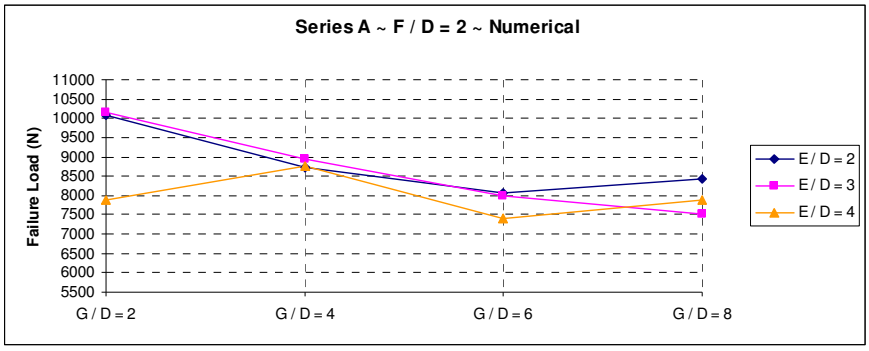



(b)

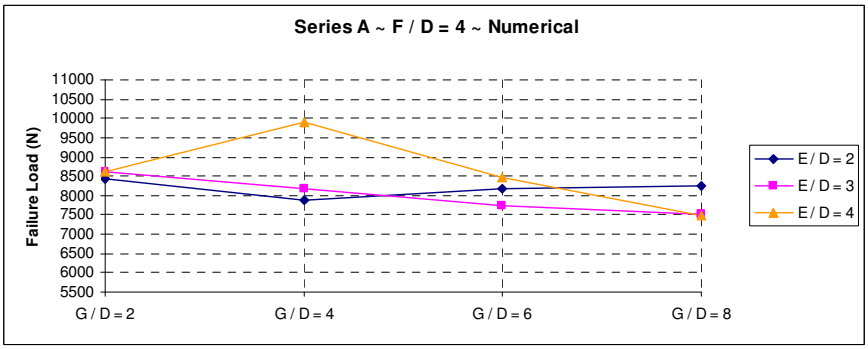



(c)

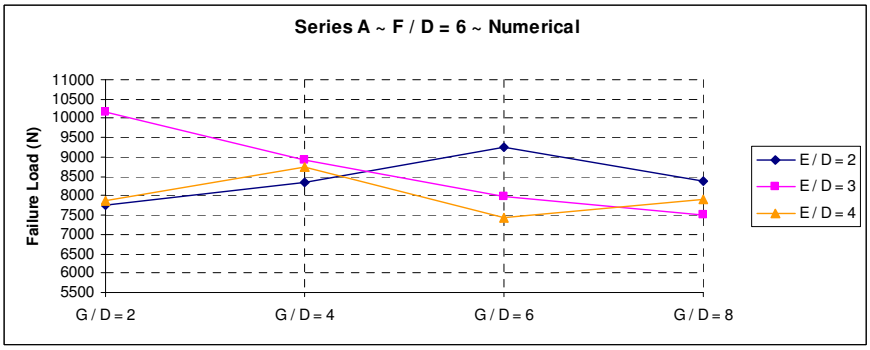
Figure 6.16 The numerical results of the effect of G/D ratio on the failure load (Change of E/D ratio in test series B)




(a)

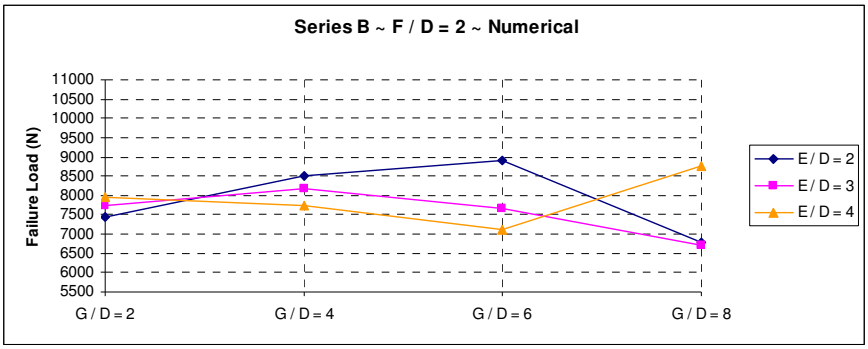



(b)

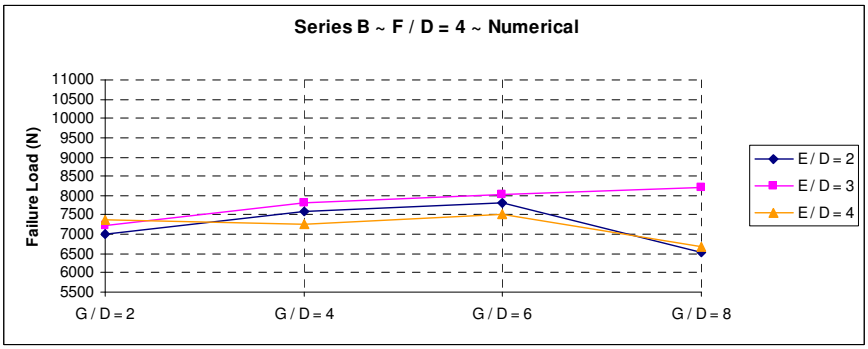



(c)

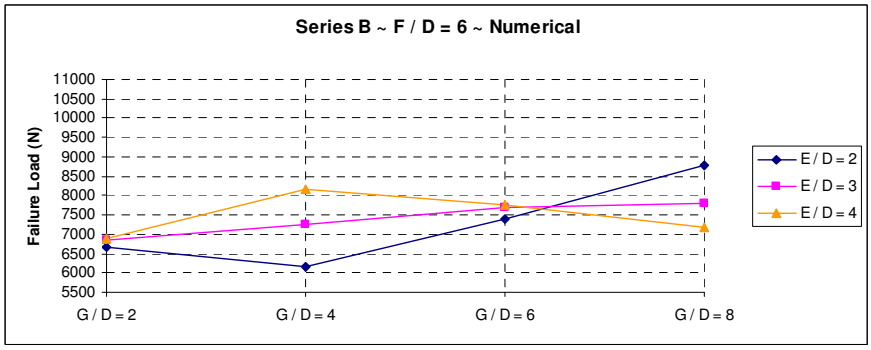
Figure 6.17 The numerical results of the effect of G/D ratio on the failure load (Change of F/D ratio in test series A)




(a)

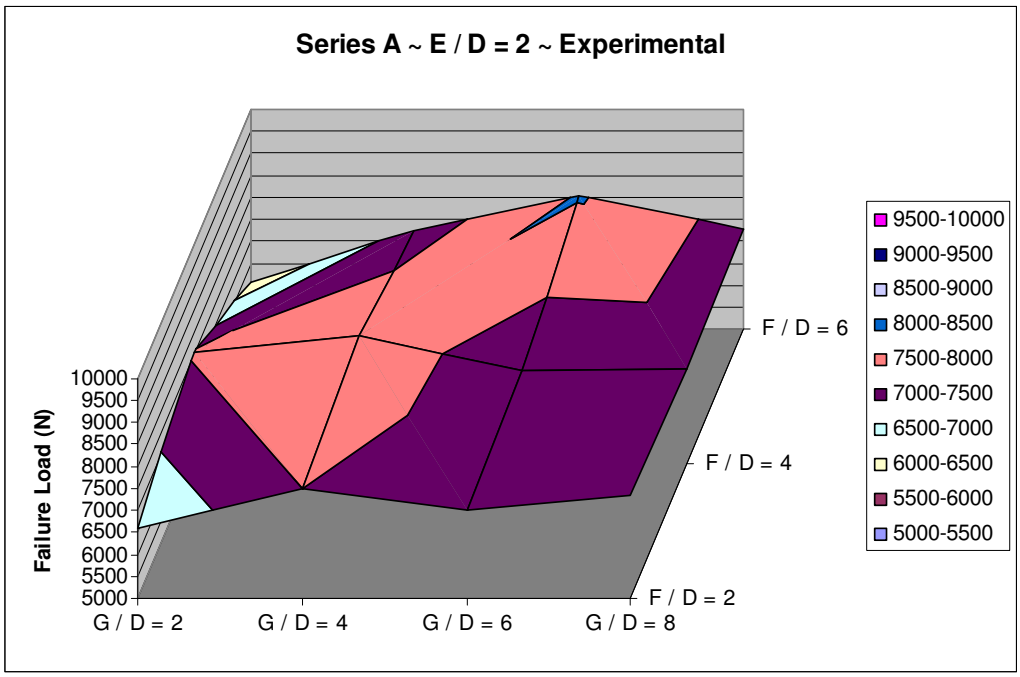



(b)

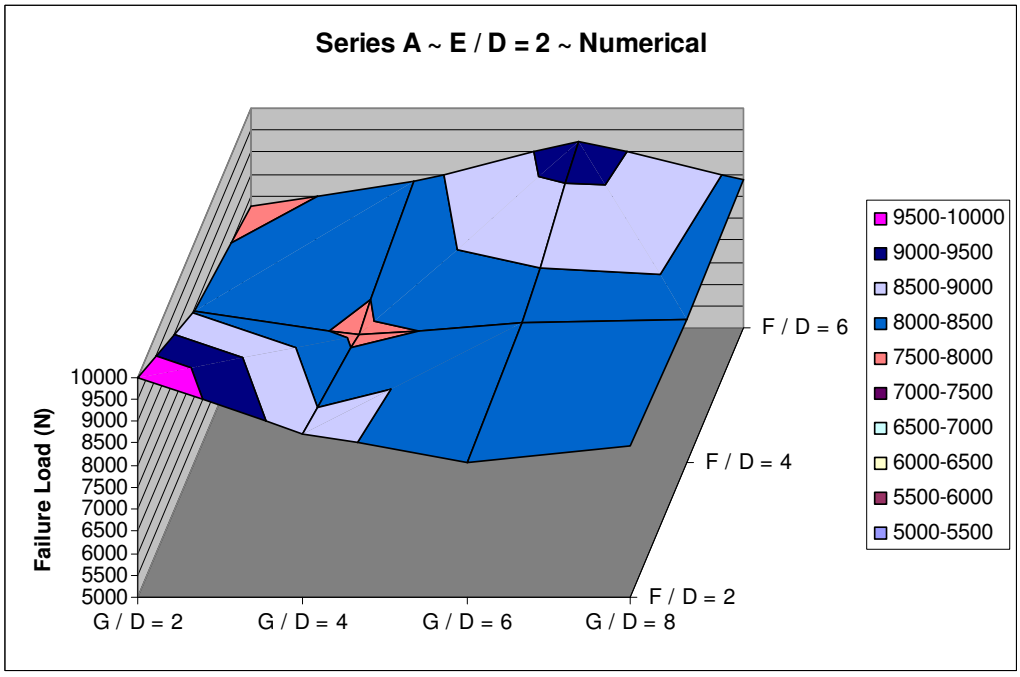



(c)

Figure 6.18 The numerical results of the effect of G/D ratio on the failure load (Change of F/D ratio in test series B)

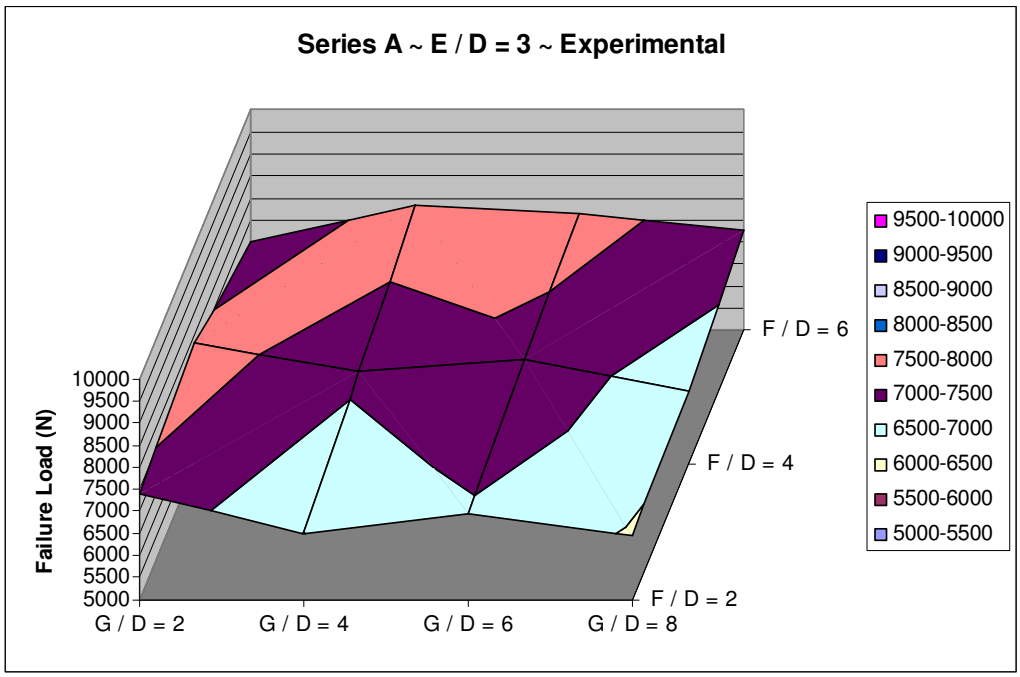



(a)

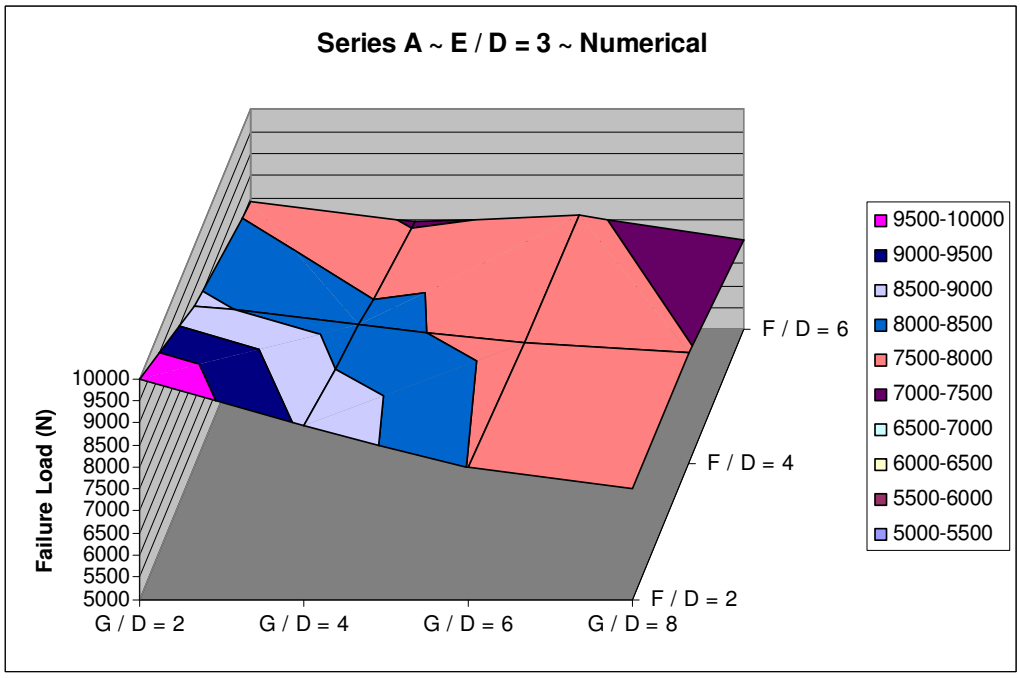



(b)

Figure 6.19 The experimental & numerical results of the composite plates with E/D=2 in Series A

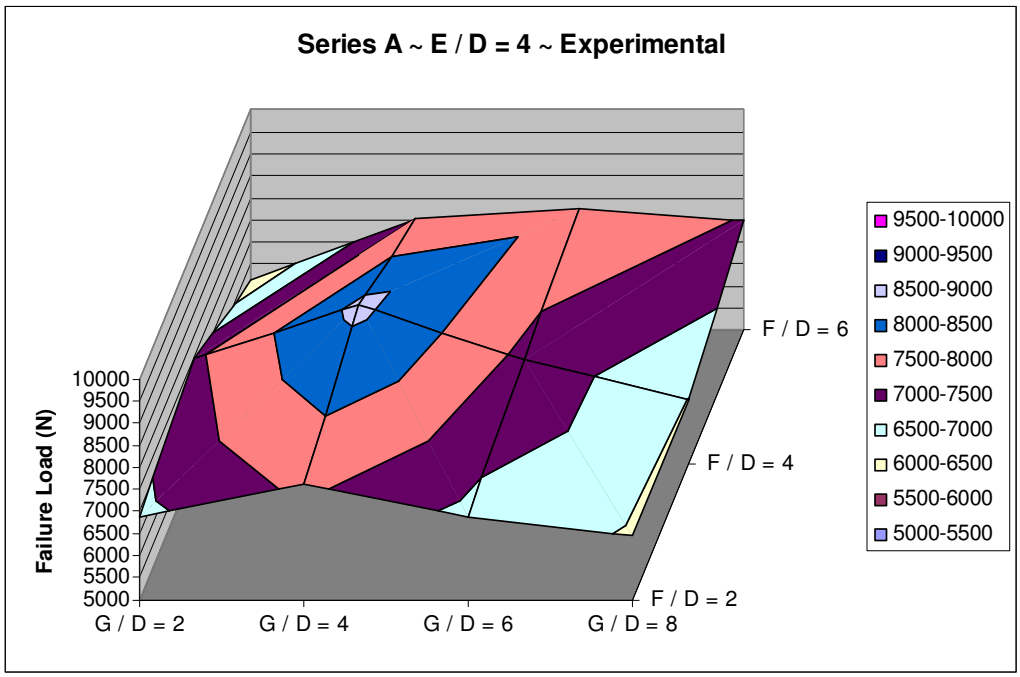



(a)

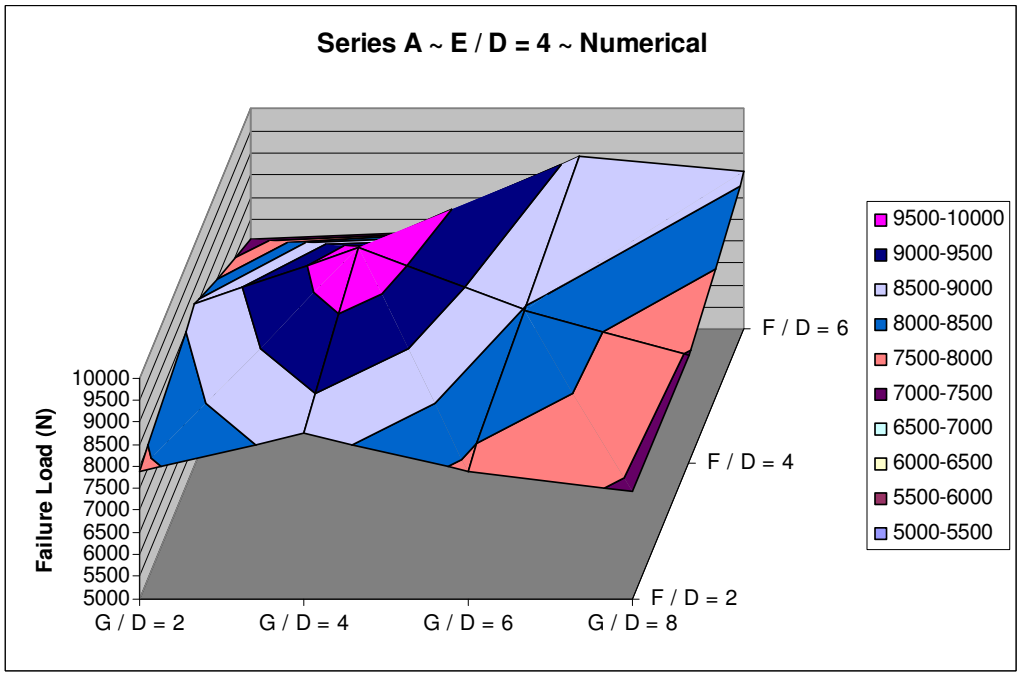



(b)

Figure 6.20 The experimental & numerical results of the composite plates with E/D=3 in Series A

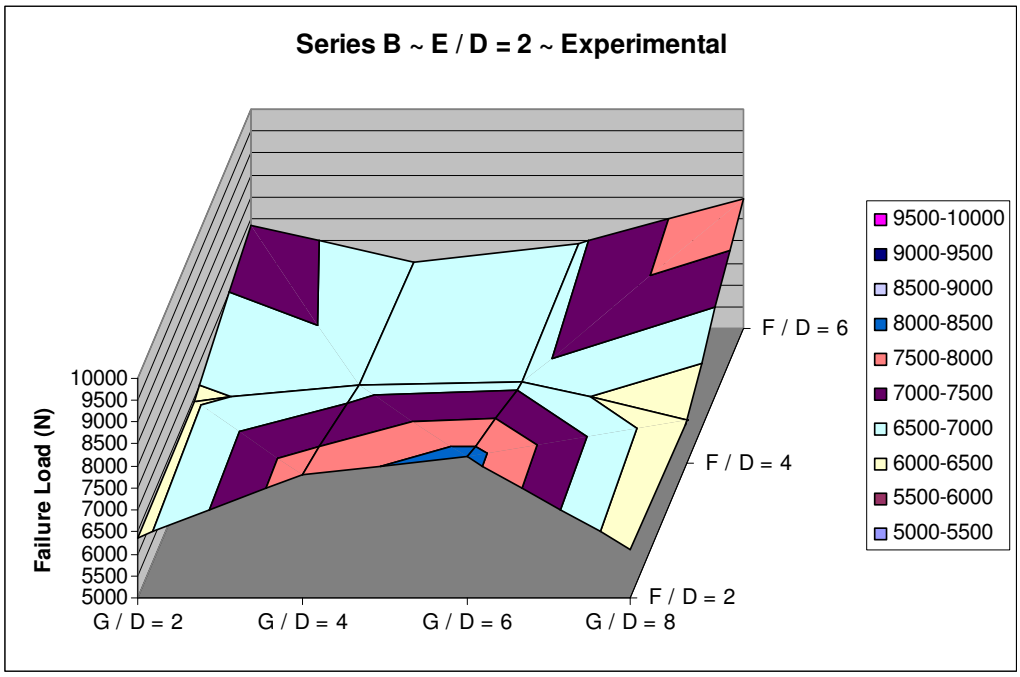



(a)

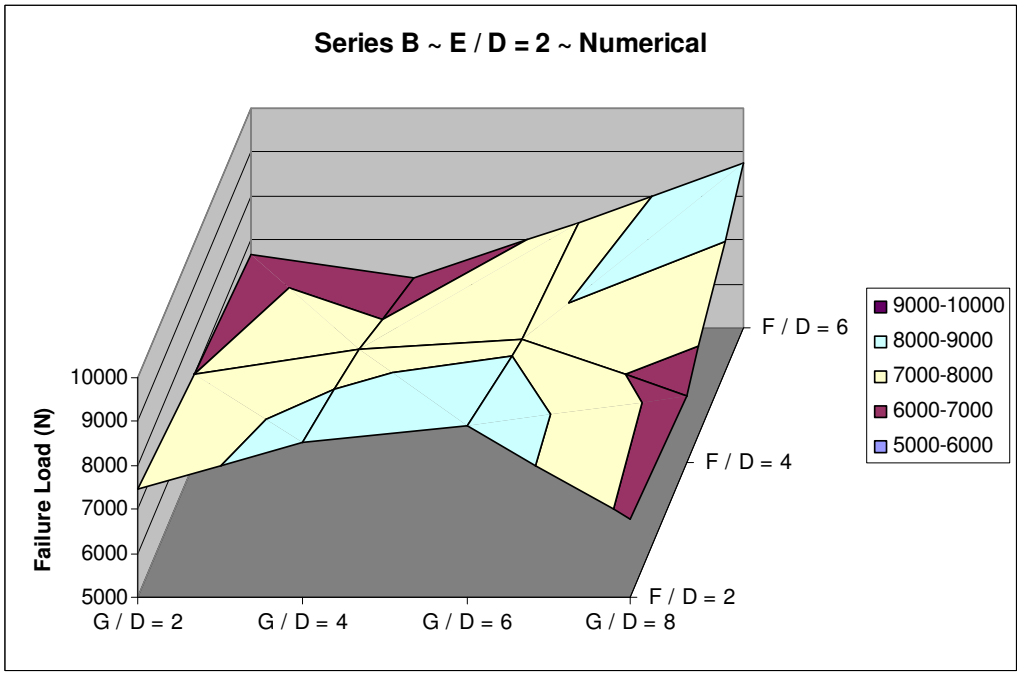



(b)

Figure 6.21 The experimental & numerical results of the composite plates with E/D=4 in Series A




(a)




(b)

Figure 6.22 The experimental & numerical results of the composite plates with E/D=2 in Series B

At experimental result of E/D=3 in series B, the minimum failure load value occurred at the maximum value of G/D & the minimum value of F/D. At the other values, the failure load has the similar values in same interval. (Fig.6.23.a)

At numerical result of E/D=3 in series B, the minimum failure load value occurred at two regions, one of them is the maximum value of G/D & the minimum value of F/D, the other one is the minimum value of G/D & the maximum value of F/D. (Fig.6.23.b)

At experimental result of E/D=4 in series B, the minimum failure load value occured at the minimum value of G/D and the maximum value of F/D. At the values of G/D=2 to G/D=6 and F/D=2 to F/D=4 the failure load have the values in same interval. (6.24.a)

At numerical result of E/D=4 in series B, the minimum failure load value occurred at the maximum value of G/D and F/D=4. If the charts have observed, it can be say that the experimental and numerical results have the same behavior in this case. (Fig.6.24.b)

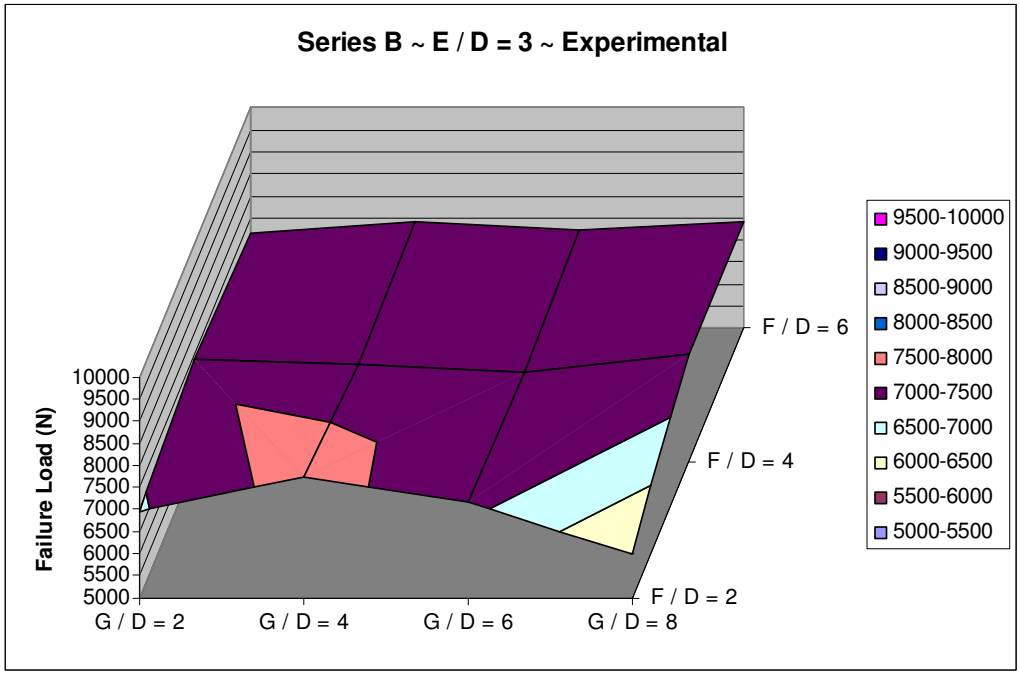
At the experimental results of E/D=2 and F/D=2, Series A & Series B have the same failure load value for G/D=2 & G/D=4, and it tended to increase. (Fig. 6.25.a)

At the numerical results of E/D=2 and F/D=2, Series A & Series B have nearly the same failure load value for G/D=4. (Fig. 6.28.a)

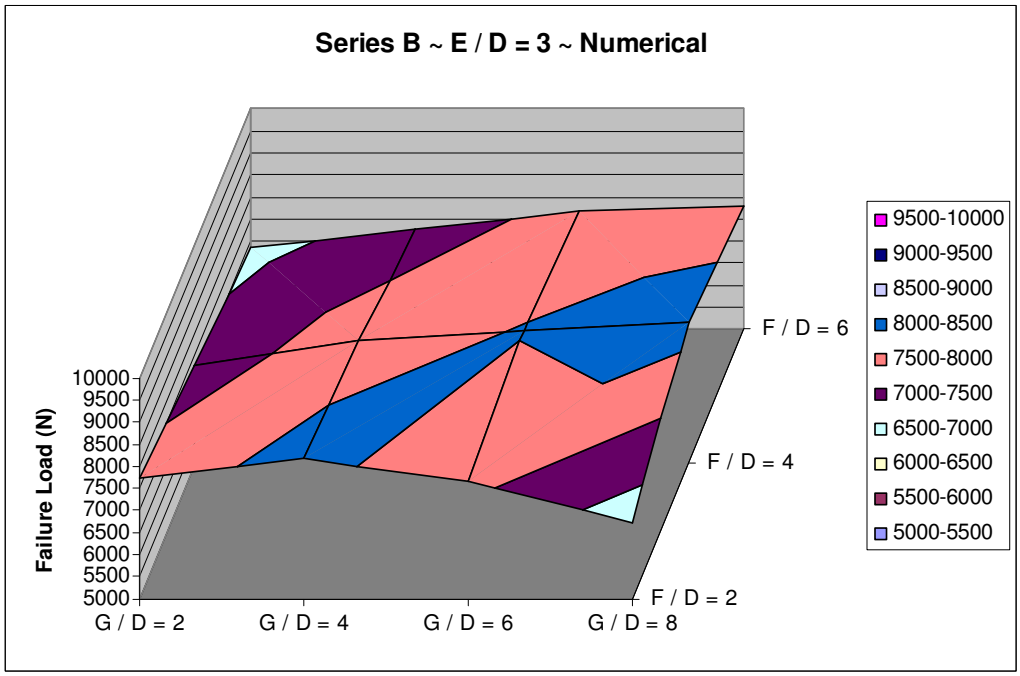
At the experimental results of E/D=2 and F/D=4, Series A & Series B have the same failure load value only for G/D=6. (Fig. 6.25.b)

At the numerical results of E/D=2 and F/D=4, Series A & Series B have nearly the same failure load value for G/D=4 & G/D=6. (Fig. 6.28.b)

At the experimental results of E/D=2 and F/D=6, Series A & Series B did not show the similarity between each other (Fig. 6.25.c) At the numerical results of E/D=2 and F/D=6, Series A & Series B showed similarity between each other (Fig. 6.28.c)

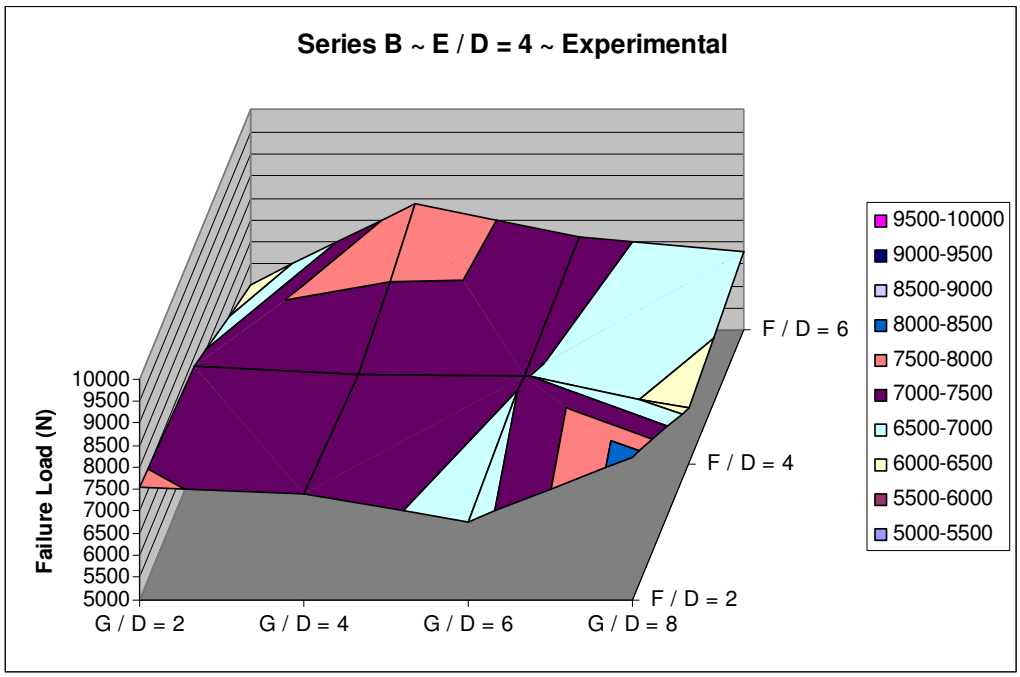



(a)

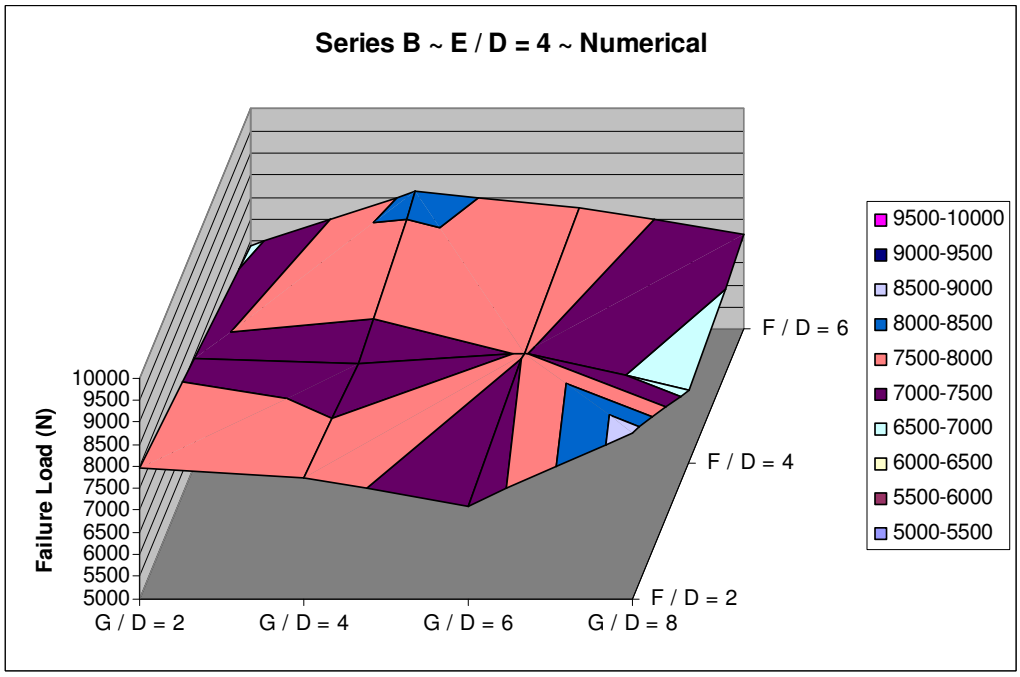



(b)

Figure 6.23 The experimental & numerical results of the composite plates with E/D=3 in Series B)

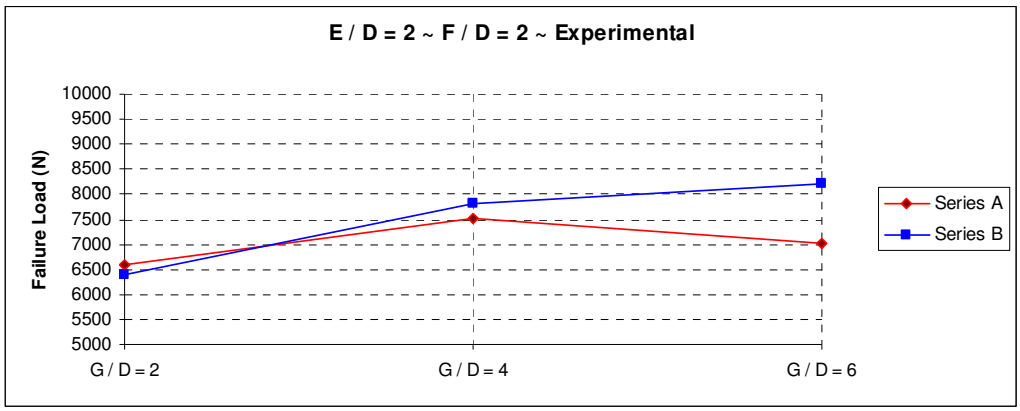



(a)

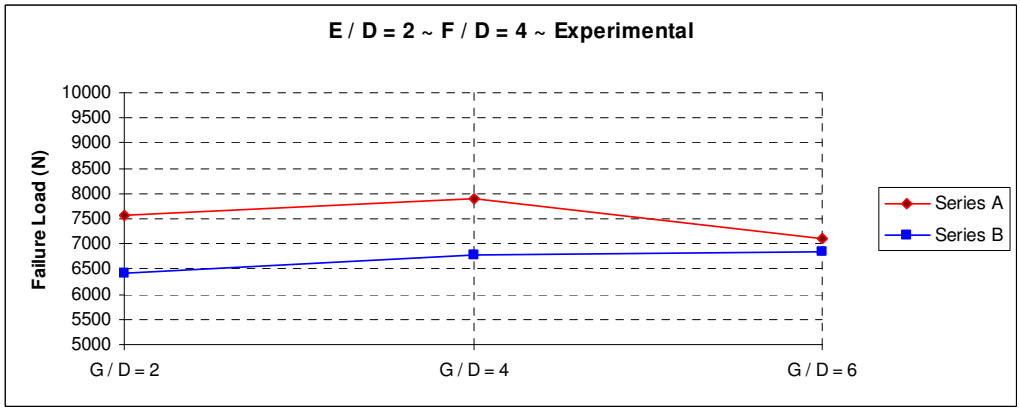



(b)

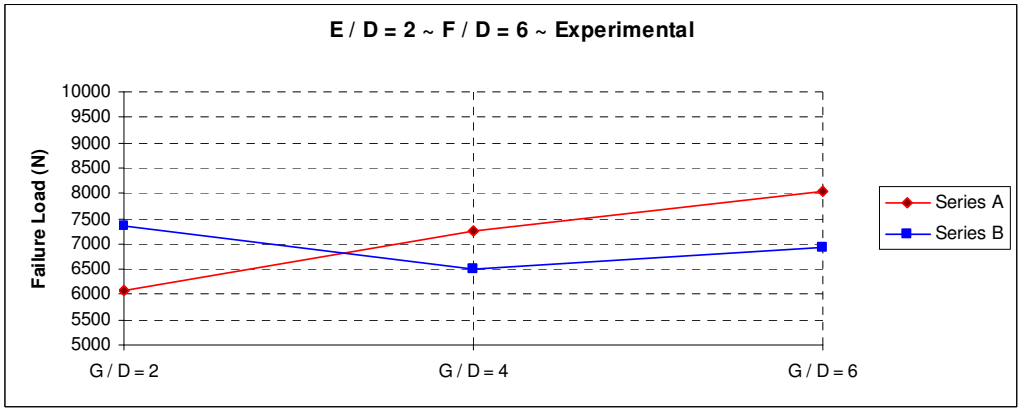
Figure 6.24 The experimental & numerical results of the composite plates with E/D=4 in Series B)




(a)

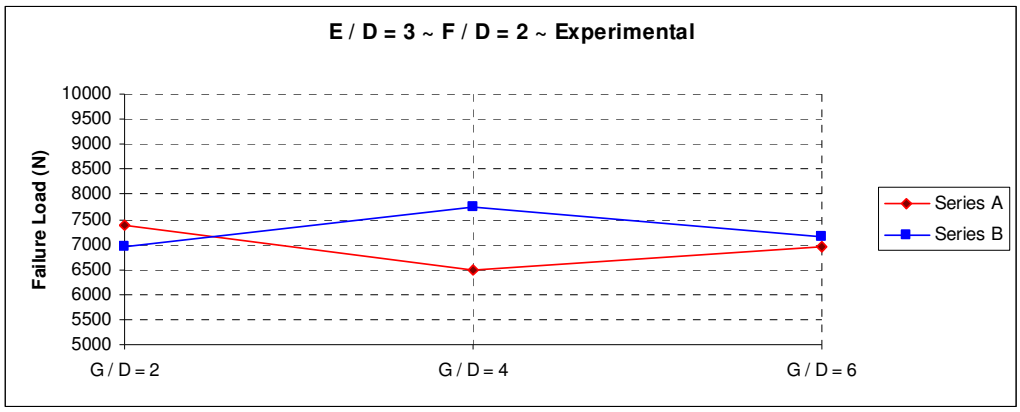



(b)

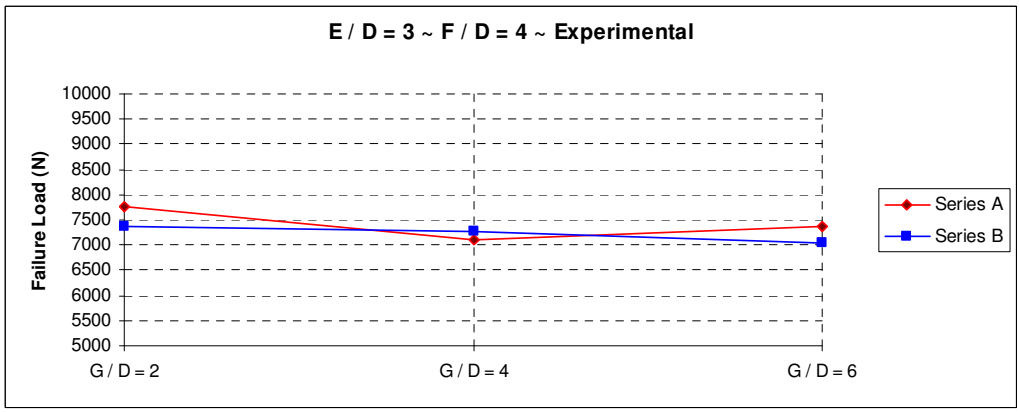



(c)

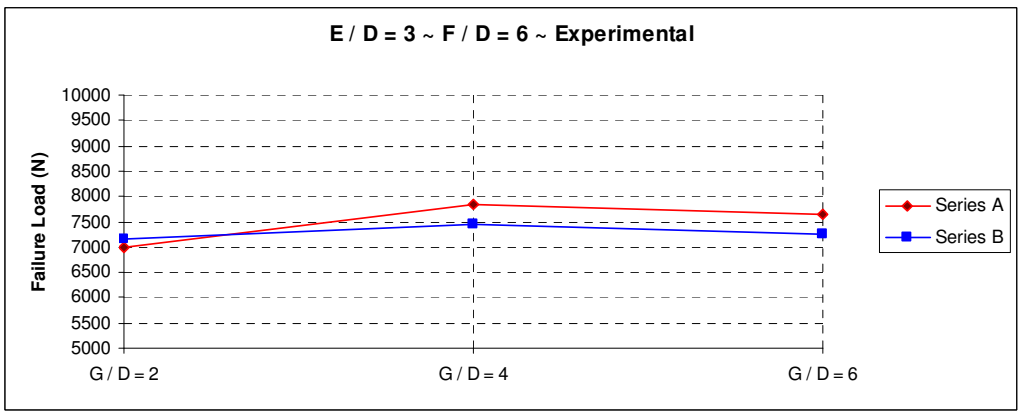
Figure 6.25 The experimental results of Series A & Series B for E/D=2




(a)

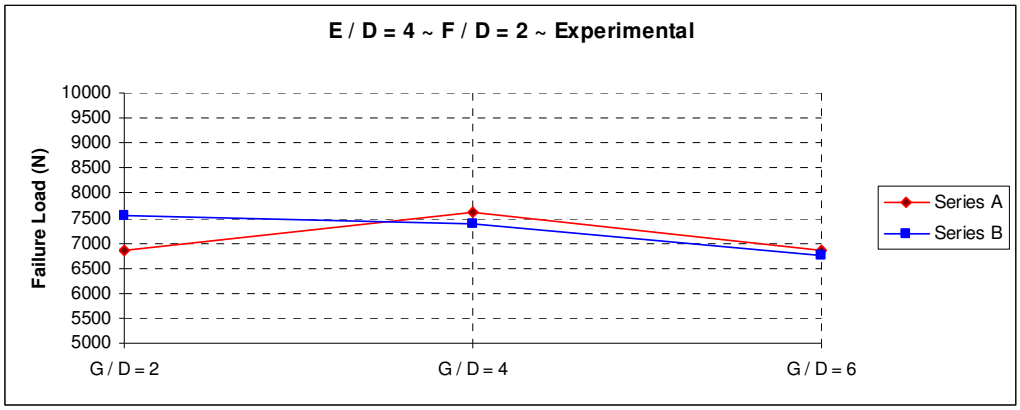



(b)

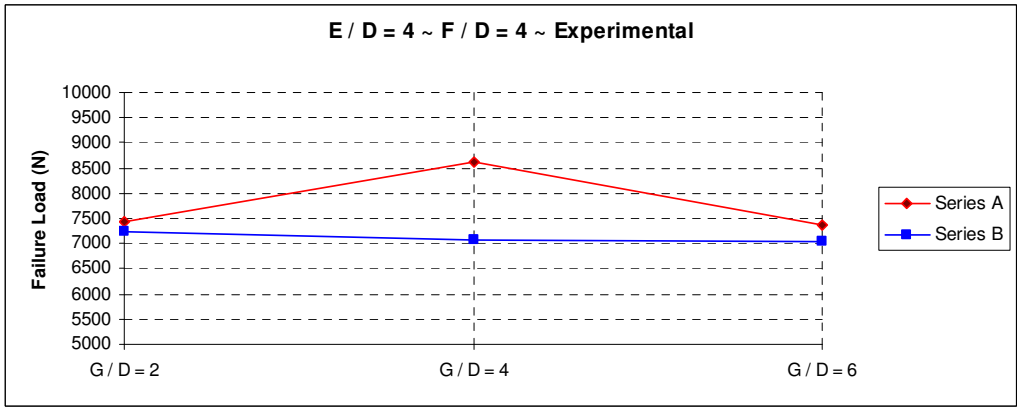



(c)

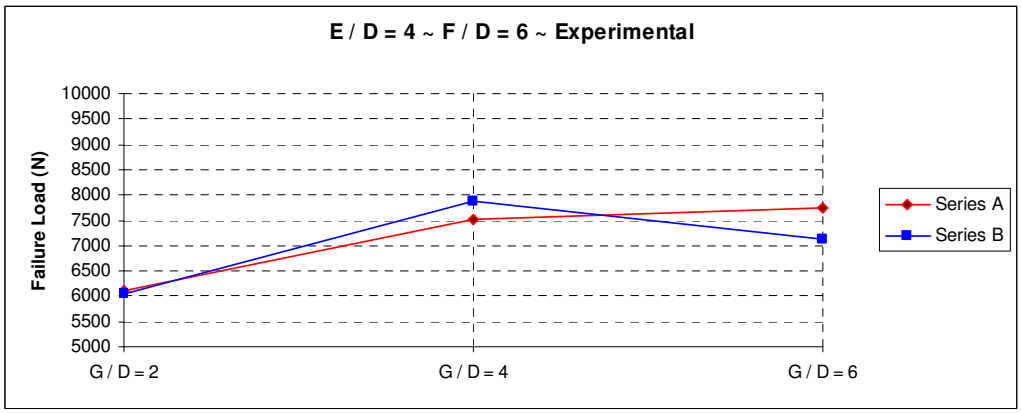
Figure 6.26 The experimental results of Series A & Series B for E/D=3




(a)

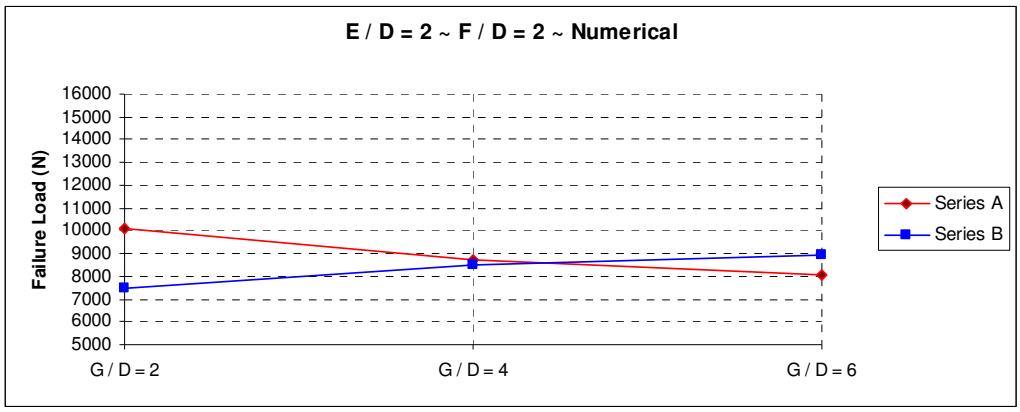



(b)

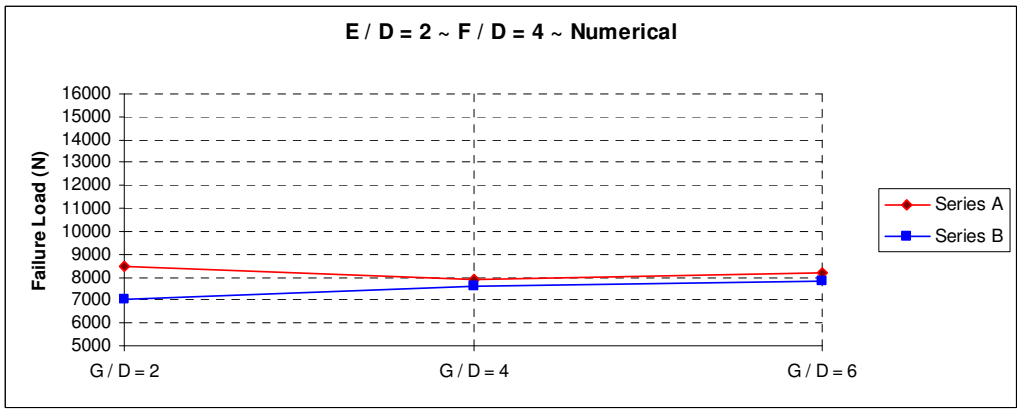



( c )

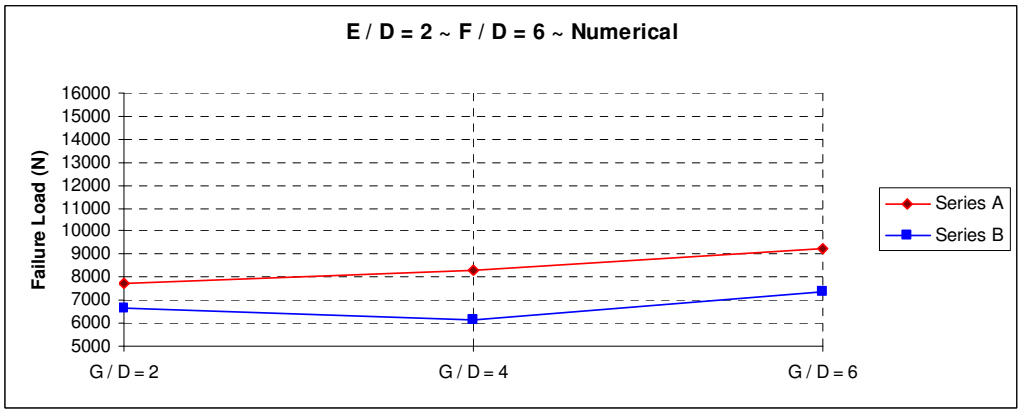
Figure 6.27 The experimental results of Series A & Series B for E/D=4




(a)




(b)




(c)

Figure 6.28 The numerical results of Series A & Series B for E/D=2

At the experimental results of E/D=3 and F/D=2, Series A & Series B have the same failure load value only for G/D=2 & G/D=6. (Fig. 6.26.a)

At the numerical results of E/D=3 and F/D=2, Series A & Series B have nearly the same failure load value for G/D=4 & G/D=6 and it tends to decrease.(Fig. 6.29.a)

At the experimental results of E/D=3 and F/D=4, Series A & Series B have the same failure load value for each G/D. There is a great similarty occured between each other (Fig. 6.26.b)

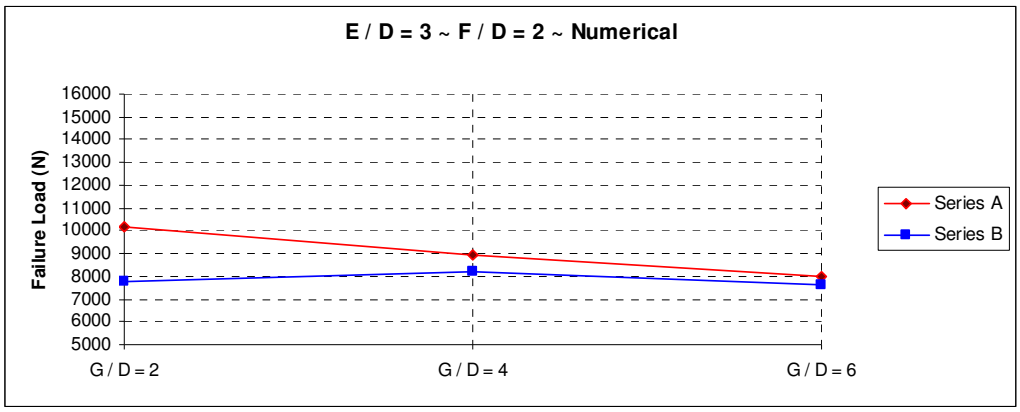
At the numerical results of E/D=3 and F/D=4, Series A & Series B have nearly the same failure load value for G/D=4 & G/D=6. (Fig. 6.29.b)

At the experimental results of E/D=3 and F/D=6, Series A & Series B showed similarity between each other (Fig. 6.26.c)

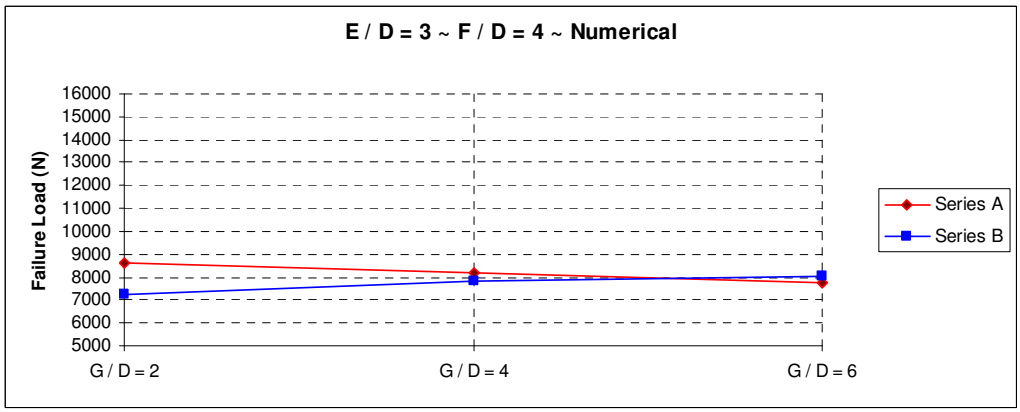
At the numerical results of E/D=3 and F/D=6, Series A & Series B have nearly the same failure load value for each G/Ds. (Fig. 6.29.c)

At the experimental results of E/D=4 and F/D=2, Series A & Series B have nearly the same failure load value for G/D=4 & G/D=6 and it tends to decrease. (Fig. 6.27.a)

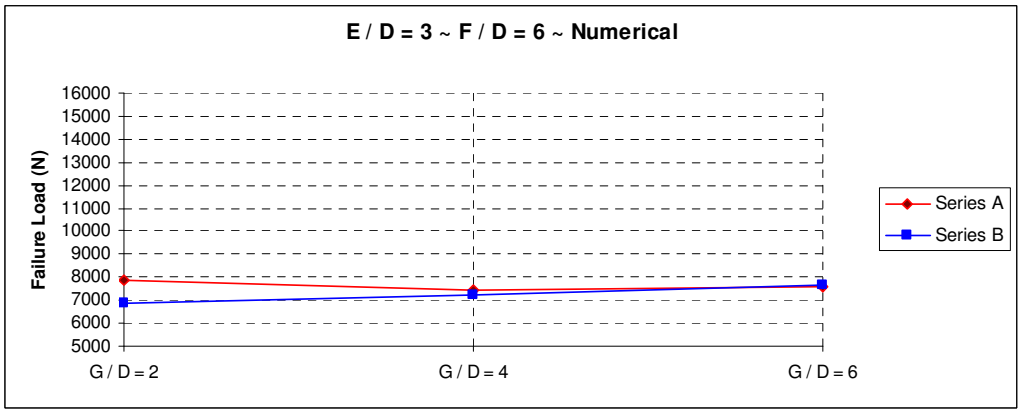
At the numerical results of E/D=4 and F/D=2, Series A & Series B have nearly the same failure load value for each G/Ds. (Fig. 6.30.a)




(a)

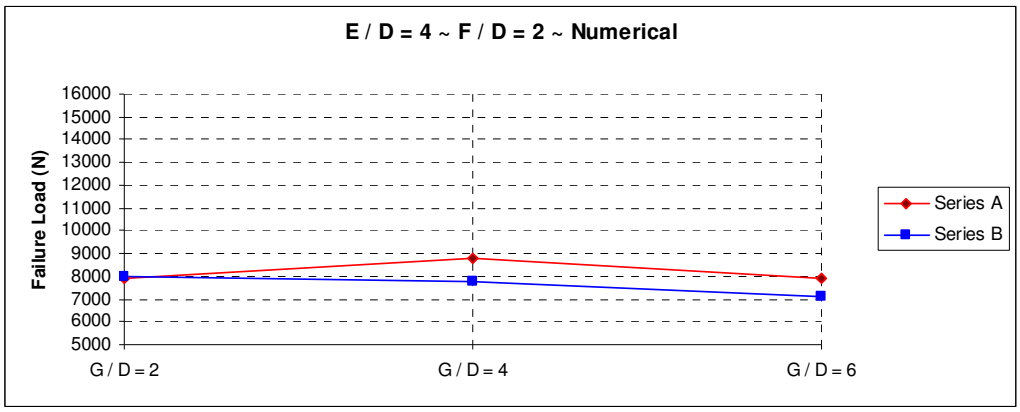



(b)

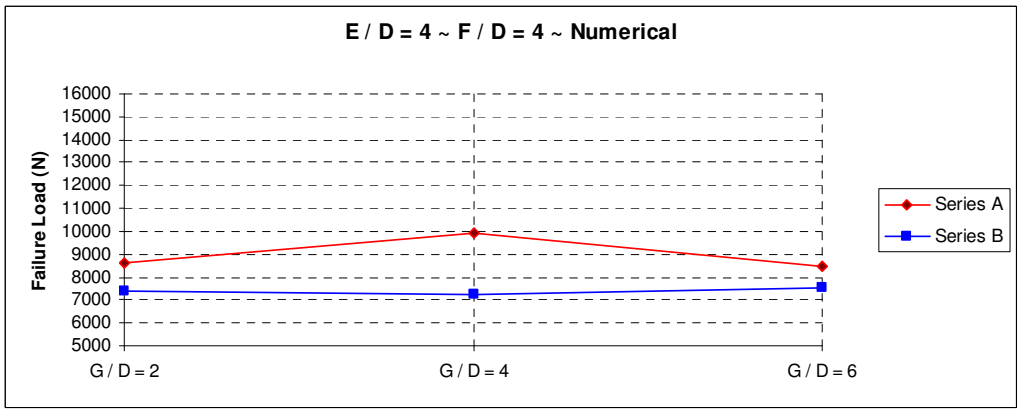



(c)

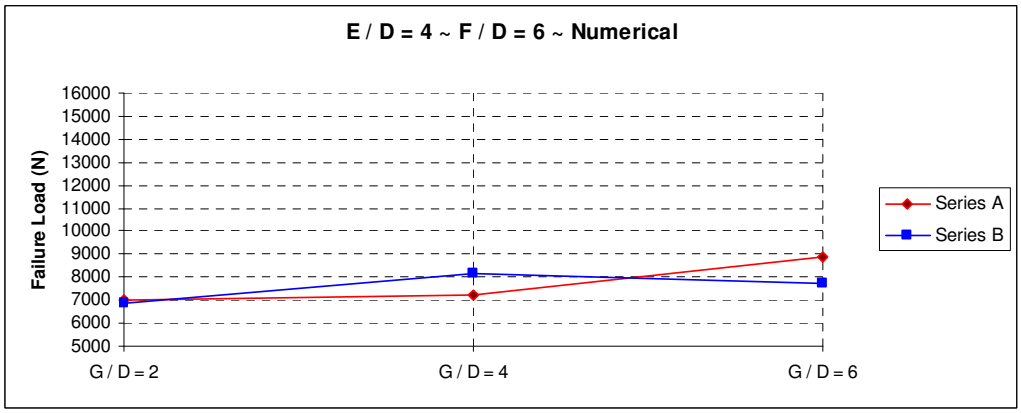
Figure 6.29 The numerical results of Series A & Series B for E/D=3




(a)




(b)




( c )

Figure 6.30 The numerical results of Series A & Series B for E/D=4

At the experimental results of E/D=4 and F/D=4, Series A & Series B have nearly the same failure load value for G/D=2 & G/D=6. (Fig. 6.27.b)

At the numerical results of E/D=4 and F/D=4, Series A & Series B did not show the similarity between each other (Fig. 6.30.b)

At the experimental results of E/D=4 and F/D=6, Series A & Series B have nearly the same failure load value for G/D=2 & G/D=4 and it tends to increase. (Fig. 6.27.c)

At the numerical results of E/D=4 and F/D=6, Series A & Series B have nearly the same failure load value for all G/D and their average values tend to increase. (Fig. 6.30.c)

For E/D=2, considering the failure load values for all of the combinations of Series A are completely different from Series B. In opposite of that considering greater E/Ds they are nearly the same values except E/D=4,F/D=4,G/D=4 and E/D=3,F/D=2,G/D=4.

The contours below are the couple of samples of the numerical study. The red regions below indicate that failure occurs since the Hashin failure criteria values are greater than 1.

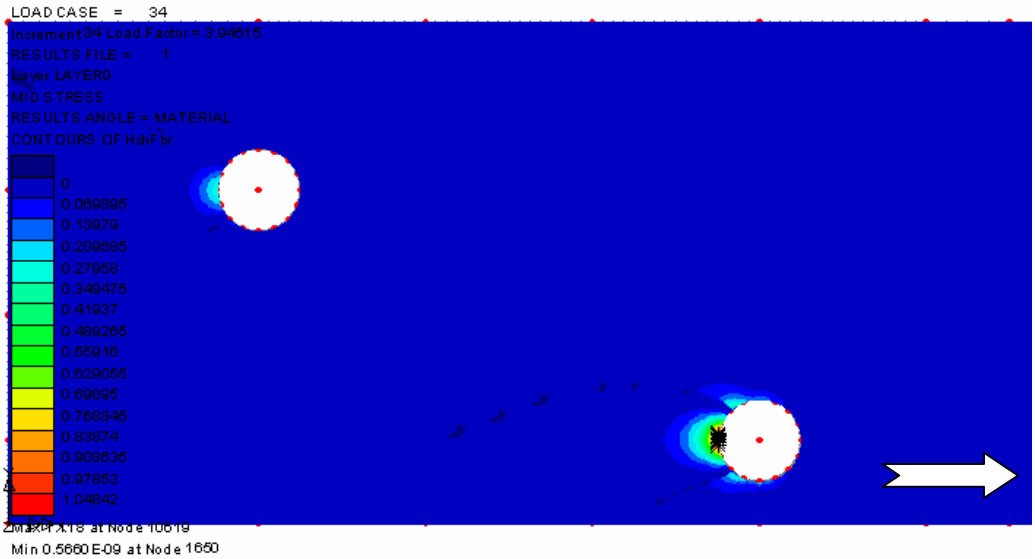



Figure 6.31 Numerical study - Hashin failure criteria of the configuration E/D=3,F/D=6,G/D=2, Series A (x indicates the region which failure has been occurred with respect to Hashin failure criteria, the failure mode is "Bearing", failure load is 7890 N)

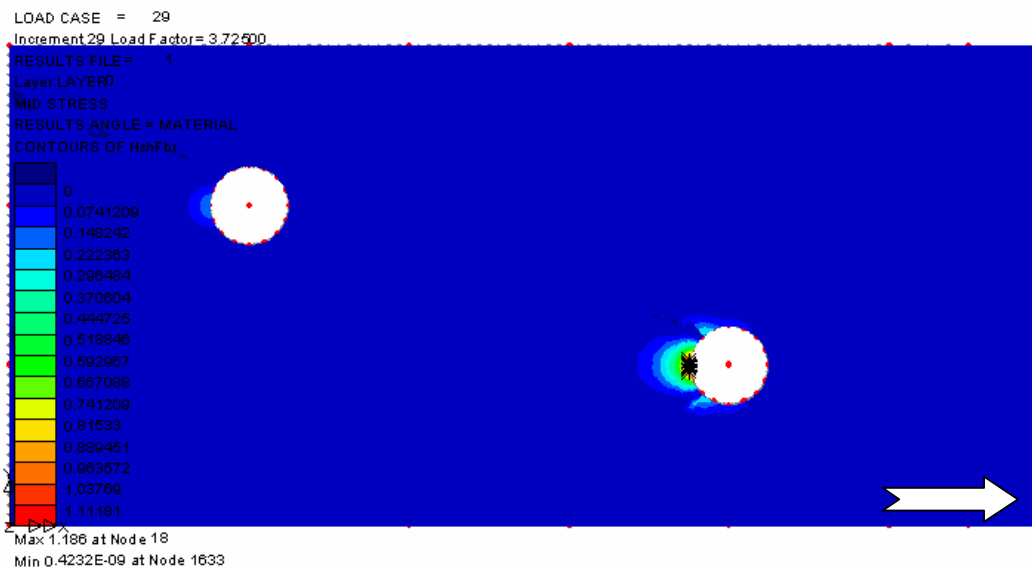



Figure 6.32 Numerical study - Hashin failure criteria of the configuration E/D=3,F/D=6,G/D=4, Series A (x indicates the region which failure has been occurred with respect to Hashin failure criteria, the failure mode is "Bearing", failure load is 7450 N)

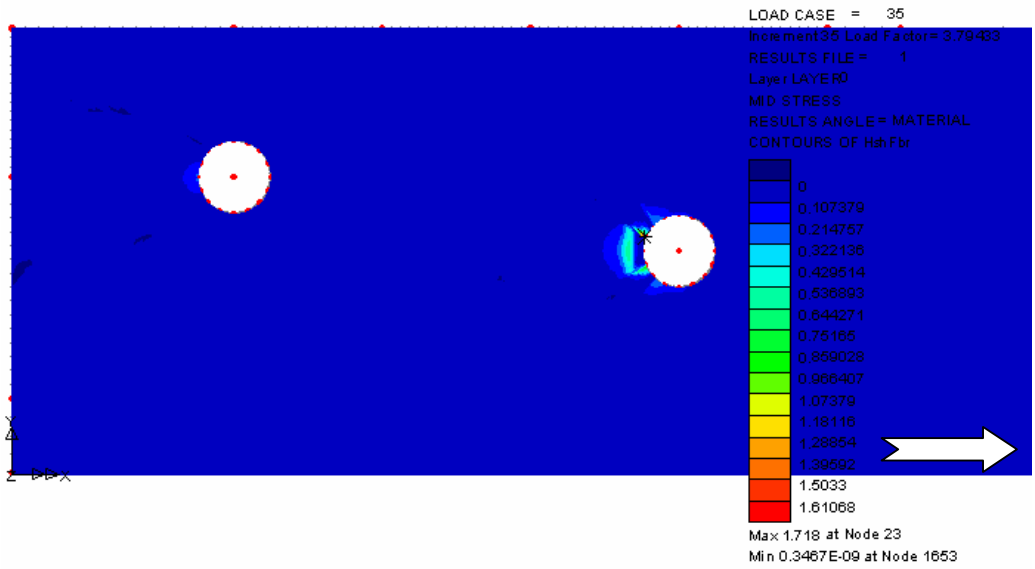



Figure 6.33 Numerical study - Hashin failure criteria of the configuration E/D=3,F/D=6,G/D=6, Series A (x indicates the region which failure has been occurred with respect to Hashin failure criteria, the failure mode is "Shear-Out", failure load is 7589 N)

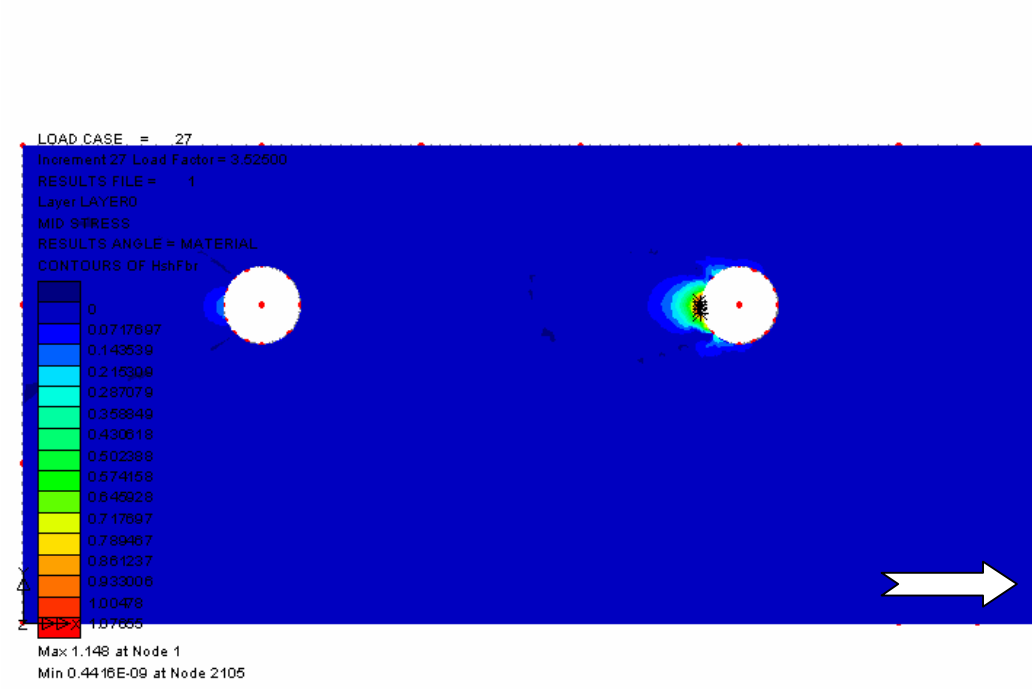



Figure 6.34 Numerical study - Hashin failure criteria of the configuration E/D=3,F/D=6,G/D=8 (x indicates the region which failure has been occurred with respect to Hashin failure criteria, the failure mode is "Bearing", failure load is 7050 N)

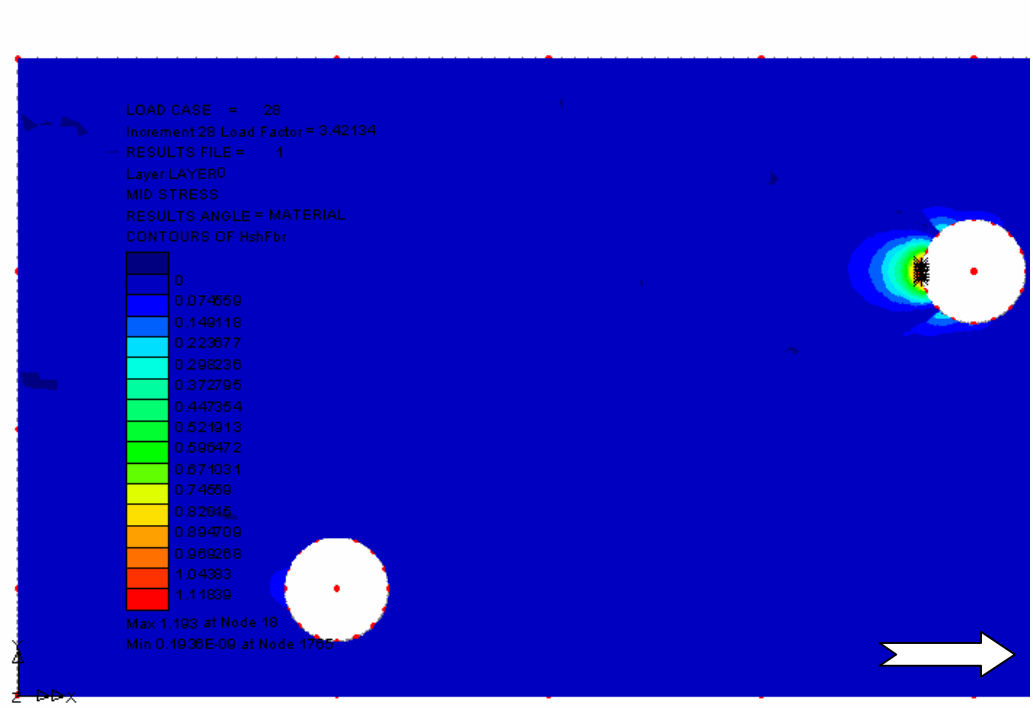



Figure 6.35 Numerical study - Hashin failure criteria of the configuration E/D=3,F/D=6,G/D=2, Series B (x indicates the region which failure has been occurred with respect to Hashin failure criteria, the failure mode is “Bearing”, failure load is 6843 N)

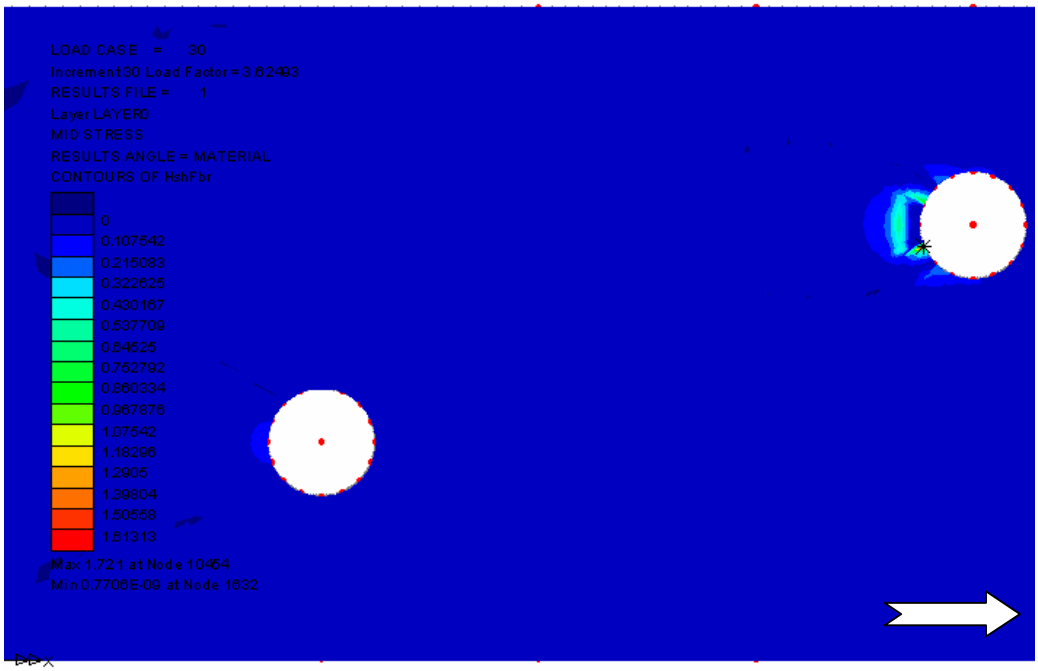



Figure 6.36 Numerical study - Hashin failure criteria of the configuration E/D=3,F/D=6,G/D=4, Series B (x indicates the region which failure has been occurred with respect to Hashin failure criteria, the failure mode is “Shear-Out”, failure load is 7250 N)

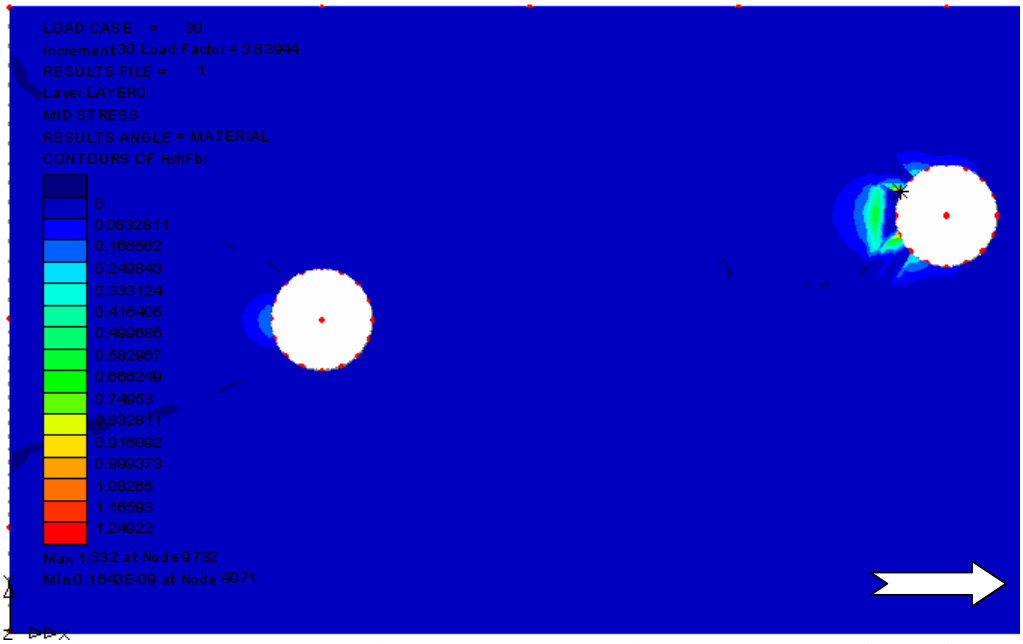



Figure 6.37 Numerical study - Hashin failure criteria of the configuration E/D=3,F/D=6,G/D=6, Series B (x indicates the region which failure has been occurred with respect to Hashin failure criteria, the failure mode is “Shear-Out”, failure load is 7679 N)

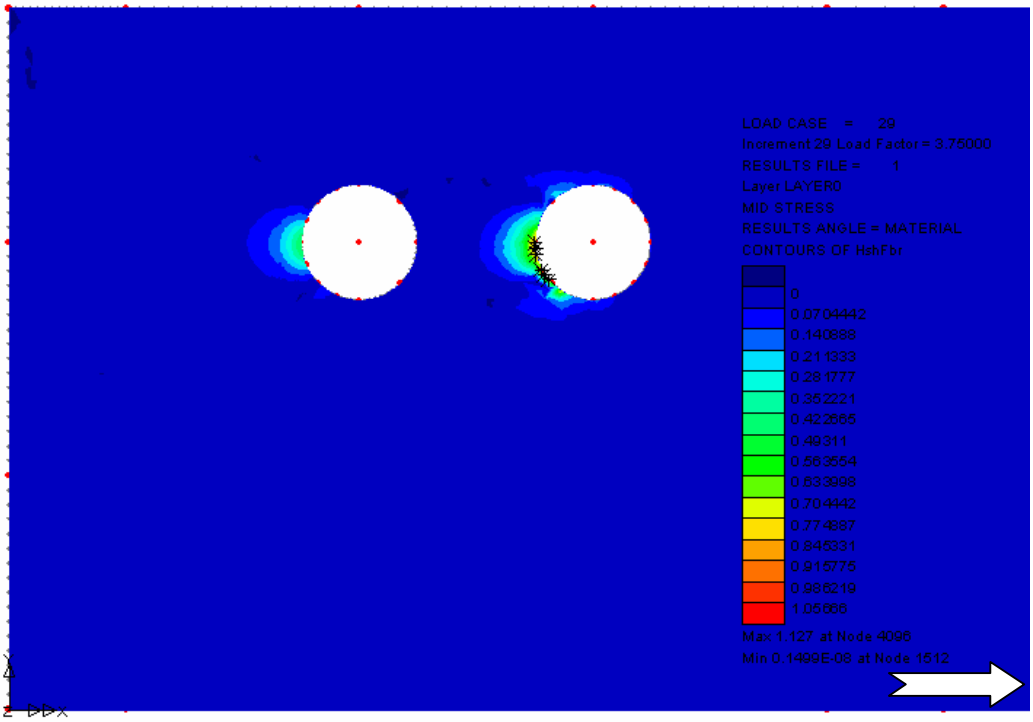



Figure 6.38 Numerical study - Hashin failure criteria of the configuration E/D=3,F/D=2,G/D=8 (x indicates the region which failure has been occurred with respect to Hashin failure criteria, the failure mode is “Bearing + Shear-Out”, failure load is 7500 N)

# CHAPTER SEVEN

# CONCLUSIONS

In this study, “failure load” and “failure mode” parameters were investigated experimentally and numerically. The specimens for each pin configuration were tested for experimental study. For the numerical study all pin configurations were modeled and analyzed by LUSAS 13.6 finite element analysis software. Geometric non-linear solution with Hashin failure criterion were selected for the numerical analysis. Failure load values and failure modes were investigated for three variables, E/D ratio (2,3,4), F/D ratio (2,4,6), G/D ratio (2,4,6,8). In both the experimental and numerical studies, “Load-Displacement” and “Failure Load-Hole Distance Ratio” curves have been plotted and compared with each other.

It was seen that curves are linear before the initial failure (elastic region). It can be say that almost all of the specimens were reached the failure loads between the displacements of 1 and 2 mm. Furthermore, specimens were carried the load up to min. 5 mm at nearly-constant load values.

However, it was seen that the greater E/D ratio-configuration-specimens continued to carry the load up to 9 mm at nearly-constant load values.

When we look at the failure modes of either Series A or Series B, the lowest value of the E/D (E/D=2), have the combination of “Bearing” and “Shear-out” modes. As known that it is not a secured mode, in practice the ratio of E/D=2 should not to be chosen.

At the same time, for all E/D versions of the arrangement F/D=2 + G/D=8 the same failure modes, combination of “Bearing” and “Shear-out”, occurred.

The remaining configurations had the “Bearing” mode, which is the most secured failure mode.

In Series A, the configuration G/D=2 & F/D=6 with lower values of E/D (2,3) the laminates are the weakest, the configuration E/D=4, F/D=4 and G/D=4 is the strongest and the most secured laminate.

In Series B, G/D=8 with lower values of E/D (2,3) & F/D (2,4) the laminates are the weakest, the configuration of E/D=2, F/D=2 and G/D=6 is the strongest and the most secured laminate.

It was seen that the failure behaviour of the laminates which have the rectangular-shaped hole configuration (G/D=8) is not depend on the E/D ratio.

In both experimental & numerical results of the configuration E/D=4 in series A, the maximum failure load occurred at G/D & F/D=4. The failure load tended to decrease while G/D increased & F/D decreased.

In both experimental & numerical results of the configuration E/D=2 in series B, the failure load tended to decrease while G/D increased & F/D decreased.

In both experimental & numerical results of the configuration E/D=3 in series B, the minimum failure load occurred at maximum value of G/D & the minimum value of F/D.

At the minimum value of E/D, (E/D=2) considering the failure load values for all of the combinations of Series A are completely different from Series B. In opposite of that considering greater E/Ds they are nearly the same values except the arrangements E/D=4,F/D=4,G/D=4 and E/D=3,F/D=2,G/D=4.

**REFERENCES**

Abd-El-Naby SFM, Hollaway L. (1993) The experimantal behaviour of bolted joints in pultruded glass/polyester material. Part 1: singlebolt joints. *J Comp Mater*;24:531–8.

Aktaş A, & Karakuzu R., (1998) Failure Analysis of Two Dimensional Carbon-Epoxy Composite Plate Pinned-Joint, *Proc. NATO Advanced Study Institute on Mechanics of CompositeMaterials and Structures*, 12–24 July 1998, Troia, Portugal, vol. 3, pp. 381–397, IDMEC/IST, Lisbon, Portugal.

Aktaş A, Karakuzu R. (1999) Failure analysis of two-dimensional carbon–epoxy composite plate pinned joint. *Mech Compos Mater Struct*;6:347–61.

Aktaş A. (2005) Bearing strength of carbon epoxy laminates under static and dynamic loading. *Composite Structures* 67, 485-489.

B. L. Larry and M. S. Mahmood, (1995) Two DimensionalModeling of Composite Pinned-Joint Failure, *J. Composite Mater*, vol. 29, pp. 671–696.

C. Fu-Kuo and C. Kuo-Yen, (1987) Post-Failure Analysis of Bolted Composite Joints in Tension or Shear-out Mode Failure, *J. Composite Mater.*, vol. 21, pp. 809–833,.

C. Fu-Kuo, S. George, and A. Richard, (1984) Failure Strength of Nonlinearly Elastic Composite Laminates Containing a Pin Loaded Hole, *J. Composite Mater.*, vol. 18, pp. 465–476.

Camanho, P.P, & Matthews, F.L. (1999). A Progressive Damage Model for Mechanically Fastened Joints in Composite Laminates. *Journal of Composite Materials*, 33, 2248-2280

Camanho, P.P., & Matthews, F.L. (1997). Stress analysis and strength prediction of mechanically fastened joints in FRP: a review. *Composites Part A, 28A*, 529-47.

Chang FK, Scott RA, Springer GS. (1982) Strength of mechanically fastened composite joints. *J Comp Mater*;16:470–94.

Chang FK. (1986) The effect of pin load distribution on the strength of pin loaded holes in laminated composites. *J Compos Mater*;20:401–8.

Chang, F.K. (1983). Strength of bolted joints in laminated composites. *Unpublished Ph.D. Dissertation, University of Michigan*

Chang, F.K., Scott, R.A., & Springer, G.S. (1984)a. Failure of Composite Laminates Containing Pin Loaded Holes- Method and Solution. *Journal of Composite Materials*, 18, 255-278.

Chang, F.K., Scott, R.A., & Springer, G.S. (1984)b. Failure Strength of Nonlinearly Elastic Composite Laminates Containing a Pin Loaded Hole. *Journal of Composite Materials*, 18, 464-477

Chen JC, Chiu CH, Chin H. (1994) On the influence of weave structure on pin-loaded strength of orthogonal 3D composites. *J Comp Mater*;30:251–62.

Chen, W-H. and S-S. Lee. (1995). "Numerical and Experimental Failure Analysis of Composite Laminates with Bolted Joints under Bending Loads," *Journal of Composite Materials*, Vol. 29, pp. 15-36

Chun M., Niu Y., (1992), *Composite Airframe Structures: Practical Design information and Data*, Florida: Conmilit Pres Ltd.

Collings TA. (1977)The strength of bolted joints in multi-directional CFRP laminates. *Composites*: 43-55.

Collings TA. (1982) On the bearing strengths of CFRP laminates. Composites:241-52.

Dano, M.L., Gendron, G., & Picard, A. (2000). Stress and Failure Analysis of Mechanically Fastened Joints in Composite Laminates. *Composite Structures*, 50, 287-296

Dano, M.L., Gendron, G., & Piccard, A. (2000). Stress and Failure Analysis of Mechanically Fastened Joints in Composite Laminates. *Composite Structures*, 50, 287-296

Dano, M.L., Kamal, E. & Gendron, G (2006). Analysis of bolted joints in composite laminates: Strains and bearing stiffness predictions. *Composite Structures, In Press, Corrected Proof.* Retrieved July 4, 2006, from www.sciencedirect.com database.

Ekh, J. (2006). Multi-Fastener Single-lap Joints in Composite Structures. *Unpublished Ph.D. Dissertation, Royal Institute of Technology, Stockholm, Sweden*

Gamble, K., M. Pilling and A. Wilson. (1995). "An Automated Finite Element Analysis of the Initiation and Growth of Damage in Carbon-Fibre Composite Materials," *Composite Structures*, Vol. 35, pp. 265-274

Green AE, Zerna W. (1968) *Theoretical elasticity*. New York: Dover Publications Inc.

Gülem, T. (2004). Failure analysıs in laminated Composites with pin-loaded hole. *Unpublished M.Sc. thesis, Dokuz Eylül University, Izmir*

H. Hiroyuki, M. Zen-Ichiro, and H. Kazushi, (1996) Strength Prediction of Mechanically Fastened Quasi-Isotropic Carbon/Epoxy Joints, *J. Composite Mater.*, vol. 30, pp. 1596–1612.

Hamada H,Maekawa ZI. (1996) Strength prediction of mechanically fastened quasi-isotropic carbon/epoxy joints. *Journal of Composite Materials*;30:1596–612.

Hassan, N.K., Mohamedien, M.A., & Rizkalla, S.H. (1996). Finite element analysis of bolted connections for PFRP composites. *Composites: Part B, 27B*, 339-349.

Herrington PD, Sabbaghina M. (1992) Effect of radial clearance between bolt and washer on the bearing strength of composite bolted joints. *J Compos Mater*;26:1826–43.

Hollmann K. (1996) Failure analysis of bolted composite joints exhibiting in-plane failure modes. *J Compos Mater*;30(3):359–83.

Hung, C.L., & Chang, F.K. (1996). Bearing Failure of Bolted Composite Joints. Part II: Model and Verification. *Journal of Composite Materials*, 30, 1359-1400.

İçten B.M., Karakuzu R.& Toygar M.E., (2006)b Failure analysis of woven kevlar fiber reinforced epoxy composites pinned joints. *Composite Structures*, 73, 443–450

Icten BM, Karakuzu R. (2002) Progressive failure analysis of pin loaded carbon–epoxy woven composite plates. *Compos Sci Technol*;62:1259–71.

Icten BM, Okutan B, Karakuzu R. (2003) Failure strength of woven glass fiber–epoxy composites pinned joints. *J Compos Mater*;37:1337–51.

Icten BM, Sayman O. (2003) Failure analysis of pin-loaded aluminium–glass–epoxy sandwich composite plates. *Compos Sci Technol*;63:727–37.

Jones R.M., (1999), *Mechanics of Composite Materials*, (2nd Ed.), USA: Taylor&Francis, Inc.

K. Usama, (1996) Notched and Pin Bearing Strengths of GFRP Composite Laminates, *J. Composite Mater.*, vol. 30, pp. 2043–2055.

Karakuzu R., Gülem T., İçten B.M. (2006)a. Failure analysis of woven laminated glass-vinylester composites with pin-loaded hole. *Composite Structures, 72, 27-32*

Khashaba UA. (1996) Notched and pin bearing strengths of GFRP composite laminates. *J Compos Mater*;30(18):2042.

Kim, S.J., Hwang, J.S., & Kim, J.H. (1998). Progressive failure analysis of pin-loaded laminated composites using penalty finite element method. *AIAA Journal*, *36*, No: 1, 75-80.

Konish HJ, Whitney JM. (1975) Approximate stress as in an orthotropic plate containing a circular hole. *J Compos Mater*;9:157–66.

Kretsis G, Matthews FL. (1985) The strength of bolted joints in glass fibre/epoxy laminates. *J Compos Mater*;16:92–102.

Lekhnitskii SG. (1968) *Anisotropic plates (English edition).* London:Gordon and Beach; (Translated by S.W. Tsai and T.Cheron).

Lessard, L.B., & Shokrieh, M.M. (1995). Two-Dimensional Modelling of Composite Pinned-Joint Failure. *Journal of Composite Materials*, 29, 671-697.

Liu D, Raju BB, You J. (1999) Thickness effects on pinned joints for composites. *J Comp Mater*;33:2–21.

M. Akay, S. Kong, and Ah Mun, (1991) Bearing Strength of Autoclave and Oven Cured Kevlar/Epoxy Laminates under Static and Dynamic Loading, *Composites*, vol. 26, pp. 451–456,

M. Hironori and K. Kenji, (1993).Bearing Strength and Damage Progress for PAN-Based and Pitch-Based Carbon Fiber Composites, *J. Composite Mater.*, vol. 27, pp. 1739–1761,

M. Ozbay, (1998) Buckling of Laminated Plates with Semicircular Holes, *J. Inst. Sci. Technol. Gazi Univ.*, vol. 10, pp. 393–401,.

M. S. Mahmood and B. L. Larry, (1996) Effects of Material Nonlinearity on the Three-Dimensional Stress State of Pin-Loaded Composite Laminates, *J. Composite Mater.*, vol. 30, pp. 839–861.

Maikuma H, Kubomura K. (1993) Bearing strength damage progress for PAM-based and pitch-based carbon fiber composites. *J Compos Mater*;27:1739–61.

Matthews F.L., Davies G.A.O., Hitchings D. & Soutis C. (2000) *Finite element modelling of composite materials and structures*, Cambridge: Woodhead Publishing Ltd. and CRC Press LLC.

Matthews FL, Quinn WJ. (1977) The effect of stacking sequence on the pin-bearing strength in glass fibre reinforced plastic. *J Comp. Mater.*;11:139–45.

Mazumdar, S.K., (2002) *Composites manufacturing : materials, product, and process Engineering*, USA: CRC Press LLC

Okutan B., Aslan Z., Karakuzu R., (2001) A study of the effects of various geometric parameters on the failure strength of pin-loaded woven-glass-fiber reinforced epoxy laminate*, Composites Science and Technology*, 61, 1491–1497.

Okutan B., Karakuzu R., (2003) The strength of pinned joints in laminated composites, *Composites Science and Technology*, 63, 893–905.

Okutan, B., Aslan, Z., & Karakuzu, R. (2001). A Study of The Effects of Various Geometric Parameters On The Failure Strength of Pin-Loaded Woven-Glass-Fiber Reinforced Epoxy Laminate. *Composite Science and Technology*, 61, 1491-1497.

Persson, E., E. Madenci and I. Eriksson. “Prediction of Delamination Initiation in Laminates with Pin-Loaded Holes,” to appear in *Journal of Theoretical and Applied Fracture Mechanics*.

Pierron F, Cerisier F, Grediac M. (2000) Numerical and experimental study of woven composite pin-joints. *J Comp Mater*; 34:1028–54.

Pyner GR, Matthews FL. (1979) Comprasion of single and multi-hole bolted joints in glass fibre reinforced plastic. *J Comp Mater*; 13:233–9.

Sallam HEM. (2003) Effect of circular hole on static and fatigue strength of unidirectional carbon-fiber/epoxy plate. *10th International colloquium on structural and geotechnical engineering, April 22–24, Cairo, Egypt: Ain Shams University;*.

Shokrieh, L. B., L. B. Lessard and C. Poon. "Three Dimensional Progressive Failure Analysis of Pin/Bolt Loaded Composite Laminates," *AGARD Conference Proceedings 590, Florence, Italy, 2-3 September 1996*.

W. Hong-Sheng, H. Chang-Li, and C. Fu-Kuo, (1996) Bearing Failure of Bolted Composite Joints. Part I: Experimental Characterization, *J. Composite Mater.*, vol. 30, pp. 1284–1314,.

Wang D.**,** Gang C., Zhengneng L. & Changhe K. (2006). Bearing Strength Analysis of Single Mechanically Fastened Joint in Stitched Laminates. *Journal of Reinforced Plastics and Composites 25, 711-724*

Whitney JM, Nuismer RJ. (1974) Stress fracture criteria for laminated composites containing stress concentrations. *J Mater*;8:253–65.